

**TEXTURED SOFT MAGNETIC Ni-Fe ALLOYS—  
STUDY OF PROCESS VARIABLES ON THE DEVELOPMENT OF  
CUBE TEXTURE IN A PERMALLOY**

A Thesis Submitted  
In Partial Fulfilment of the Requirements  
for the Degree of  
**MASTER OF TECHNOLOGY**

by  
**P. SARKAR**

to the

**DEPARTMENT OF METALLURGICAL ENGINEERING  
INDIAN INSTITUTE OF TECHNOLOGY KANPUR  
JANUARY 1979**

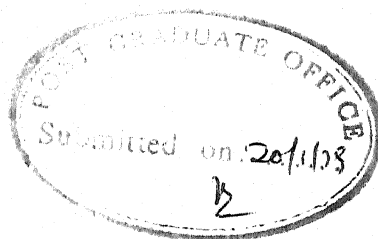
L. I. F. KANPUR  
CENTRAL LIBRARY

Acc. No. **A** **58753**

**3** JUL 1979


ME-1979-M-SAR-TEX



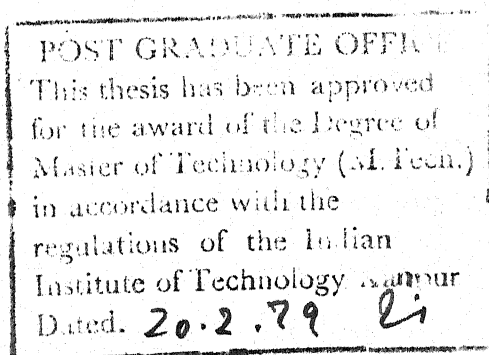


## CERTIFICATE

Certified that this work on 'Textured Soft Magnetic Ni-Fe Alloys - Study of Process Variables on the Development of Cube Texture in a Permalloy' by P. Sarkar has been carried out under my supervision and that this has not be submitted elsewhere for a degree.

  
( K.P. Gupta )  
Professor

Department of Metallurgical Engineering  
Indian Institute of Technology, Kanpur.



## ACKNOWLEDGEMENTS

I avail this opportunity to express my heartfelt indebtedness to Professor K.P. Gupta for his lively interest, inspiring guidance illuminating suggestions and constant help throughout the problem infested path of this work. In my weal and woe, he always stood by me. His sweet demeanour always enabled him to oblate my frustration whenever that had a chance to creep in my life.

To repay the debts, I owe to him is a dream only, I am grateful to Dr. A.K. Majumdar and Dr. S.N. Kaul for their help during the magnetic measurements, an essential part of this work.

I must acknowledge Mr. B. Somnath, the ever smiling man behind the computation involved in this work. Lot of thanks and regards are due to Mr. P.K. Nandi for his immense help in designing the electrical equipments.

I wish to offer a lot of thanks to Mr. V.P. Gupta for materialisation of the different schemes into actual experiment apparatus and accurate tracing of figures.

I am also thankful to Mr. D.K. Biswas, Mr. M.L. Pandey, Mr. K.P. Mukherjee, Mr. S.N. Sikdar and Mr. Chaurasia for their kind help throughout the work.

Lot of Thanks are due to my Lab. Partners, Messrs V.P. Srivastava, R.C. Misra, D.D. Ahirwar, M.K. Sardar and K.R. Subramaniam for helping me in various ways during the course of investigation.

How can I forget my friends Messrs R.N. Chatterjee, S. Dutta, S. Ganguly, P.K. Ghosh, S.N. Paul, P. Mukherjee, P. Sarkar, P. Ghosh, A. Sen, N.C. Biswas, V.V. Ramanna Rao, K. Hariprasad, S. Nath and B.P. Rao. Their entertaining company enlightened me in my days of frustration. Their constant help in various ways enabled me to complete this work. I may forget many things, but the sweet memories with them will never fade in my life.

I must acknowledge the financial support of Department of Science and Technology (India) which made this work possible for investigation.

I am also grateful to Mr. Hari Ram for his beautiful cyclostyling and Mr. Tripathi for ammonia printing.

At last but not the least, I must thank Mr. M.R. Nathwani for painstakingly typing the almost illegible manuscript.

P. SARKAR

## SYNOPSIS

The present investigation involves the study of some process variables on the development of cube texture in 48 permalloy. To carry out this work, some experimental set up like controlled atmosphere annealing furnace, magnetic test equipment etc. have been fabricated. The process variables, taken into consideration for the development of cube texture, are percent reduction in thickness in cold rolling, temperature of annealing, time of annealing and addition of impurities or alloying elements. Texture developed was studied through x-ray diffraction technique using a texture goniometer. Prominent cube texture together with some secondary textures appears to be produced when the alloys are cold rolled to 96% without intermediate annealing and is followed by annealing at  $1058^{\circ}\text{C}$  for 4 hrs. The secondary textures get reduced considerably when the alloys contain reasonable amount of manganese ( $\sim 1\%$ ) and cold rolled to 96% at elevated temperature ( $\sim 250^{\circ}\text{C}$ ) prior to annealing at  $1058^{\circ}\text{C}$  for 4 hrs.

# TABLE OF CONTENTS

Contents	Page
LIST OF TABLES	x
LIST OF FIGURES	xi
SYNOPSIS	
I. INTRODUCTION	1
I.1 Permalloys-Survey of Literature	4
I.1.1 Phase equilibrium	4
I.1.2 Nontextured permalloys	5
I.1.2.1 Fabrication and heat treatment of permalloys tapes and wires	5
I.1.2.2 Magnetic properties of nontextured permalloys	5
I.1.3 Textured iron-nickel alloys	10
I.1.3.1 Cube texture in Fe-Ni alloys	10
I.1.3.2 Effect of impurities on texture and magnetic properties of Fe-Ni alloys	12
I.1.3.3 Effect of inclusion, grain diameter and size on texture and magnetic properties	13
I.2 Fabrication of cube textured permalloys with appropriate magnetic property	21
I.2.1 Melting and hot working	22
I.2.2 Cold rolling	22
I.2.3 Annealing of Fe-Ni alloys	24
I.2.3.1 Effect of rate of cooling and atmosphere of annealing on magnetic properties.	25

	Page
I.2.4 Magnetic annealing	26
I.3 Statement of the problem	33
II. FABRICATION OF EQUIPMENT	37
II.1 Furnace for hot rolling	38
II.1.1 Design consideration	38
II.1.2 Constructional details	39
II.1.3 Testing of the furnace	40
II.2 Controlled atmosphere annealing furnace	41
II.2.1 Design consideration	41
II.2.2 Constructional details	42
II.2.3 Power supply	44
II.2.4 Testing of furnace	44
II.3 Gas purification train	45
II.3.1 Design consideration	45
II.3.2 Constructional details	46
II.4 Epstein test frame	46
II.4.1 Design consideration	52
II.4.2 Constructional details	52
II.4.3 Testing of Epstein test frame	53
II.5 Magnetic annealing furnace and power supply	53
II.6 Sheet specimen holder for Laué technique	54

	Page
I.2.4 Magnetic annealing	26
I.3 Statement of the problem	33
II. FABRICATION OF EQUIPMENT	37
II.1 Furnace for hot rolling	38
II.1.1 Design consideration	38
II.1.2 Constructional details	39
II.1.3 Testing of the furnace	40
II.2 Controlled atmosphere annealing furnace	41
II.2.1 Design consideration	41
II.2.2 Constructional details	42
II.2.3 Power supply	44
II.2.4 Testing of furnace	44
II.3 Gas purification train	45
II.3.1 Design consideration	45
II.3.2 Constructional details	46
II.4 Epstein test frame	46
II.4.1 Design consideration	52
II.4.2 Constructional details	52
II.4.3 Testing of Epstein test frame	53
II.5 Magnetic annealing furnace and power supply	53
II.6 Sheet specimen holder for Laue technique	54

	Page
III. EXPERIMENTAL PROCEDURE	68
III.1 Melting and homogenization of alloys	69
III.2 Hot rolling	71
III.3 Cold rolling	71
III.4 Annealing of alloys under controlled atmosphere	73
III.5 Specimen thinning for X-ray diffraction work	74
III.6 Texture determination using x-ray diffraction technique	76
III.6.1 Determination of $\theta_{(hkl)}$	76
III.6.2 Determination of $\mu_t$	77
III.6.3 Determination of correction factor	78
III.6.4 Measurement of intensity and plotting of pole figures	79
III.7 Metallographic investigation	80
III.8 Magnetic measurements	84
IV. RESULTS	91
IV.1 X-ray study	92
IV.1.1 Bragg angle determination	92
IV.1.2 Texture determination	92
IV.2 Magnetic measurements	94
V. DISCUSSION	129
V.1 Study of cold rolled texture	132
V.2 Study of annealed texture of 48 permalloy with small amount of Mn	134



## Page

V.2.1	Identification of peak positions in pole figures	138
V.2.2	Effect of percent reduction on the annealed texture	139
V.2.3	Effect of annealing temperature on annealed texture	141
V.2.4	Effect of annealing time on the annealed texture	141
V.3	Identification of other process variables	142
V.4	Study of permalloys with new process variables	144
V.4.1	Cold rolled texture	145
V.4.2	Annealing textures	145
V.5	Magnetic study of 48 permalloys	147
VI.	CONCLUSION	155
	REFERENCES	158
	APPENDIX	162
Table 1.	Program for calculation of intensity correction factor for various $\mu t$ and $-\alpha$ for different values of $\theta$ .	163
Table 2.	Intensity correction factor for different $\mu t$ and $\theta$ values.	168
Table 3.	Components of Epstein test frame.	190

## LIST OF TABLES

- Table I : Magnetic properties of soft magnetic materials based on Ni-Fe.
- Table II : Effect of deoxidizer on initial permeability of 49 permalloy.
- Table III : Epstein test frame data for 200 gms HSL Si steel samples.
- Table IV : Processing data for 48 permalloys.
- Table V : Chemical thinning solutions for Fe-Ni alloys.
- Table VI : Diffractometer conditions used for texture determination.
- Table VII : Bragg angle of reflection ( $\theta_{hkl}$  in terms of  $2\theta_{hkl}$ ) for different samples.
- Table VIII : Relative peak intensity at different pole locations of different heat treated samples.
- Table IX : Effect of percent reduction on annealing texture at a fixed temperature ( $1058^{\circ}\text{C}$ ) and time (4 hrs).
- Table X : Effect of temperature on annealing texture of cold rolled samples at a fixed time (4 hrs.)
- Table XI : Effect of time of annealing on texture formation at different temperature.
- Table XII : Effect of cold rolling temperature and Mn content for 96% cold rolled and annealed ( $1058^{\circ}\text{C}$ , 4 hrs) samples.

## LIST OF FIGURES

	<u>Page</u>
Figure 1. : Fe-Ni binary diagram.	7
Figure 2. : Effect of heat treatment on initial permeability of Fe-Ni alloys.	8
Figure 3. : Maximum permeability of Fe-Ni alloys due to different heat treatment.	8
Figure 4. : Coercive force of Fe-Ni alloys of ordinary purity.	9
Figure 5. : Maximum permeability of 78 permalloys on annealing in a magnetic field.	9
Figure 6. : (B-H) vs. H curves for Nickel single crystal measured along different crystallographic directions.	15
Figure 7. : Recrystallization textures in Fe-Ni-Cu alloys.	16
Figure 8. : B-H loop of 50 Ni-Fe alloy for different sheet thicknesses.	16
Figure 9. : Quality of cube texture produced in 50 Ni-Fe alloy as a function of rolled grain thickness. (A) Fe-Ni alloy with 0.028% Si, (B) Fe-Ni alloy with 0.67% Si.	17
Figure 10. : Magnetic properties of Mo-permalloy as a function of sulfur content.	18
Figure 11. : Permissible annealing temperature range for 50 Ni-Fe alloys at different impurity contents.	19

	<u>Page</u>
Figure 12. : (111) pole figure for cold rolled copper.	31
Figure 13. : (200) pole figure for cold rolled copper.	31
Figure 14. : Effect of cooling rate and composition of alloys (near 76% Ni, 2.6% Cr) on initial permeability.	32
Figure 15. : Permeability vs. flux density curves for 58 Ni-Fe alloys: (A) After primary heat treatment at 1200°C, (B) After subsequent magnetic annealing at 470°C and (C) a conventional 50 Ni-Fe alloy.	33
Figure 16. : Magnetostriction vs. flux density curves for 53 Ni-Fe alloys: (A) after magnetic annealing at 450°C and (B) before magnetic annealing (after primary annealing at 1200°C).	33
Figure 17. : Initial Permeability ( $\mu_0$ ) and squareness ( $B_r/B_m$ ) vs. temperature of magnetic annealing for 58 Ni-Fe alloys.	33
Figure 18. : The dependence of induced uniaxial anisotropy on the annealing temperature for Fe-Ni alloys.	34
Figure 19. : Temperature vs. voltage curve for hot working furnace.	48
Figure 20. : Heat treatment furnace.	49
Figure 21. : Longitudinal temperature profile of the annealing furnace.	50
Figure 22. : Hydrogen gas purification train and Argon and Hydrogen gas mixer arrangement.	51

	<u>Page</u>
Figure 23. : Details of Epstein test frame.	57
Figure 24. : Circuit diagram of Epstein test frame.	58
Figure 25. : Secondary voltage vs. primary current curve obtained for Epstein test frame.	59
Figure 26. : Ratio of secondary voltage to current vs. primary current curves for the Epstein test frame.	60
Figure 27. : Primary voltage vs. secondary voltage curves for the Epstein test frame.	61
Figure 28. : B-H loop obtained for 200 gms of hot rolled Si-Steel Strips.	62
Figure 29. : Circuit diagram of the D.C. power genera- tion unit for magnetic annealing furnace.	64
Figure 30. : Details of the sheet specimen holder for Laue technique.	65
Figure 31. : Laue pattern of LiF single crystal fixed to the sheet specimen holder. The diffrac- tion pattern corresponds to the bottom most part of crystal.	66
Figure 32. : Laue pattern of the same LiF single crystal fixed to the sheet specimen holder as in Fig. 31. The diffraction pattern corres- ponds to the top most part of the crystal. The crystal was only displaced vertically with the help of the vertical slide.	66
Figure 33. : Diffractometer geometry for transmission technique.	82

- Figure 34. : Use of a polar net to plot the diffracted beam intensity measured in the transmission technique of texture determination. 83
- Figure 35. : (111) pole figure of sample 1(a), 90% cold rolled at room temperature. 97
- Figure 36. : (111) pole figure of sample 2, 94% cold rolled at room temperature. 97
- Figure 37. : (111) pole figure of sample 2(a), 96% cold rolled at room temperature. 98
- Figure 38. : (111) pole figure of sample 3, 97% cold rolled at room temperature. 98
- Figure 39. : (111) pole figure of sample 4(b), 96% cold rolled at 200°C. 99
- Figure 40. : (111) pole figure of sample 4(c), 96% cold rolled at 400°C. 99
- Figure 41. : (111) pole figure of sample 5(b), 96% cold rolled at 150°C. 100
- Figure 42. : (111) pole figure of sample 5(c), 96% cold rolled at 250°C. 100
- Figure 43. : (111) pole figure of sample 1 annealed at 1058°C for 4 hrs. 102
- Figure 44. : (111) pole figure of sample 1(a) annealed at 1058°C for 4 hrs. 102
- Figure 45. : (111) pole figure of sample 1(a) annealed at 1058°C for 7½ hrs. 103
- Figure 46. : (111) pole figure of sample 2 annealed at 1058°C for 1 hrs. 103

Figure 47.	: (111) pole figure of sample 2 annealed at 1058°C for 2 hrs.	104
Figure 48.	: (111) pole figure of sample 2 annealed at 1058°C for 4 hrs.	104
Figure 49.	: (111) pole figure of sample 2 annealed at 1100°C for 4 hrs.	105
Figure 50.	: (111) pole figure of sample 2(a) annealed at 1058°C for 4 hrs.	105
Figure 51.	: (111) pole figure of sample 2(a) annealed at 1058°C for 8 hrs.	107
Figure 52.	: (111) pole figure of sample 2(a) annealed at 1058°C for 16 hrs.	107
Figure 53.	: (111) pole figure of sample 2(a) annealed at 1120°C for 4 hrs.	108
Figure 54.	: (111) pole figure of sample 2(a) annealed at 1120°C for 6 hrs.	108
Figure 55.	: (111) pole figure of sample 2(a) annealed at 1120°C for 8 hrs.	109
Figure 56.	: (111) pole figures of sample 2(a) annealed at 1120°C for 10 hrs.	109
Figure 57.	: (111) pole figure of sample 3 annealed at 1058°C for 2 hrs.	110
Figure 58.	: (111) pole figure of sample 3 annealed at 1058°C for 4 hrs.	110
Figure 59.	: (111) pole figure of sample 3(a) annealed at 1058°C for 4 hrs.	112
Figure 60.	: (111) pole figure of sample 3(a) annealed at 1058°C for 8 hrs.	112

Figure 61.	:	(111) pole figure of sample 3(a) annealed at 1058°C for 16 hrs.	113
Figure 62.	:	(111) pole figure of sample 3(a) at 1120°C for 4 hrs.	113
Figure 63.	:	(111) pole figure of sample 3(a) annealed at 1120°C for 6 hrs.	114
Figure 64.	:	(111) pole figure of sample 3(a) annealed at 1120°C for 8 hrs.	114
Figure 65.	:	(111) pole figure of sample 3(a) annealed at 1120°C for 10 hrs.	115
Figure 66.	:	(111) pole figure of sample 4(b) annealed at 1058°C for 4 hrs.	115
Figure 67.	:	(111) pole figure of sample 4(c) annealed at 1058°C for 4 hrs.	117
Figure 68.	:	(111) pole figure of sample 5(a) annealed at 1058°C for 4 hrs.	117
Figure 69.	:	(111) pole figure of sample 5(b) annealed at 1058°C for 4 hrs.	118
Figure 70.	:	(111) pole figure of sample 5(c) annealed at 1058°C for 4 hrs.	118
Figure 71.	:	(111) pole figure of sample 6(b) annealed at 1058°C for 4 hrs.	119
Figure 72.	:	(200) pole figure of sample 6(b) annealed at 1058°C for 4 hrs.	119
Figure 73.	:	Stereogram showing peak intensity locations of (111) and (200) poles for sample 6(b).	120



Figure 74.	:	Magnetisation vs field strength curves for sample 2 after various processing stages.	122
Figure 75.	:	Magnetisation vs. field strength curves for 48 permalloy specimens annealed at 1058°C for 4 hrs.	123
Figure 76.	:	Microstructure of 48 permalloy sample after annealing.	136
Figure 77.	:	(111) pole figures for annealed copper with cube texture.	137
Figure 78.	:	(200) pole figure for annealed copper with cube texture.	137

## CHAPTER I

### INTRODUCTION

2

## CHAPTER I

### INTRODUCTION

Soft magnetic alloys are used for making transformer cores. Generally there are two types of transformers - (1) transformers for low frequency ( $\sim 50$ - $60$  Hzs) use in which usually bcc Fe-Si alloys are used and (2) transformers for high frequency ( $> 50$ - $60$  Hz) use. For the latter case fcc Fe-Ni base alloys are used due to their very high initial permeability, low loss and small coercive force. The Fe-Ni base alloys are known by various trade names depending on the variation in Fe and Ni contents, alloying element content and specific thermal and/or mechanical treatments. The Fe-Ni alloys are usually called permalloys whereas a certain copper added Fe-Ni alloy is called  $\mu$ -metal, a certain copper and molybdenum<sup>added</sup>/Fe-Ni alloy is called 1040 alloy and molybdenum added Fe-Ni alloys are called Mo-permalloys and supermalloys.

Commercial permalloys contain 40 to 80%Ni (alloy compositions are given in weight percent unless otherwise stated). They are usually named according to their nickel content, e.g., 45 peralloy contains 45%nickel. The usual commercial permalloys are 48 permalloy, 65 permalloy, 78 permalloy even though quite often other permalloy compositions are found in specific uses. Magnetic properties of permalloys can be varied quite extensively through suitable heat treatment. For suitably heat treated permalloys (permalloy treatment) the magnetic permeability is found to increase with increase in Ni content and reaches a maximum at about 78%Ni. Isoperm and  $\mu$ -metals are two

copper bearing permalloys containing about 45 to 50% Ni and 75% Ni respectively and copper varying from 5 to 15%. Commercial  $\mu$ -metal contains about 5% Cu with or without some small amount of Cr. Copper containing permalloys respond to permalloy treatment. The most important Mo-permalloys, 4-79 Mo permalloy and supermalloy, contain 4% and 5% Mo respectively. Addition of small amount of molybdenum causes a large increase in initial permeability, low coercive force and high electrical resistivity. The only important molybdenum and copper containing commercial permalloy is 1040 alloy which contains about 14% copper 3% molybdenum, 72% nickel and rest iron. The most remarkable property of this alloy is its high initial permeability and low coercivity. For easy comparison, the magnetic properties of various Fe-Ni alloys are given in Table I together with some typical uses of these materials.

Even though Fe-Ni base alloys are in commercial use in our country, the required material is not made here but is imported from abroad. The processing of those materials is not difficult but the development of optimum properties depend on careful choice and variations of processing parameters which are usually not given out in detail in literature. Hence under a general plan to study these group of alloys this investigation concentrates on the study of permalloys. A more detailed survey of permalloys is thus given in the following sections.

## I.1 Permalloys-Survey of Literature

### I.1.1 Phase equilibria

The Fe-Ni phase diagram is given in Fig. 1. A continuous series of solid solution of Fe in Ni (fcc) occurs at higher temperatures but at room temperature it is stable above 40% Ni. The fcc solid solution, however, undergoes an order-disorder transformation with a maximum critical temperature of  $\sim 500^{\circ}\text{C}$  at the  $\text{FeNi}_3$  composition. The rate of ordering is reported to be sluggish, taking about a week at  $450^{\circ}\text{C}$  for complete ordering<sup>1,2</sup>. The critical temperature for ordering decreases with increase in Fe content. Neutron irradiation has been found to bring about an ordering reaction in 50 Ni-Fe alloy<sup>3</sup>. The fcc Fe-Ni alloys are ferromagnetic - the curie temperature also goes through a maximum ( $\sim 612^{\circ}\text{C}$ ) at about 65% Ni composition. If the Fe-Ni alloys are not allowed to produce LRO, the SRO state may bring about magnetic anisotropy in Fe-Ni alloys through suitable magnetic treatment<sup>4,5</sup>.

The Fe-Ni alloys can be classified into two categories with respect to the crystallographic orientation of their grains - (1) nontextured permalloys in which the grains are randomly oriented with respect to each other and (2) textured permalloys in which the grains are oriented with one of their crystallographic direction parallel to each other. The processing of the two varieties of permalloys are different and are discussed in some detail in the following sections.

### I.1.2 Nontextured Permalloys

#### I.1.2.1 Fabrication and heat treatment of permalloy tapes and wires

Permalloys are generally melted in arc or induction furnace under an alkaline slag or in controlled atmosphere of hydrogen or argon. About 0.5% Mn is added for better ductility and easy fabrication. Usually 0.2% Al is added for deoxidation. Carbon is kept usually below 0.1%. The arc or induction melted ingots are heated to 1200°C and hot rolled to about 3/4" thickness. The hot rolled material is then cold rolled to 0.002" thick strips. Then it is again annealed in closed pots at 900°-950°C for 1 hour followed by cooling at a maximum rate of 100°C/hr upto 600°C. Finally an air quench is accomplished by removing the completely fabricated material from the furnace at 600°C and cooling it in still air by placing it on a copper plate. This treatment is called 'double treatment' or 'permalloy treatment'.

#### I.1.2.2 Magnetic properties of nontextured permalloys

Magnetic properties of permalloy are dependent on composition of alloys and heat-treatment given. Increase in Ni content increases both initial and maximum permeability which reaches a maximum at about 78% Ni if permalloy treatment is given (Figs. 2 and 3). Coercive force is also minimum for double treated 78 permalloys (Fig. 4). It has been found that optimum magnetic properties can be produced<sup>6</sup> if the magnetic field is present during the cooling of alloy between curie temperature and 350°C. The magnitude

## FIGURE CAPTIONS

- FIG. 1. Fe-Ni binary diagram.
- FIG. 2. Effect of heat treatment on initial permeability of Fe-Ni alloys.
- FIG. 3. Maximum permeability of Fe-Ni alloys due to different heat treatment.
- FIG. 4. Coercive force of Fe-Ni alloys of ordinary purity.
- FIG. 5. Maximum permeability of 78 permalloys on annealing in a magnetic field.

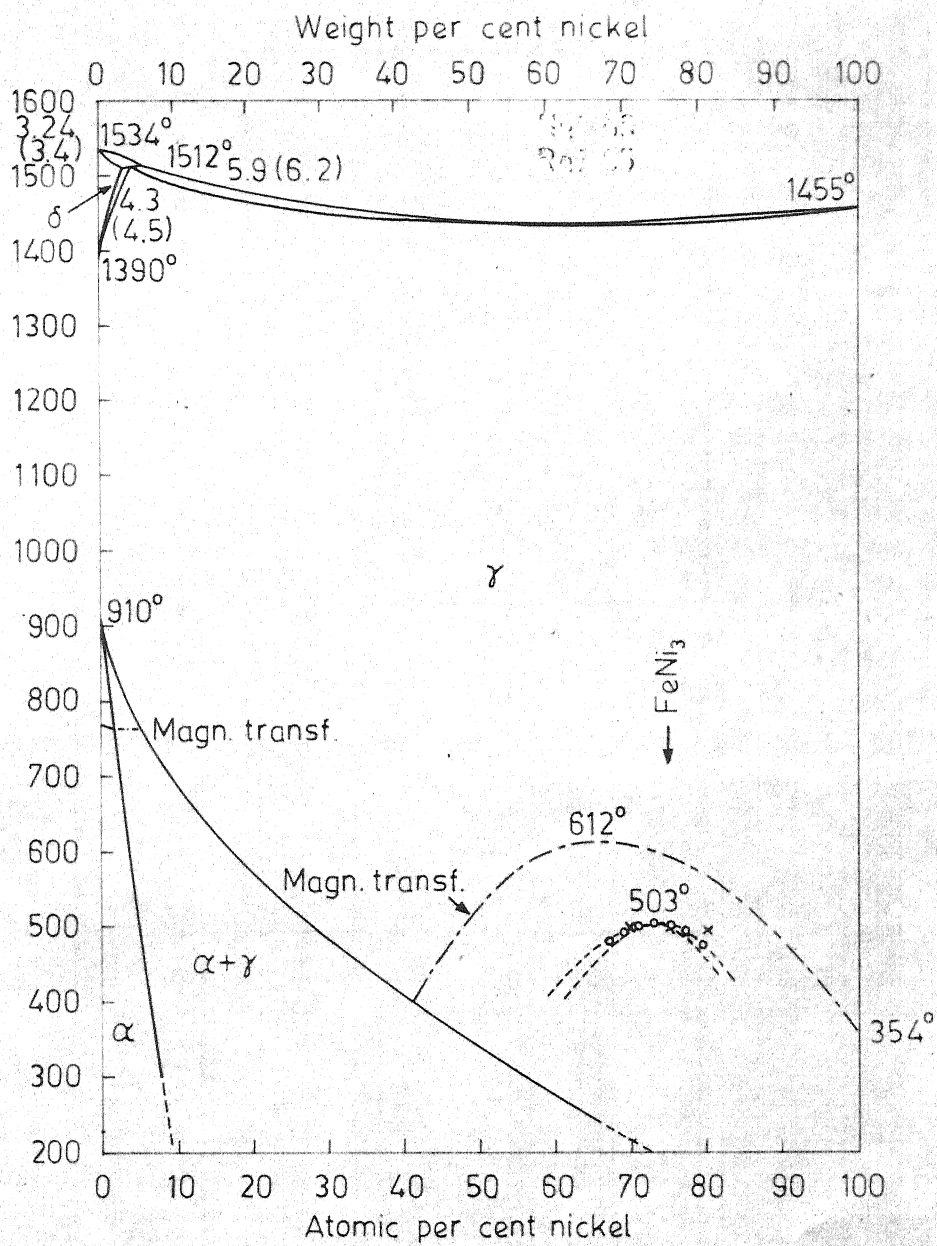


Fig. 1



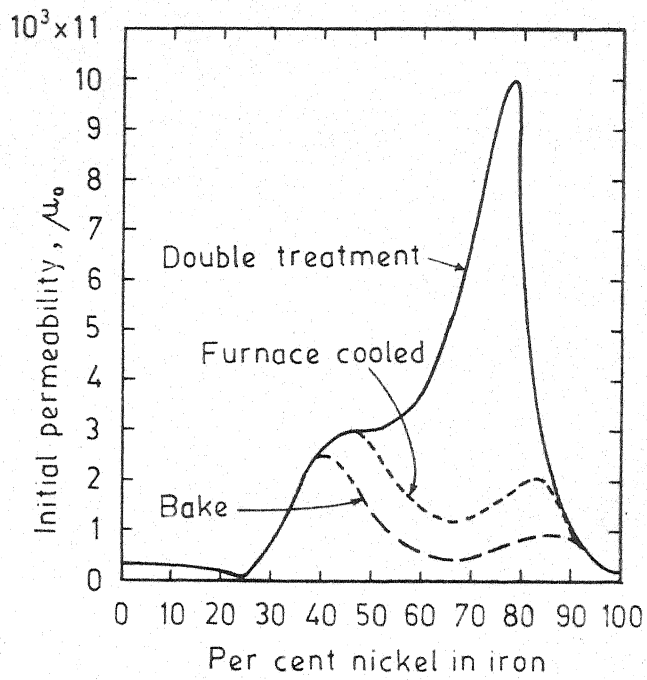


Fig. 2

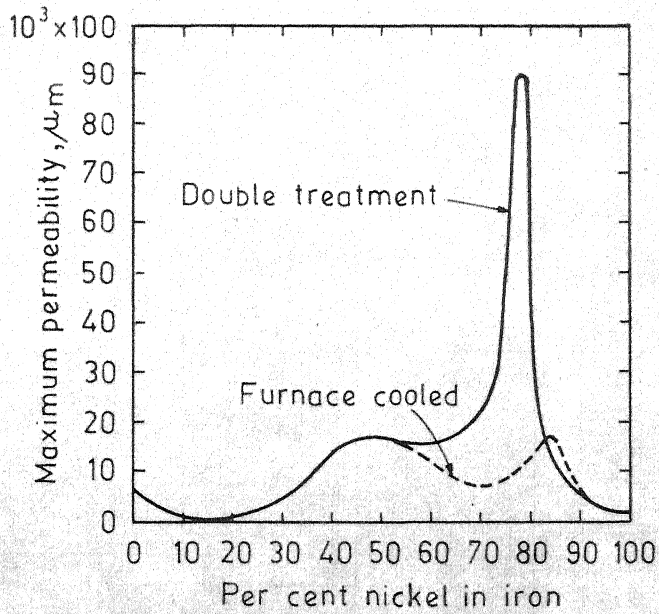


Fig. 3

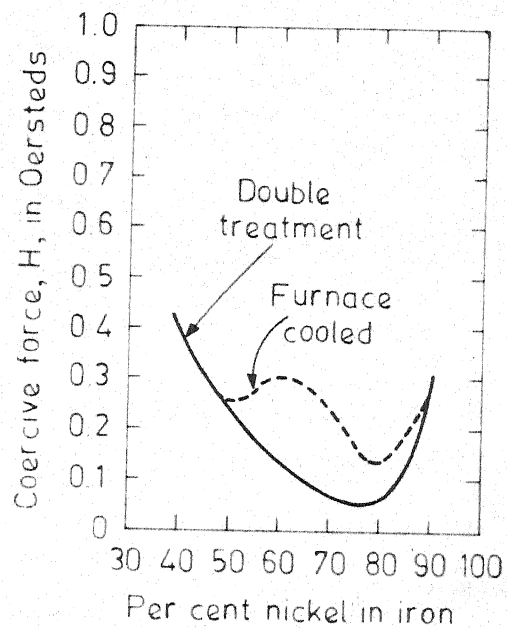


Fig. 4

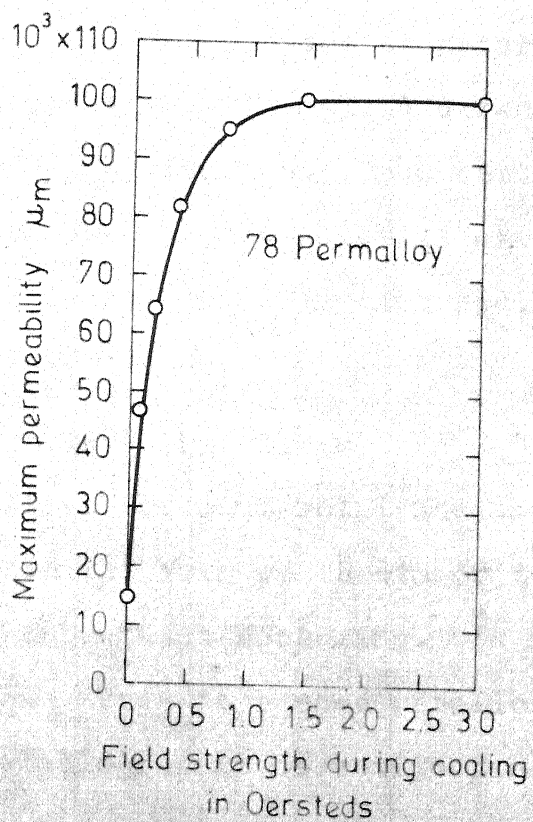


Fig 5

of the magnetic field necessary for this purpose is very small. For example, for 78 permalloy the required field strength is  $\sim 1.0$  Oe (Fig. 5).

### I.1.3 Textured Iron-Nickel Alloys

A polycrystalline material is said to possess a texture if all or major part of its crystals are oriented in such a way that one crystallographic direction of all the grains become parallel to each other. Texture is very important for magnetic materials because the magnetic properties are anisotropic in nature. For example, the magnetisation vs. field <sup>strength</sup> curve for single crystal of Ni (fcc structure) shows that (Fig. 6) of the three crystallographic directions  $\langle 111 \rangle$ ,  $\langle 110 \rangle$  and  $\langle 100 \rangle$ , the easiest direction of magnetisation is along the  $\langle 111 \rangle$  direction. All the Fe-Ni alloys of interest are with fcc structure and show the same type of behaviour as Ni, i.e.  $\langle 111 \rangle$  direction is the easiest direction of magnetisation. Thus better magnetic properties can be achieved in the alloy if all its grains can be oriented with a desired crystallographic direction parallel to each other.

#### I.1.3.1 Cube texture in Fe-Ni alloys

The Fe-Ni alloys for commercial use as transformer material is usually in the form of sheets or tapes produced by cold rolling and subsequent annealing. In cold rolling, one crystallographic plane tends to become parallel to the rolled surface and one crystallographic direction tends to become parallel <sup>to the</sup> rolling direction. For Fe-Ni alloys, like many other fcc metals (e.g., Cu), the rolling texture is given approximately as  $(110)[112]$  or more precisely as  $(123)[412]$  major

+ (145)[211] minor<sup>8</sup>. The cold rolled texture is not the desired one as the easy magnetic direction does not align itself to the rolling direction. When the cold rolled sheets are annealed various kinds of annealing textures, which are different from the rolling texture, can be produced, none of which corresponds to the desired one. When the cold rolled material is annealed under a very specific set of conditions, it is possible to produce quite perfect cube texture  $\{100\}\langle 001\rangle$ , in which  $\{100\}$  plane is parallel to the rolling plane and  $\langle 001\rangle$  direction is parallel to the rolling direction. Thus, even though the most easy direction cannot be obtained in Fe-Ni sheets, it is possible to achieve perfect alignment of the third easy direction of magnetization. Compared to a random texture or a texture with a still harder magnetic direction parallel to the rolling direction, it is advantageous to produce cube textured Fe-Ni sheets and tapes. Early studies of Muller<sup>9</sup> indicates that cube texture in Fe-Ni base alloys can be developed over wide composition range as shown in Fig. 7.

The studies of fcc metals and alloys, e.g. Cu, indicate that perfect cube texture development requires fulfilment of several conditions. These conditions may be summerised as<sup>10</sup>

- (1) requirement of very high deformation by cold working prior to annealing,
- (2) Employment of high annealing temperature,
- (3) Employment of long annealing time,
- (4) Small penultimate grain size.

As all the Fe-Ni alloys of interest have fcc structure, the same guidelines may be used for the development of cube texture in permalloys.

#### I.1.3.2 Effect of impurities on texture and magnetic properties of Fe-Ni alloys

The Fe-Ni base alloys are usually prepared from pure elements. The usual impurities are those present in the parent materials. These are C, S, Si, Mn, O<sub>2</sub> etc. Benford<sup>11</sup> has studied the effect of Si on the sharpness of cube texture produced in 50 wt% Ni-Fe alloys (Fig. 9). It appears from the figure that the rolled sheets, thickness between 0.004" to 0.006", produces sharp cube texture in alloy containing 0.028% Si (curve A) whereas still smaller thickness, 0.002" to 0.003", is required to produce similar texture sharpness in an alloy containing 0.67% Si. Thus Si addition appears to be detrimental to the cube texture formation.

Colling and Aspd<sup>en</sup><sup>12</sup> and Ames<sup>13</sup> separately studied the effect of S on the magnetic properties of 49 Ni-Fe alloys and Mo-permalloys respectively. Colling and Aspd<sup>en</sup> found that high permeability could be achieved in their alloys if S content was kept below 12 ppm. Ames likewise found that the permeability decreased with increase in S whereas coercivity increased (Fig. 10).

The only systematic study of the effect of the impurities on the annealing temperature for producing best magnetic properties has been made by Savitski<sup>14</sup>. In this study, the alloys were prepared from electrolytic Fe and Ni at the equiweight composition with intentional additions

of S (0.025% added as FeS), oxygen (0.015% added as  $\text{Fe}_2\text{O}_3$ ), Si (0.025%) and Mn (0.5% and 1%). Alloys were processed in the conventional way of permalloy production and the results were summarised as the effect of impurities on temperature range of annealing in which good magnetic properties (good loop squareness, low coercive field, high incremental permeability and high saturation density) can be produced. The results are shown in Fig. 11 which can be summarised as follows:

- (1) Mn additions are beneficial as it gives reasonably wide permissible annealing temperature range to produce good magnetic properties.
- (2) Oxygen alone drastically narrows the permissible annealing temperature region.
- (3) Si tends to lower the permissible annealing range when it is present alone or with Mn and oxygen.
- (4) S tends to narrow the permissible annealing range and drastically pushes it to higher temperature.

Thus among all the alloying elements, only Mn appears to improve all the four magnetic properties.

#### I.1.3.3 Effect of inclusion, grain diameter and size on texture and magnetic properties

Apart from dissolved impurities, inclusion, grain-size etc. have also marked effect on texture and magnetic properties. Ananthraman, Coles and Slepian<sup>15</sup> studied the effect of inclusion on the stability of cube texture. Using electron microscopic study, they concluded that cube texture in 50 Ni-Fe-alloys would be stable if the inclusions

## FIGURE CAPTIONS

- FIG. 6. (B-H) vs. H curves for Nickel single crystal measured along different crystallographic directions.
- FIG. 7. Recrystallization textures in Fe-Ni-Cu alloys.
- FIG. 8. B-H loop of 50 Ni-Fe alloy for different sheet thicknesses.
- FIG. 9. Quality of cube texture produced in 50 Ni-Fe alloy as a function of rolled grain thickness.  
(A) Fe-Ni alloy with 0.028% Si, (B) Fe-Ni alloy with 0.67% Si.
- FIG. 10. Magnetic properties of Mo-permalloy as a function of sulfur content.
- FIG. 11. Permissible annealing temperature range for 50 Ni-Fe alloys at different impurity contents.

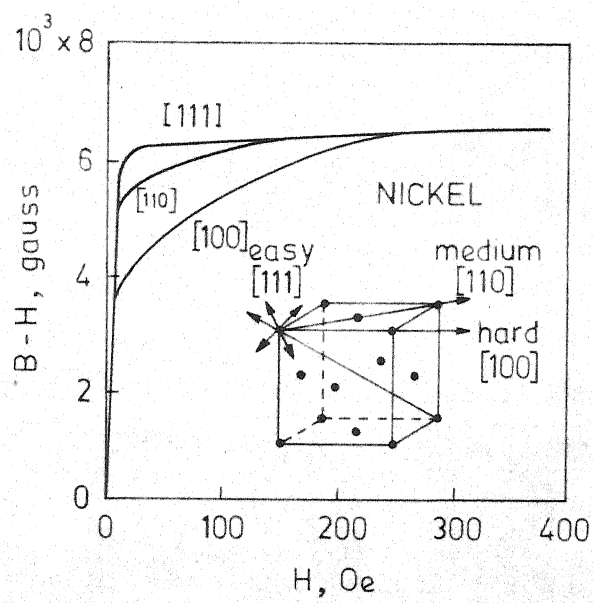


Fig. 6



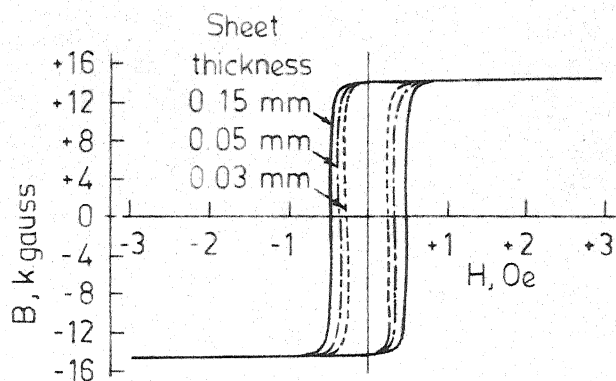


Fig. 8

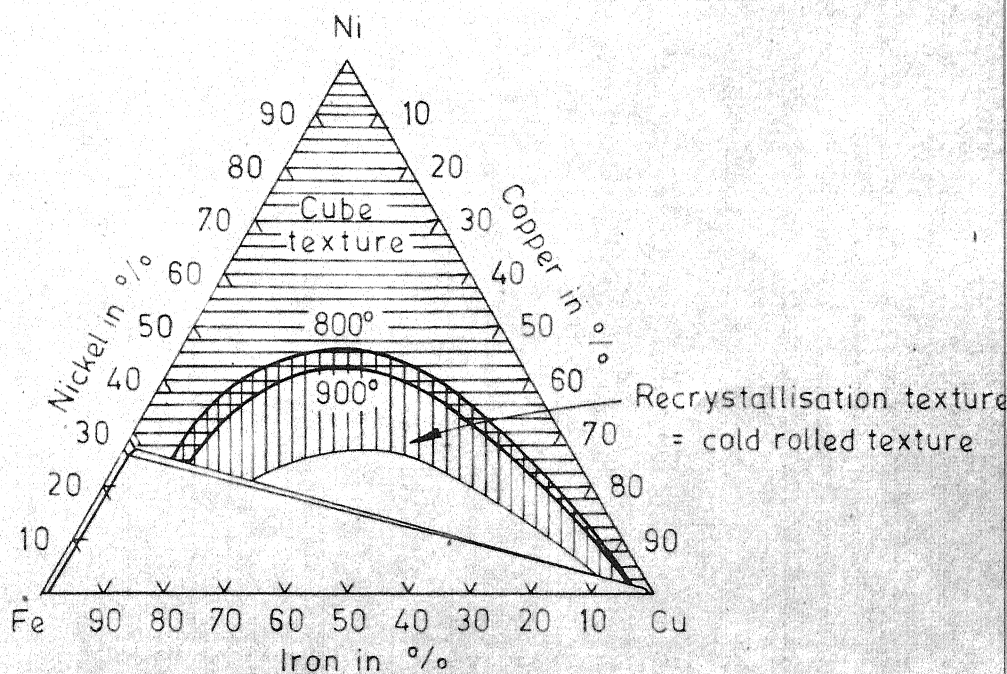


Fig. 7

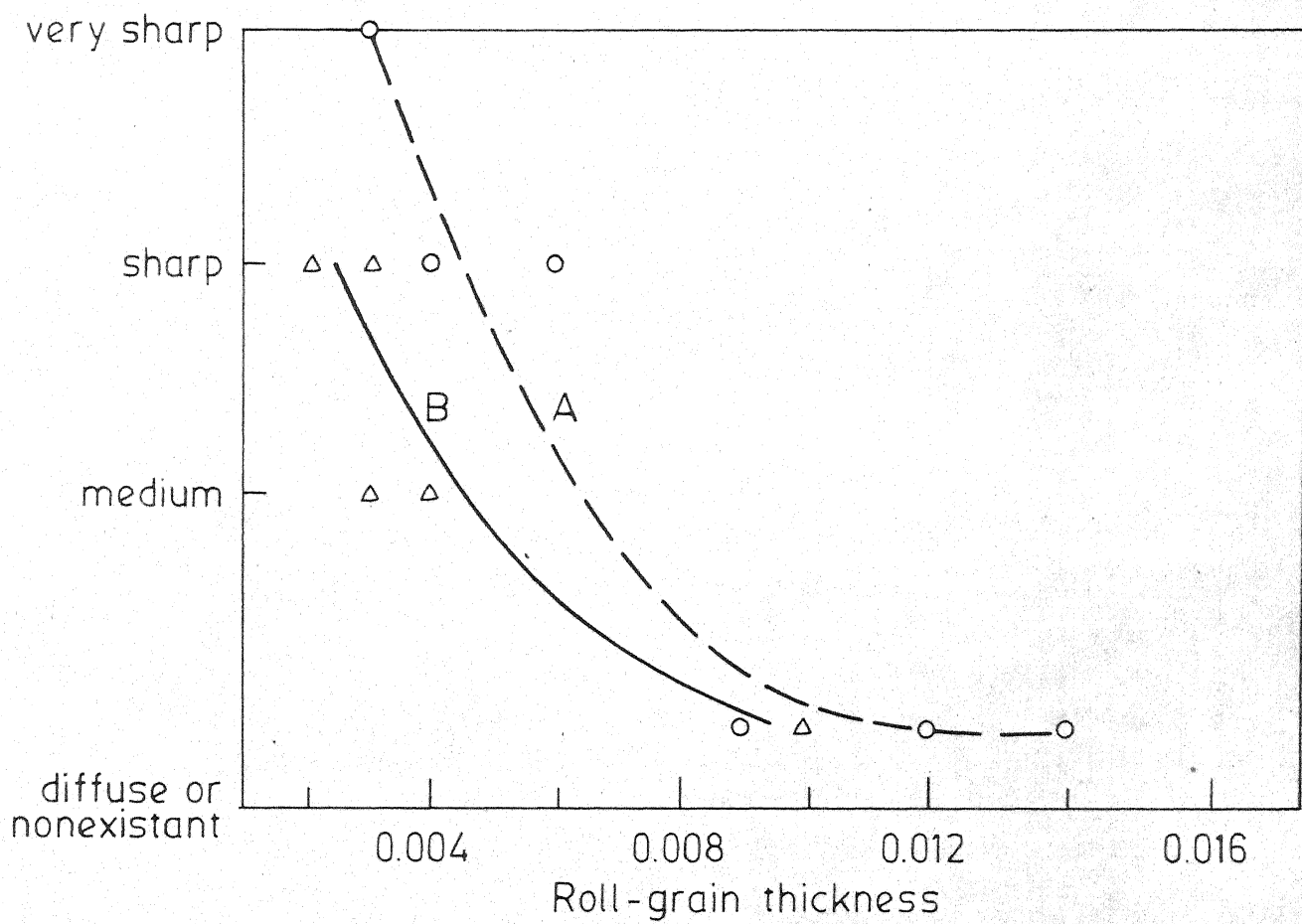


Fig. 9

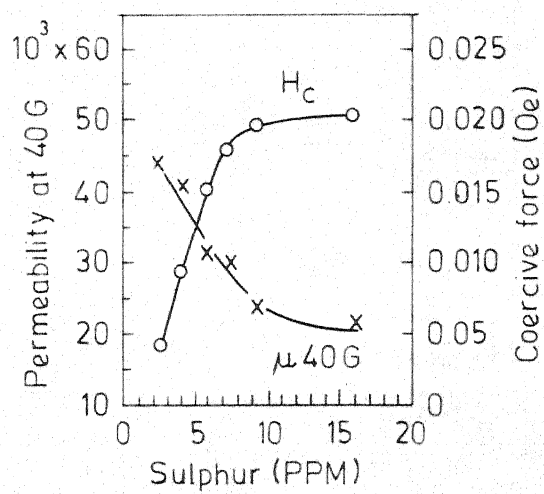
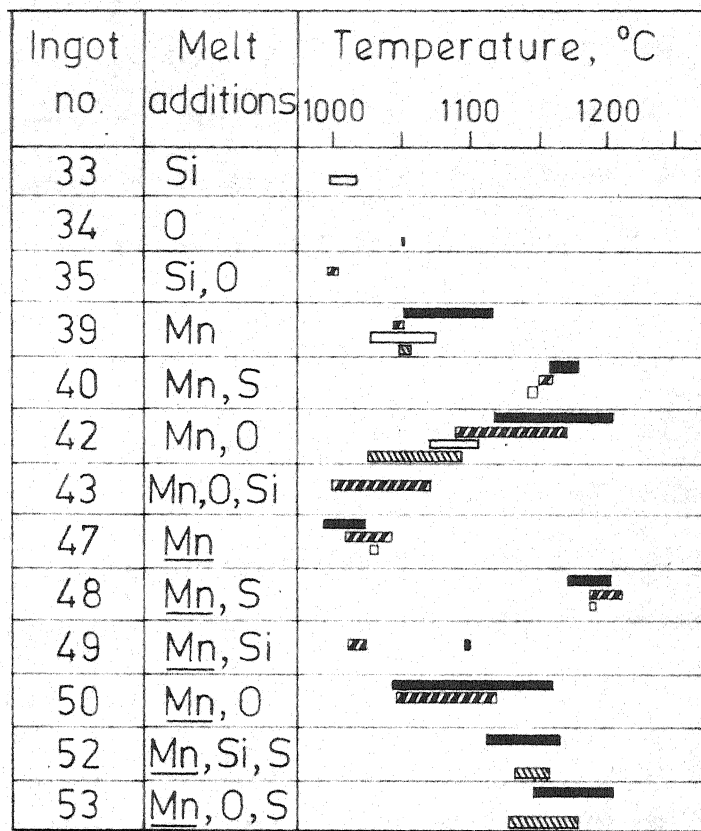


Fig. 10



### Symbols




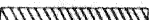
-  Hot rolled at high temperature
-  Hot rolled at low temperature
-  Hot rolled at high temp. and annealed after hot rolling
-  Hot rolled at low temp. and annealed after hot rolling
- Mn 1.0 % manganese
- Mn 0.5 % manganese
- Si 0.25 % silicon
- S 0.025 % sulfur
- O 0.015 % oxygen

Figure 11

were very finely dispersed (submicron size) in the material. If dispersion is not fine, secondary recrystallization would occur very easily after annealing at  $1050^{\circ}\text{C}$  (within 2 hours) whereas in the finely dispersed alloys, it occurs with difficulty after annealing above  $1250^{\circ}\text{C}$  for several hours.

Benford<sup>11</sup> has studied the effect of penultimate grain size on cube texture of 50% Ni-Fe alloys. According to him the sharpness of cube texture of this alloy is dependent on penultimate grain size (P G S) or rolled grain thickness (RGT) which is a function of PGS and percent reduction. RGT was calculated by assuming the grains of a slab to get reduced in thickness in proportion to the slab reduction, an assumption used also by Cook and Richards<sup>16</sup>. It was found that RGT of 0.004" to 0.006" produced sharp cube texture (Fig. 8). Dahl and Pawlek<sup>17</sup> have also found similar behaviour in their 50% Ni-Fe alloys. A decrease in hysteresis loop occurs due to RGT effect is also evident from the results reported by Wasserman and Wenner<sup>18</sup> (Fig. 8).

Littman, Harris and Ward<sup>19</sup> studied the effect of grain size on texture of 48% Ni-Fe alloys and observed that the grain structure should be homogenous and should consist of either very small  $\{100\} \langle 001 \rangle$  primary grains or large  $\{120\} \langle 001 \rangle$  secondary grains free from annealing twins. Mixture of large and small grains appears to cause greater magnetic loss because of the difference in the hysteresis characteristics between the large and small grains.

Alder and Pfeiffer<sup>20</sup> studied the effect of grain size and inclusion on coercive field of 47.5%<sub>v</sub> Ni-Fe alloys and determined two empirical relations as given below:

$$H_c = \frac{15}{16} \pi \frac{\gamma_w}{\mu_o M_s} \frac{1}{d_k} \quad \dots (1)$$

where  $\gamma_w$  is wall energy,  $M_s$  is saturation magnetisation,  $\mu_o$  is initial permeability,  $H_c$  is coercive field and  $d_k$  is average grain diameter.

and,  $H_c \simeq H_{c0} + H_{ci}$

$$\simeq 8\left(\frac{\text{mA}}{\text{cm}}\right) + 28\left(\frac{\text{mA}}{\text{cm}}\right) N_F \times 10^{-6} \text{ cm}^2 \quad \dots (2)$$

where  $H_{c0}$  = Coercive field for pure alloy,  $H_{ci}$  = coercive field for inclusions,  $N_F$  = No of particles/cm<sup>2</sup> and  $d_i$  is average diameter of inclusions in the range of 0.02 to 0.5  $\mu\text{m}$ .

## I.2 Fabrication of cube textured permalloys with appropriate magnetic property

To produce cube texture, the alloys are prepared and processed through several stages. These are

- (1) Melting and hot working,
- (2) Cold rolling,
- (3) Annealing to produce the desired texture,
- (4) Magnetic annealing or cooling in magnetic field.

For development of texture usually the latter three stages are more important than the first one. The details of each processing step are given in this section.

### I.2.1 Melting and hot working

From the previous discussion it has been seen that to develop appropriate texture in the alloys the impurity content should be as low as possible. Now a days, most of the melting is done in controlled atmosphere induction furnace. The atmosphere usually used is argon but sometimes hydrogen also is used. Deoxidizers are added to the melt to lower down its oxygen content. Colling and Aspden<sup>21</sup>, however, have found that highest initial permeability is obtained if no strong deoxidizer is used. The adverse effect of strong deoxidizers such as Si and Al are attributed to the increased susceptibility of the alloy to internal oxidation in a dry hydrogen annealing furnace. The effect of deoxidizers on initial permeability, as found by Colling and Aspden, is given in Table II.

The alloys after melting are usually cast in steel moulds. The cast alloy is then hot rolled or hot forged. This is done only to reduce the thickness of the alloy and has no effect in producing the final texture. Sometimes the hot-worked alloy is annealed before further processing. Some investigators<sup>22</sup> have reported that it is detrimental to the final magnetic property whereas some others<sup>23</sup> have indicated that there is no effect of intermediate annealing in producing cube texture.

### I.2.2 Cold rolling

Cold rolling is a very important step for developing cube texture. The desired cold rolled texture to produce cube texture is copper type texture (Figs. 12 and 13). The



amount of cold rolling is very critical. According to some investigators<sup>24</sup>, the cold reduction should be at least 85% or more whereas some others<sup>25,26</sup> indicate that cold reduction should be at least 90%. Excess cold reduction, on the other hand, has been found detrimental to cube texture formation<sup>23,27</sup>. Generally the amount of cold reduction varies from 90-98% depending upon the material.

Besides the amount of cold reduction, cold reduced sheet thickness appears to have considerable effect on the achievement of cube texture. It has been found<sup>(23)</sup> that for 50% Ni-Fe alloy cube texture cannot be produced when the sheet thickness is 0.001" whereas sheet thickness greater than 0.001" gives good cube texture. For sheet thickness greater than 0.001", cube texture can also be produced by annealing even after etching off of the surface layers. This probably suggests that the nucleation of cube texture occurs deep within the material where material is less disturbed than the surfaces of cold rolled material. When the sheet is too thin ( $< 0.001"$ ) the central less disturbed layer practically vanishes thereby producing unfavourable condition for nucleation of cube oriented grains whereas for thicker materials removal of surface layers (disturbed layer) by etching leaves behind the less disturbed inner layers which are favourable for nucleation of cube oriented grains.

In cold rolling of metals and alloys, the following interesting observations have been made<sup>28</sup>:

- (1) The nature and degree of preferred orientation are independent of roll diameter (at least from



1½" to 24"), reduction per pass (tested from 10% to 30%) and rolling speed.

- (2) For unidirectional rolling 180° rotation of the specimen (end over end rolling) does not have any effect on texture.
- (3) The application of tension to the strip as it passes through the rolls does not have any effect on the orientation but smaller diameter rolls gives greater range of scattering about the transverse direction<sup>29,30,31</sup>.

### I.2.3 Annealing of Fe-Ni alloys

Cube texture is an annealing texture. It is produced by annealing the cold rolled sheets at appropriate temperature for appropriate time. Temperature and time of annealing for producing cube texture varies from material to material. According to Bumm and Miller<sup>32</sup> time and temperature should be such that both recrystallization and grain growth can occur. But at the same time secondary recrystallization should be prevented<sup>33</sup> because the secondary grains produced from primary cube texture are of different orientations (e.g. (120)[201] or (102)[20 $\bar{1}$ ] or (112)[hkl] where [hkl] is a high indices direction). Secondary recrystallization also takes place if the cold deformation is non-uniform or if the rate of heating during annealing is too high. Usually for Fe-Ni alloys the temperature and time of annealing varies from 1050°C-1250°C and 4 hours to 16 hours respectively<sup>23,25,26</sup>.

### I.2.3.1 Effect of rate of cooling and atmosphere of annealing on magnetic properties

Rate of cooling after annealing appears to be very important for developing initial permeability of Fe-Ni alloys. D.J. Snee<sup>34</sup> studied the effect of cooling rate on initial permeability of  $\mu$  metal of different compositions. The alloys were annealed in dry hydrogen and then cooled at rates 10°C/hr to 1100°C/hr. His observations are shown in Fig. 14 which indicates that  $\mu_0$  goes through maximum at certain cooling rates varying from alloy to alloy. An empirical equation was derived relating permeability with alloy composition and cooling rate (100°C/hr to 550°C/hr) using regression analysis and is given by

$$\begin{aligned}\mu_0 = & [43.090 + 0.0065 R X - 2.4403 X^2 + 17.438 Y \\ & - 0.01914 R Y + 14.886 X Y + 0.00001 R^2 X Y \\ & - 24.9499 Y^2 - 0.0001777 R^2 Y^2 + 13.0252 X Y^2 \\ & + 11.4260 X^2 Y] \cdot 10^3 \quad \dots (3)\end{aligned}$$

where R = cooling rate, X = %Ni and Y = %Cr

The calculated values from above equation show good agreement with experimental results.

Generally hydrogen or argon gas is used as the annealing atmosphere. From the available literature it is not very clear wheather or not atmosphere of annealing has any effect on magnetic property. According to Kehr<sup>35</sup> and Coffi<sup>36</sup> highest permeability can be obtained by annealing in hydrogen atmosphere because hydrogen is a strong reducing agent and is reportedly capable of removing impurities like oxygen, carbon, nitrogen and sulfar from the material being

annealed. Stefan and Arato<sup>37</sup> have annealed 50% Ni-Fe alloys in two conditions, one in pure dry hydrogen and the other in vacuum in the order of  $10^{-3}$  torr. They, however, concluded that these two conditions did not produce appreciable change in texture or in magnetic properties of Fe-Ni alloys.

#### I.2.4 Magnetic annealing

Magnetic annealing means annealing of a material under a magnetic field at some suitable elevated temperature which is below the curie temperature of the alloy. It was first tried by Kelsall<sup>38</sup> for 78.5% Ni-Fe alloy. In Fe-Ni alloys [100] orientation shows good response to magnetic annealing where as [111] does not<sup>26</sup>. Thus, the permeability and squareness of the B-H loop for the cube textured alloy is expected to increase through magnetic annealing.

Martin et. al.<sup>26</sup> studied the effect of magnetic annealing on 53 to 58% Ni-Fe alloys, as shown in Figs 15 to 17. From Figs. 15 and 16 it is found that permeability increases and magnetostriction decreases with magnetic annealing. This is due to short range directional ordering of Fe-Ni atom pairs. Since magnetic coupling energy of a pair of atoms generally depends on the kind of atoms, in this case Fe-Fe, Fe-Ni, Ni-Ni, magnetic annealing of Fe-Ni alloys below their curie temperature, but above their critical temperature of LRO, tends to align the atom pairs with minimum coupling energy in the field direction. Fast cooling of alloys after the above magnetic annealing freezes this short range directional order structure. This gives rise

21

to uniaxial anisotropy with easy axis of magnetisation along the field direction and subsequent measurement in this direction produces square hysteresis loop. If an applied field is absent, the anisotropy becomes aligned randomly by local magnetisation of the domains resulting in constricted B-H loop<sup>39</sup>. In Fig. 15, with increasing annealing temperature the initial permeability curve shows a peak at 470°C and a decreased loop squareness. These results can be explained in terms of relationship between crystal anisotropy constant  $K_1$  and uniaxial anisotropy const  $K_u$ . Pfeifer<sup>40</sup> concluded that high initial permeability was achieved when  $K_1 \approx K_u$  and a rectangular loop is produced when  $K_u > K_1$ . For Fe-Ni alloys uniaxial anisotropy decreases as the annealing temperature approaches the curie point<sup>41</sup> (Fig. 18). The crystal anisotropy increases with magnetic annealing temperature<sup>40</sup> and the highest initial permeability in 58% Ni-Fe alloy is observed at 470°C where  $K_1$  and  $K_u$  are similar. At lower temperature where  $K_u$  is greater than  $K_1$  a rectangular hysteresis loop is observed.

The field required for magnetic annealing is very low (e.g., ~100 Oe) and time of annealing varies from 2 to 6 hrs<sup>40</sup>. The rate of cooling after magnetic annealing should be very high (at least 30°C/sec)<sup>41</sup>. A puzzling and still unexplained aspect of magnetic annealing in permalloys is the observation that field heat treatment is not effective if too little oxygen is present in the specimen<sup>42</sup>. Similar results also have been found in 2% Mo permalloys<sup>43</sup>.

### I.3 Statement of the Problem

The literature review presented in the previous sections shows that improvement in the magnetic properties of permalloys can be achieved through the development of a suitable texture (cube texture) and through suitable magnetic annealing or cooling. Development of texture and suitable magnetic properties in permalloy requires an experimental set up which involves facilities for hot and cold rolling, controlled atmosphere annealing, magnetic annealing, magnetic and x-ray characterization. While several basic facilities like rolling mill, texture goniometer etc. were available, no suitable facility for controlled atmosphere annealing, magnetic testing etc. was available and had to be developed. Hence a part of the present work involved fabrication and setting up of suitable facilities for carrying out work on textured magnetic materials.

In the present investigation, cube texture development in 48 permalloy has been taken up due to its great commercial importance. The available literature gives only general procedures for the development of cube texture but it possibly does not give the exact process to be employed in order to develop perfect cube texture in Ni-Fe alloys. This is borne out by the fact that different authors claim the importance of different process parameters for obtaining the best results. The different process variables available from the literature can be summarised as percent cold reduction, annealing temperature and annealing time. Effect of alloying elements, like Si, on the development of cube

texture have been studied. Whether any other process parameter is important for producing maximum amount of cube oriented grains is not clearly indicated in any published literature. Hence, the effect of the indentified process parameters (as identified above) on the development of cube texture in 48 permalloy has been attempted. The available literature indicate that high amount of deformation (85 to 98 pct. reduction in thickness), high annealing temperature ( $900^{\circ}\text{C}$  to  $1200^{\circ}\text{C}$ ) and long annealing time (2 hrs to 16 hrs) are required to produce perfect cube texture. Eventhough the composition of the perm-alloys remain practically the same, the wide variation in the choice of process parameters in one investigation and another indicate that the choice of a set of parameters is possibly typical of a given alloy prepared under a given condition. This may also indicate that the minor elements (impurities or intentionally added ones) are possibly quite important. Hence, besides the three process parameters, composition of alloy in terms of minor alloying elements is also considered in this investigation as a possible process variable.

The alloys are proposed to be melted under argon atmosphere, hot forged or hot rolled, cold rolled and finally annealed under protective atmosphere of argon or hydrogen gas. The texture produced is proposed to be studied through the use of x-ray diffraction technique employing a transmission texture goniometer or a Laue camera. Magnetic tests are proposed to be done using a magnetometer and an Epstein test frame. The major emphasis of this work is in finding the proper choice of process parameters to develop perfect cube texture.

## FIGURE CAPTIONS

- FIG. 12. (111) pole figure for cold rolled copper.
- FIG. 13. (200) pole figure for cold rolled copper.
- FIG. 14. Effect of cooling rate and composition of alloys (near 76%<sub>p</sub> Ni, 2.6%<sub>p</sub> Cr) or initial permeability.
- FIG. 15. Permeability vs. flux density curves for 58 Ni-Fe alloys: (A) After primary heat treatment at 1200°C, (B) After subsequent magnetic annealing at 470°C and (C) a conventional 50 Ni-Fe alloy.
- FIG. 16. Magnetostriction vs. flux density curves for 53 Ni-Fe alloys: (A) after magnetic annealing at 450°C and (B) before magnetic annealing (after primary annealing at 1200°C).
- FIG. 17. Initial Permeability ( $\mu_0$ ) and squareness ( $B_r/B_m$ ) vs. temperature of magnetic annealing for 58 Ni-Fe alloys.
- FIG. 18. The dependence of induced uniaxial anisotropy<sup>(E)</sup> on the annealing temperature for Fe-Ni alloys.

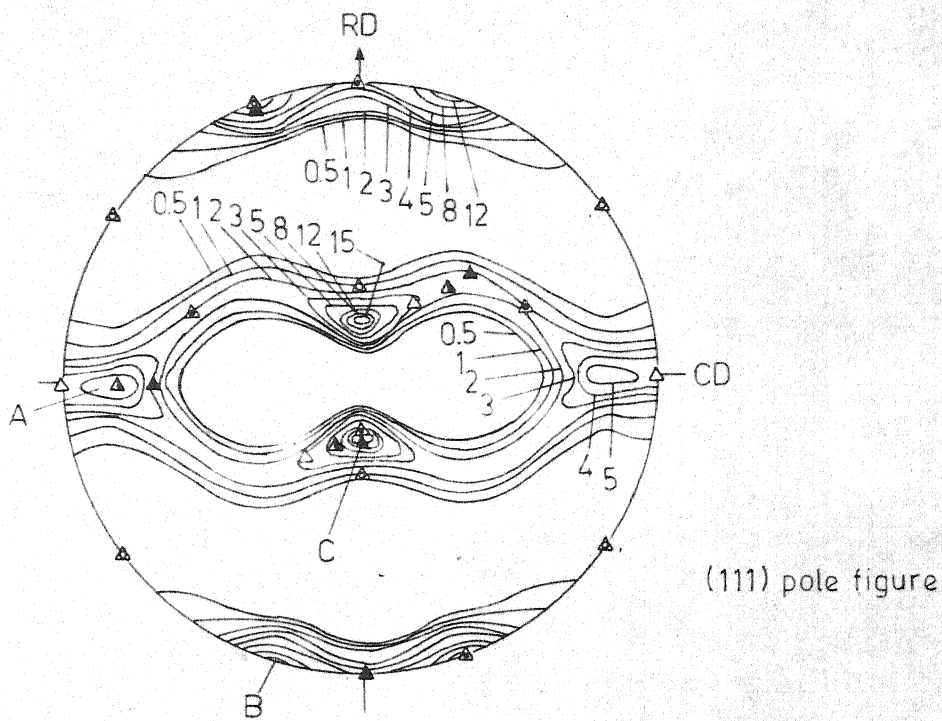


Fig. 12

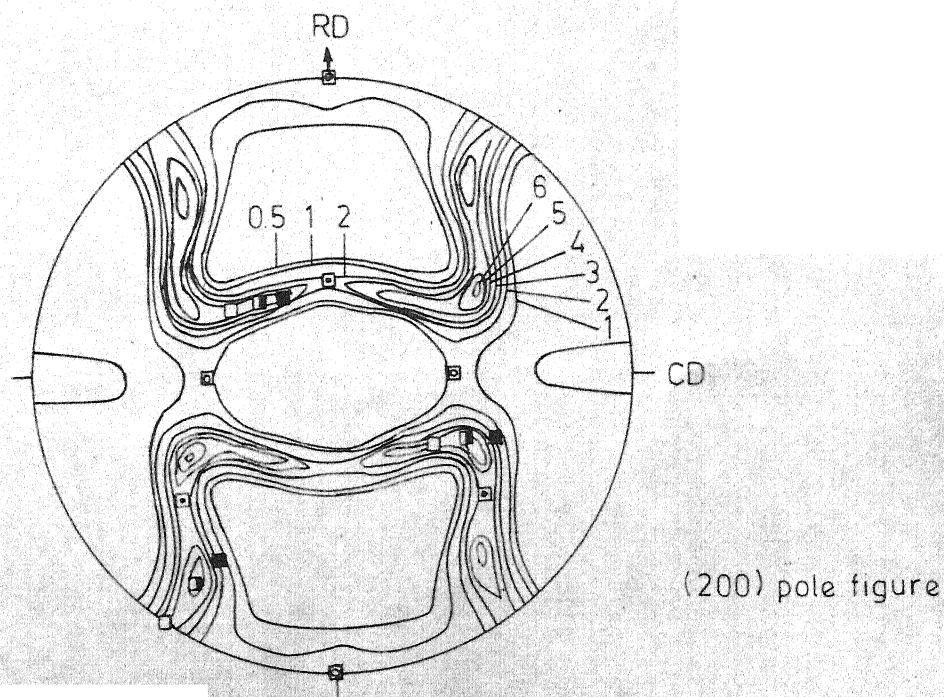


Fig. 13



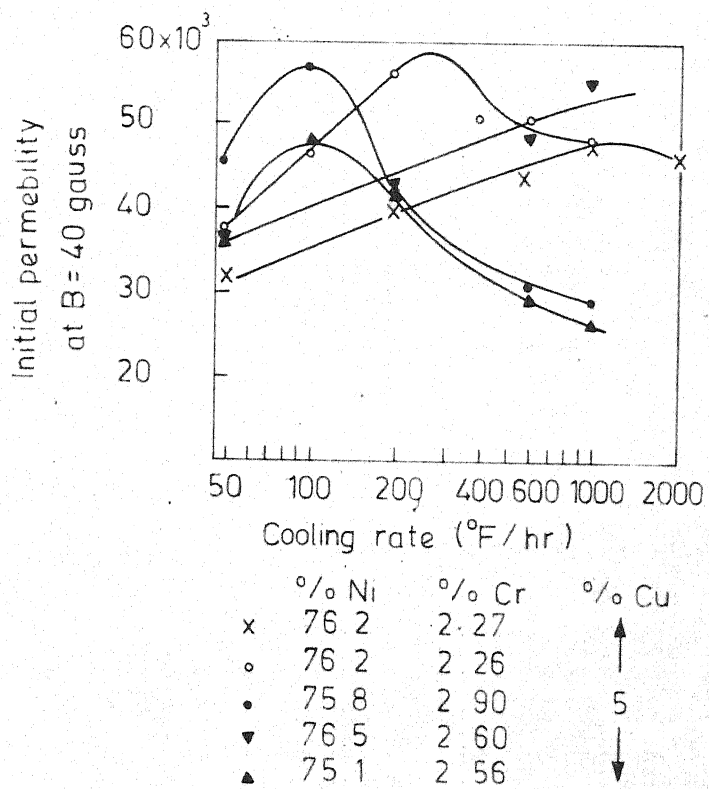


Fig. 14

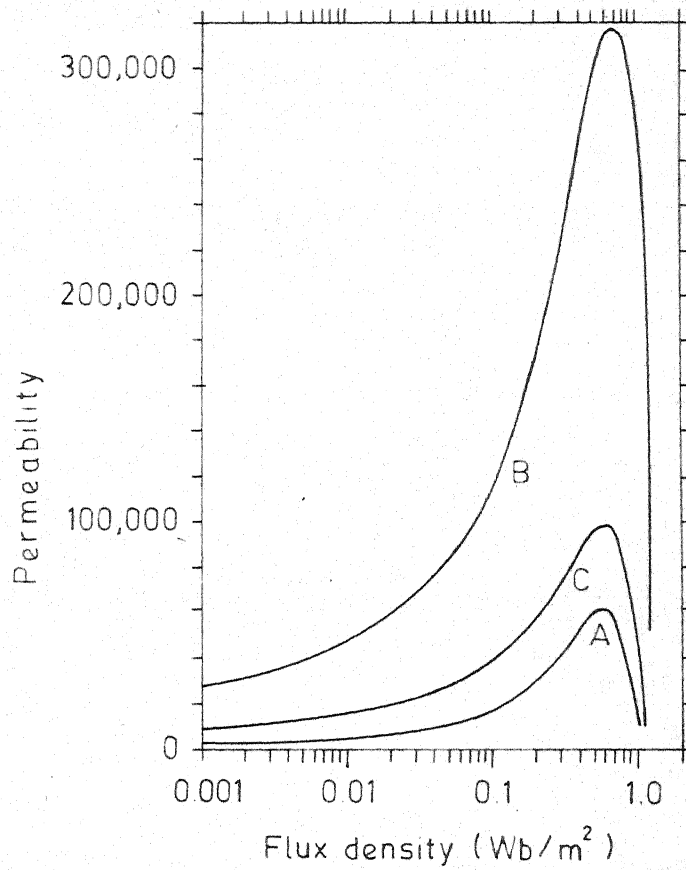


Fig. 15

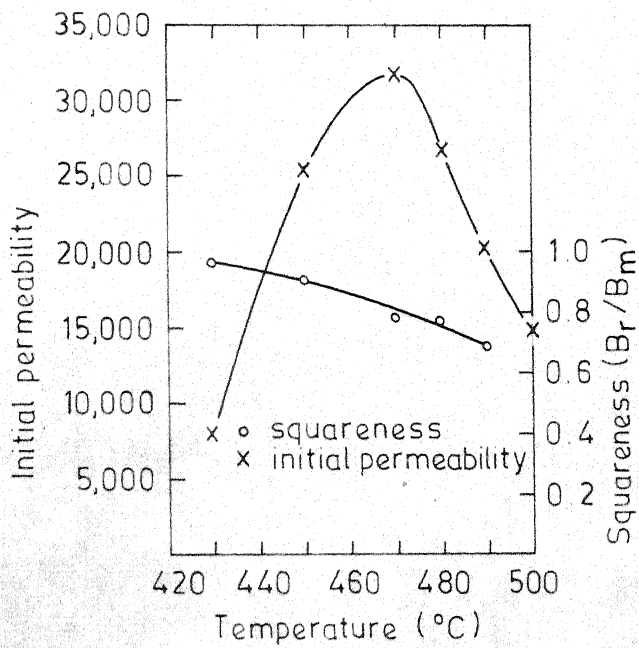


Fig. 17

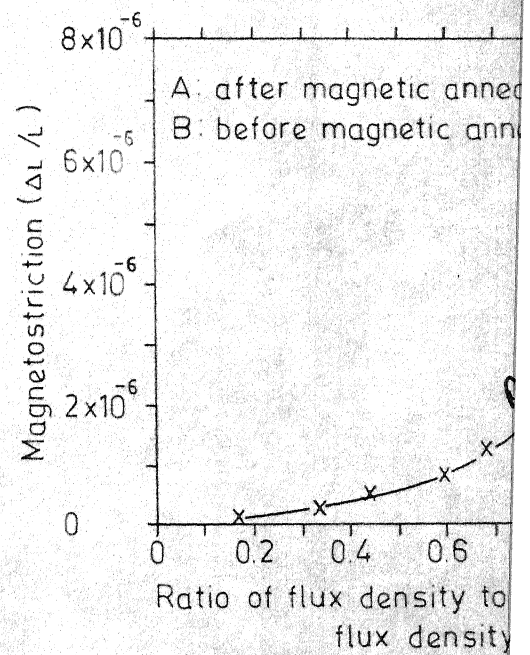


Fig. 16

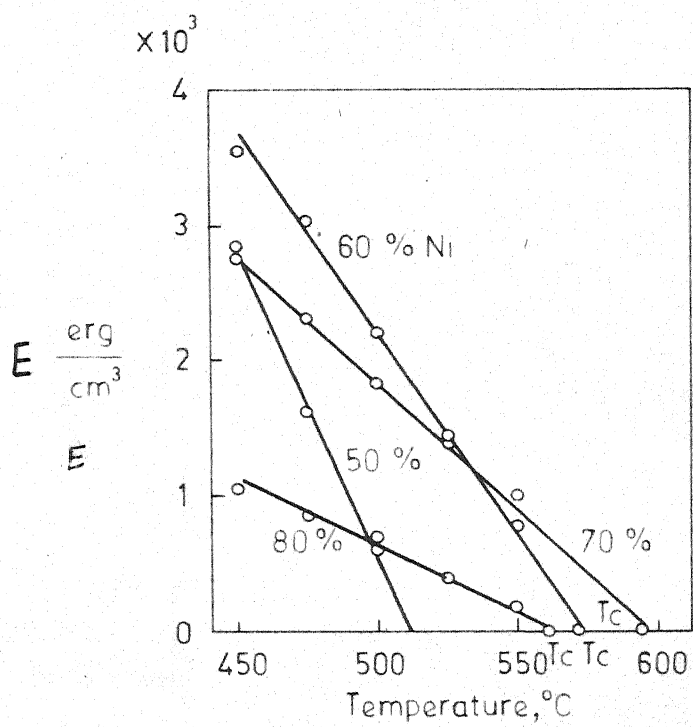


Figure 18

Materials and composition	Heat Treatment Temp °C	Condition	Permeability		H <sub>c</sub> in Oe	B <sub>s</sub> in Gauss	T <sub>c</sub> in °C	Hyst loss at W <sub>h</sub> erg/cm <sup>3</sup>		Uses
			Initial	Maximum						
1. 45 permalloy	950°C		-	-	-	-	-	700	10000	telephone transformers
	1050°C	H <sub>2</sub>	2500	25000	0.3	16000	440	1200	16000	coils and sensitive relays.
	1200°C	annealed	3500	50000	0.07	16000		100	1000	
2. 68 permalloy (68Ni 32Fe)	1000°C	Field cooled	1200	250000	0.03	13000	600	120	13000	
3. 4-79 perm-alloy (79Ni, 17Fe, 4Mo)	1100°C	H <sub>2</sub>	20000	100000	0.05	8700	420	40	5000	transformers
	1350°C	annealed	-	-	-	-	-	8	5000	transmitting weak signals at very high frequencies
4. μ-Metal (75Ni, 18Fe, 2Cr, 5Cu)	1175°C	H <sub>2</sub> annealed	20000	100000	0.05	6500	430	-	-	cores of current transformers and inductance of radio apparatus
	1050°C	-	-	-	-	-	-	50	5000	transformers transmitting weak signals at very high frequency.
5. Supermalloy (79Ni, 16Fe, 5 Mo)	1300°C	H <sub>2</sub> annealed	100000	1000000	0.002	2000	400	4	5000	
6. 1040 alloy (3Mo, 14Cu, 72 Ni, 11Fe)	1100°C	H <sub>2</sub> annealed	40000	100000	0.02	6000	240	200	6000	

H<sub>c</sub> - Coercive force, B<sub>s</sub> - Saturation Induction, T<sub>c</sub> - curie temperature

W<sub>h</sub> - Hysterisis loss, B<sub>m</sub> - Flux density at which loss was measured

TABLE II

Effect of Deoxidizer on Initial Permeability  
of 49 permalloy

Deoxidizer Conc. (wt %)	Initial permeability
1 % Mn	13450
0.52 % Mn	13450
0.48 % Si	12300
0.98 % Si	9050
0.29 % Al	7500
0.31 % Al	7300

## CHAPTER II

### FABRICATION OF EQUIPMENT

## CHAPTER II

### FABRICATION OF EQUIPMENT

To carry out investigation on textured magnetic alloys, like Fe-Ni alloys, the following facilities are required:

- i) Melting in induction furnace under controlled atmosphere,
- ii) Furnace for hot working of alloys,
- iii) Hot and cold rolling, facility,
- iv) Controlled atmosphere annealing furnace with provision for magnetic cooling,
- v) Magnetic annealing furnace,
- vi) Magnetic measurement facility,
- vii) X-ray diffractometer with texture goniometer,
- viii) Facility for using Laue technique with sheet metal specimen.

Several of these required facilities, e.g., controlled atmosphere induction melting furnace, hot and cold roller and x-ray diffractometer with texture goniometer were available. The other facilities had to be developed. A brief account of the design and constructional details of fabricated equipment are presented in the following sections.

#### II.1 Furnace for Hot Rolling

##### II.1.1 Design consideration

Since no tilt pour arrangement is possible with available controlled atmosphere induction furnace, alloys melted, are allowed to solidify in the crucible. The ingots

are of cylindrical shape, diameter varying between 0.8" to 1.25". These ingots required hot working (rolling or forging) to break down the cast structure and to reduce the ingots into rectangular parallelepiped shape for proper cold rolling. For Fe-Ni alloys hot working temperature is generally in the range of  $1000^{\circ}\text{C}$ - $1200^{\circ}\text{C}$ . For this purpose, a high temperature furnace capable of going upto  $1200^{\circ}\text{C}$  is needed. Since the melt size is small, a Kanthal A wire wound tubular furnace is considered suitable for this work. This furnace is easy to construct and can be used continuously at  $1150^{\circ}\text{C}$  and for a short time at  $1200^{\circ}\text{C}$ . Accurate control of temperature for hot working is not required because the working temperature is not a fixed one but is a range of temperature varying between  $1000^{\circ}\text{C}$  to  $1200^{\circ}\text{C}$ . Because of this reason the furnace need not have a very wide uniform temperature zone. A variation of  $\pm 10^{\circ}\text{C}$  within 4" to 6" around the centre of the furnace can be tolerated.

#### II.1.2 Constructional Details

A 2.5" ID and 18" long Mullite tube was wound with 18 gauge Kanthal A wire and was used in a 15" aluminum shell to make the furnace. The furnace winding used was 6 turns/inch over the central 15" length followed by 8 turns/inch for the 1.25" at the two ends. An one fourth inch layer of alumina cement paste was applied on the tube to keep the wire in position so as to prevent short circuit and exposure of hot wire to the atmosphere. The gap between the shell and the tube was packed by an insulating material



(Magnesia-asbestos powder). The furnace was mounted on a structure fitted with wheels so that it could be taken to any place as desired. For placing the ingots inside the furnace and for their easy withdrawal after attaining the temperature, a 12" long specimen holder of mild steel plate was made. Inside the furnace tube, two pieces of refractory bricks shaped in semi-cylindrical form, was placed in the cylindrical furnace tube to provide a flat hearth along the length of the furnace. Plugs of refractory insulating bricks covered both ends of the furnace. Through the back refractory plug a thermocouple was inserted into the hot zone for monitoring the furnace temperature. At the operating end of the furnace a permanent platform of cement asbestos plate was provided for easy insertion and withdrawal of the specimens. The platform was so placed that its top surface was level with the hearth and it also prevented the hearth brick to slip out during specimen withdrawal.

As the furnace did not need very accurate control of temperature, a temperature controller was not attached to it. At maximum temperature the current flowing through the furnace was 5 amp. Hence a standard 15 amp. out let was sufficient for the power connection to the furnace. A continuously variable voltage transformer was used for proper selection and maintainance of temperature.

### II.1.3 Testing of the Furnace

The furnace temperature selection was through selection of a suitable applied voltage across the furnace

terminals. Near  $1100^{\circ}\text{C}$  a hot zone of about 4" length with a temperature variation of  $\pm 10^{\circ}\text{C}$  was obtained in the furnace. For ease of temperature selection, a voltage temperature curve was required. To obtain this, the furnace was kept at a fixed voltage overnight to attain a steady temperature corresponding to the set voltage and the temperature of the hot zone was measured with a platinum vs. platinum 10% rhodium thermocouple. The voltage temperature curve obtained is shown in Fig. 19. The temperature attained at a given voltage is also a function of ambient temperature. Since the data was obtained over a period of few months (during actual use of the furnace for hot working operation) the ambient conditions may have varied to some extent and is possibly the reason for the observed scatter of data points. However, the characteristics can be represented reasonably well with a straight line, as is expected, and is sufficient for the present purpose because there is no real need for accuracy of setting the temperature of the furnace.

## II.2 Controlled Atmosphere Annealing Furnace

### II.2.1 Design consideration

This furnace is meant for annealing the cold rolled specimen in vacuum or in an atmosphere of argon and hydrogen gases. An impervious furnace tube with provision for evacuation and gas inlet/outlet is thus needed. Since vacuum or gas seals are usually made by flanges attached to the furnace tube through sealing wax, adequate cooling arrangement of flanges is necessary. Some of the Fe-Ni

alloys are known to improve their magnetic properties if they are cooled in a small magnetic field. This can be done in the same furnace after the principal annealing treatment is over or the specimen may be cooled to room temperature and then magnetic cooling can be done by reheating the specimen in a different furnace. In this design, annealing in the same furnace was preferred. This needed a provision for specimen withdrawal from the hot zone to a cooler part of the furnace where a magnetic field is present. Two types of specimens are required to be annealed in the furnace - (1) Sheet specimen of size approximately 3" x 1" for texture study and (2) strip specimen of  $\frac{1}{2}$ " x 4" size, approximately 35 to 40 pieces at a time, for magnetic loss measurement. Since annealing temperature could be somewhat critical in developing perfect texture, the furnace with a long hot zone with a reasonably uniform temperature in the hot zone is desired. The furnace was designed keeping the above features in mind.

## II.2.2 Constructional details

The annealing furnace is essentially similar in construction to the furnace for hot working except that it has two tubes, the outer having the furnace winding and the inner one serves the purpose of controlled atmosphere annealing chamber (Fig. 20). The second tube is a 30" long impervious mullite tube of  $2\frac{1}{4}$ " O.D. and 2" I.D. To the two open ends of this tube, two watercooled brass flanges were sealed with Apiezon black wax. The two flanges had

two brass caps with O-ring seals to produce a gas tight annealing chamber. One brass cap had been fitted with facilities for introduction of any desired gas and for evacuation of the annealing chamber. The other brass cap was fitted with a specially designed valve outlet which could be connected to a vacuum gauge or a gas bubbler. To introduce specimen into and to withdraw it from the hot zone without breaking vacuum or gas seal, an O-ring sliding joint was fitted at the centre of the front brass cap through which a one eighth inch diameter stainless steel rod could be pushed in or out. The specimen tray was attached to one end of this stainless steel rod. To reduce the heat loss from the hot zone and to prevent the end caps to get unduly heated, two radiation shields were provided on the end caps.

The inside tube of the furnace assembly was put somewhat unsymmetrically in the outer tube so that it was sticking out on one side more than the other. To this side, a 5" long aluminum former having a single layer of copper wire wound on it was put to serve as a solenoid generating a small axial field. The coil was designed to produce a magnetic field of about 100 Oe. . . . . If the specimen required magnetic cooling, the specimen could be pulled out of the hot zone and put into the magnetic coil without breaking gas seal and thereby produce a cooling in a magnetic field.

The wax seal used, melts at a temperature of  $70^{\circ}\text{C}$ . Hence a continuous water flow is essential. Since the water supply was found inadequate, an overhead tank with a capacity

to hold about 1000 litres of water was constructed. This ensured stoppage of frequent furnace breakdown and ensured a continuous operation, especially when long annealing was desired.

### II.2.3 Power Supply

The furnace required accurate temperature control. The furnace power was provided through a variable voltage auto transformer through a suitable relay. An APLAB indicating on/off type temperature controller (range  $0^{\circ}\text{C}$  to  $1200^{\circ}\text{C}$ ) was used to operate the relay at the set temperature. The power supply and control arrangement was mounted on the same slotted angle frame which supported the furnace. A thermocouple (Pt vs. Pt + 10% Rh couple) was used as a temperature sensor to the temperature controller and was placed between the two furnace tubes for sensitive temperature control. To generate magnetic field in the coil, a small D.C. power supply unit was constructed to give a variable magnetic field through control of input current to the magnetic coil.

### II.2.4 Testing of Furnace

The furnace was slowly heated by increasing the input power supply voltage at the rate of about 30 V/hr. A slow heating is desired for avoiding thermal shock and long life of the annealing chamber. At first the furnace was tested for vacuum operation. It has been found that if the mechanical pump operates for about half an hour, vacuum comes down to 30 micron. The leak rate, when the pump

was isolated, was found to be quite small indicating that there was no leak in the system. Since the furnace was basically to be used with an atmosphere of inert gas or mixed gas mentioned earlier, the furnace was not tested for higher vacuum. Even though annealing was to be performed in a gas atmosphere creation of vacuum was desired to cut down the time of flushing out air from the furnace and to cut down the volume of inert gas required for flushing.

In order to see, what kind of temperature variation exists along the length of the furnace tube, the temperature profile of the furnace was determined (Fig. 21). The furnace appears to have a 1" uniform temperature zone at the centre of the furnace at which temperature variation is within a degree. For a 3" zone at the centre of the furnace, the total variation is about  $4^{\circ}\text{C}$  (i.e.  $\pm 2^{\circ}\text{C}$ ). For a 4" zone at the furnace centre, the variation of temperature is  $\pm 4^{\circ}\text{C}$ . Along the diameter of the furnace tube at least a 1" wide zone with uniform temperature ( $\pm 2^{\circ}\text{C}$ ) exists. The temperature control of the furnace at the set temperature has been found to be within  $\pm 1^{\circ}\text{C}$ .

## II.3 Gas Purification Train

### II.3.1 Design consideration

As mentioned in an earlier section, annealing of Ni-Fe alloys<sup>is</sup> usually carried out in a gas atmosphere ~~argon~~, hydrogen or controlled mixture of argon and hydrogen may be used. Since the bottled gases are not pure and contains oxygen, moisture etc., a gas purification train was needed. Oxygen from inert gas can be removed by passing the gas

through heated (at about  $700^{\circ}\text{C}$ ) Cu and Ti chips and moisture can be removed by passing through anhydrous calcium chloride. For hydrogen purification, a Cu chip furnace together with moisture absorber is needed. Some times a suitable mixture of argon and hydrogen gas is desired. For this purpose a gas mixer together with flow control arrangement for individual gases is needed. These features were kept in mind in the construction of the gas purification train.

### II.3.2 Constructional details

Since an argon gas purification train was available, a hydrogen purification train and a gas mixer was constructed. The schematic diagram of it is shown in Fig. 22. The impure hydrogen and pure argon come through two different  $\frac{1}{4}$ " O.D. Cu tubes. The needle valve on these tubes can be used to control the flow rate of either gas. The Ar and  $\text{H}_2$  lines are interconnected through a needle valve so that the hydrogen line can be flushed with argon before passing hydrogen gas. The two gas bubblers, containing diffusion pump oil, in the two gas lines were used as flow rate indicator. The purified and dried  $\text{H}_2$  and Ar gases go through a mixer containing glass beads before going into the furnace. A suitable cold trap may be used to control the dryness of the gas.

### II.4 Epstein Test Frame

The specific core loss of a material is defined as 'the total power in watts expended per kilogram of magnetic

## FIGURE CAPTIONS

FIG. 19. Temperature vs. voltage curve for hot working furnace.

FIG. 20. Heat treatment furnace.

FIG. 21. Longitudinal temperature profile of the annealing furnace.

FIG. 22. Hydrogen gas purification train and Argon and Hydrogen gas mixer arrangement.



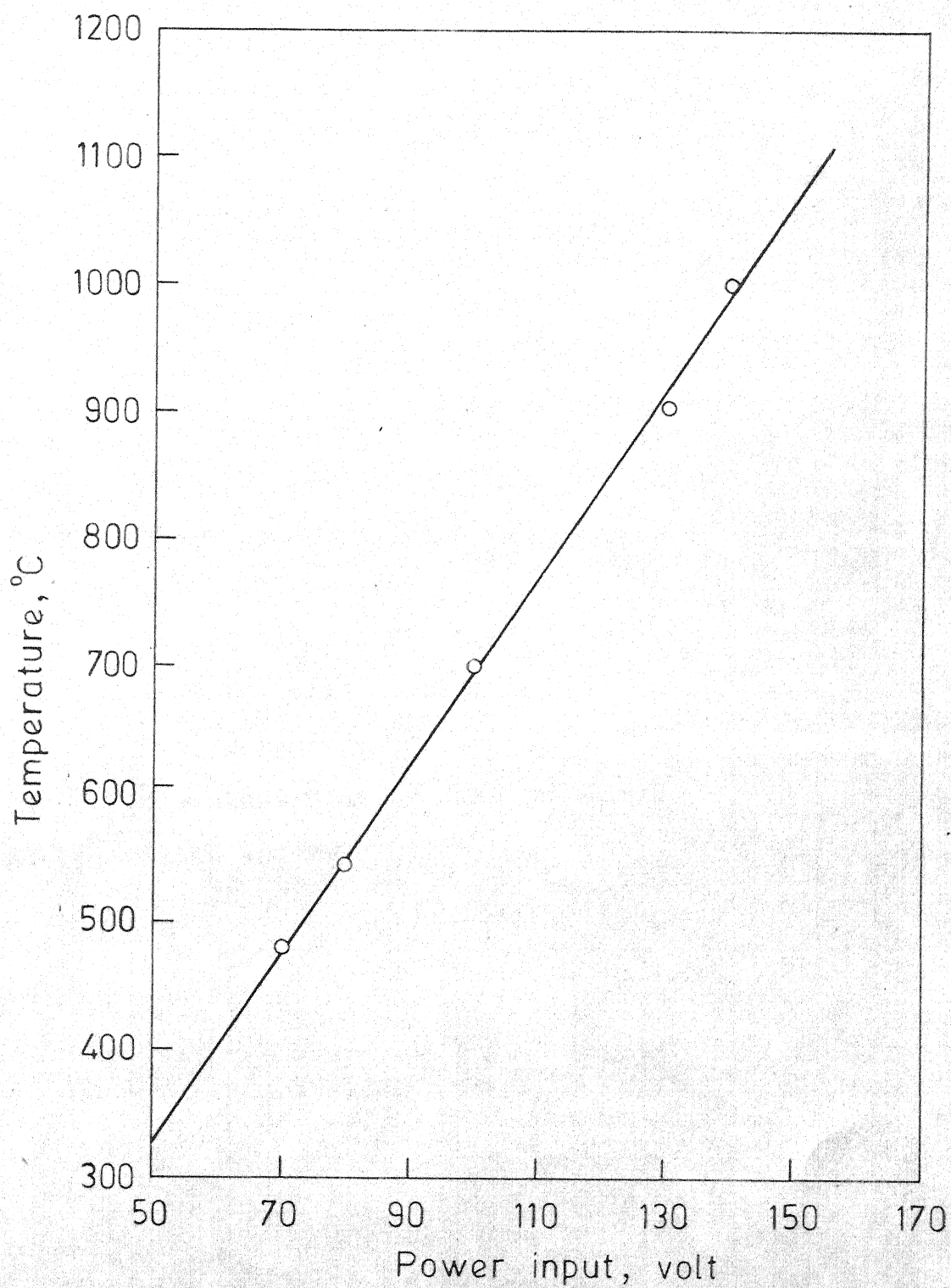
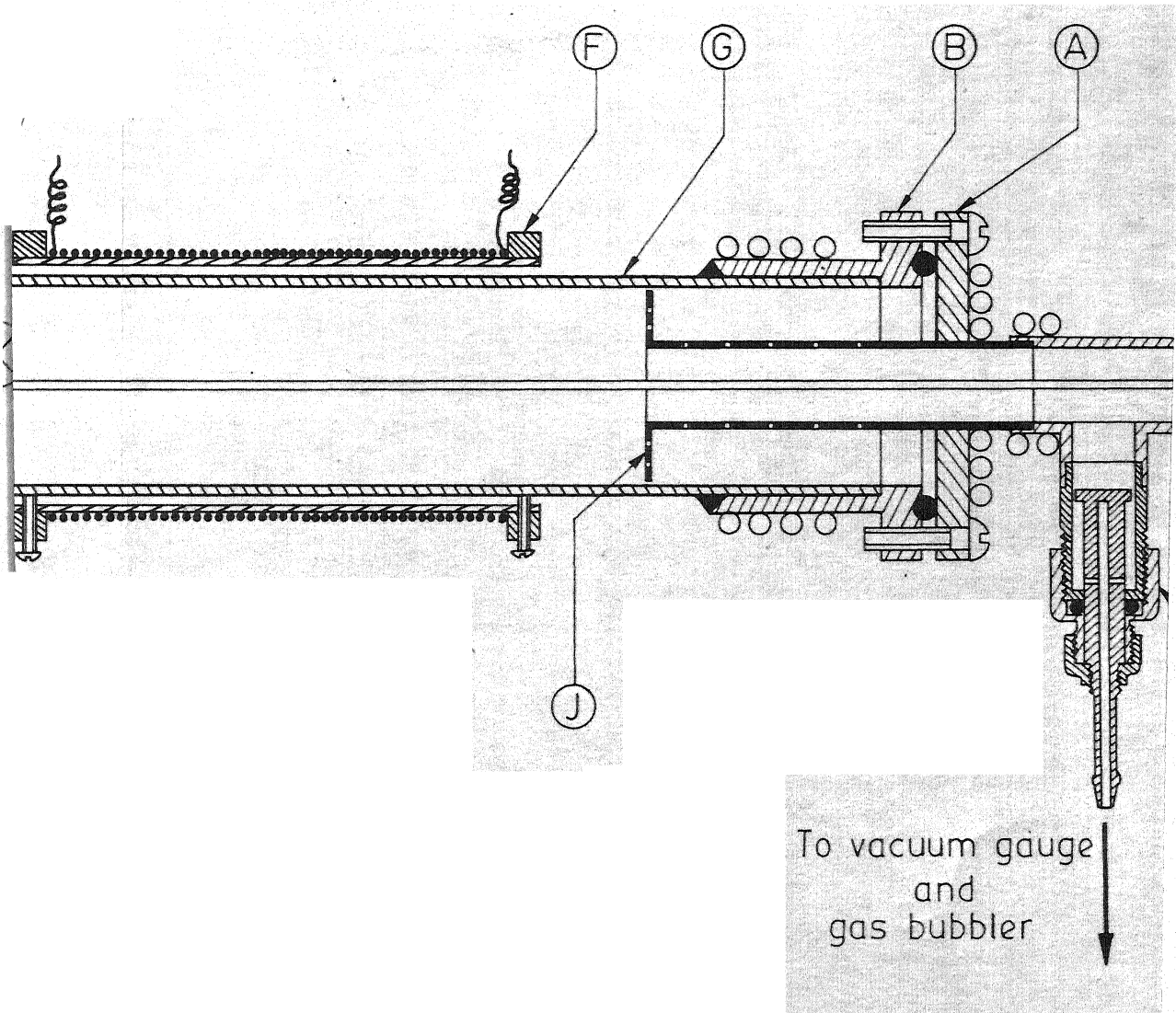


Fig. 19

## Parts List of Annealing Furnace

- A. Flange cover
- B. Water cooled brass flange
- C. Control thermocouple
- D. Stainless steel specimen tray
- E. Stainless steel pull rod
- F. Solenoid
- G. Impervious mullite tube
- H. Pull rod sliding seal
- I. Dual purpose vacuum valve
- J. Stainless steel radiation shield
- K. Black wax seal



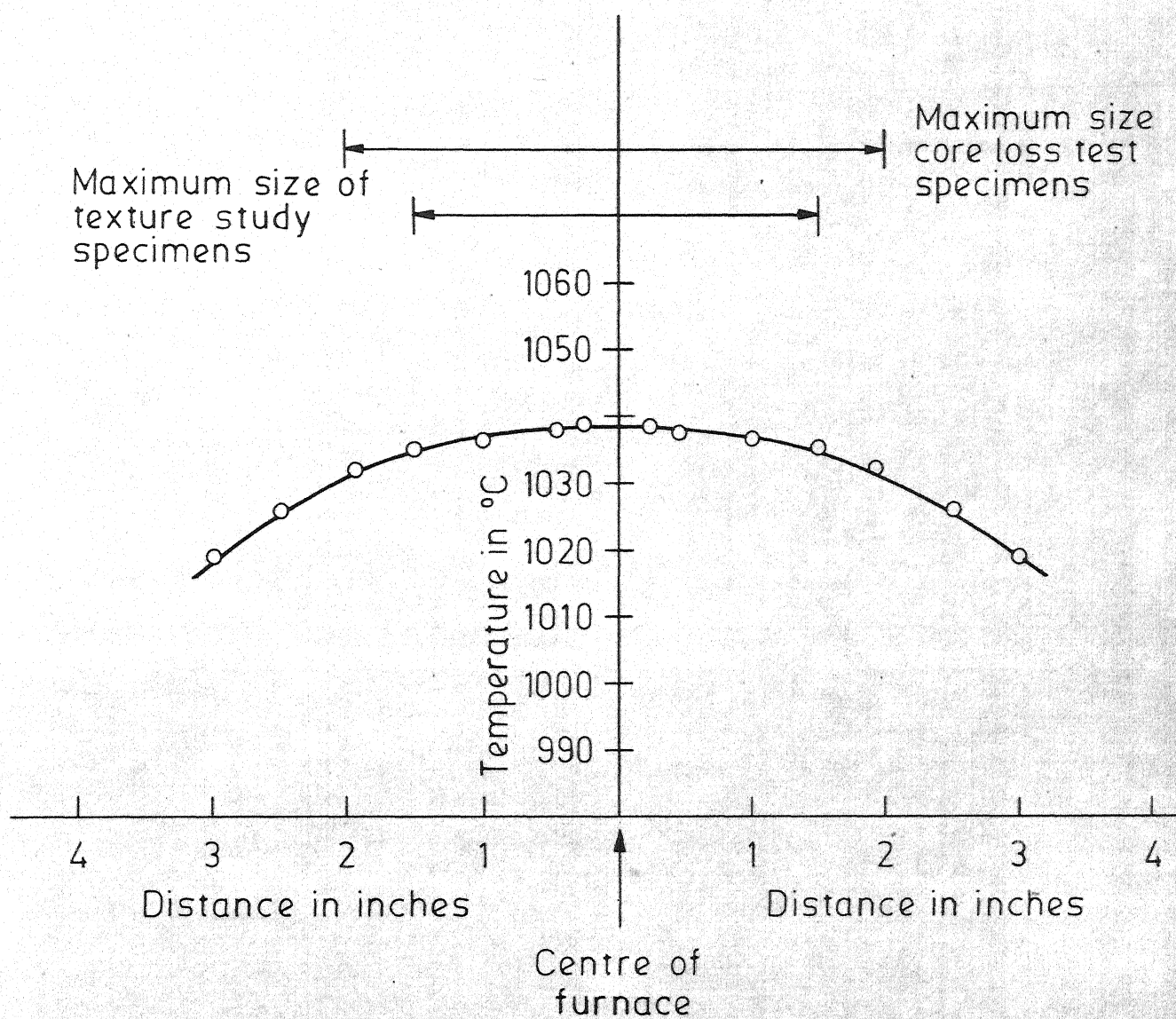


Fig. 21

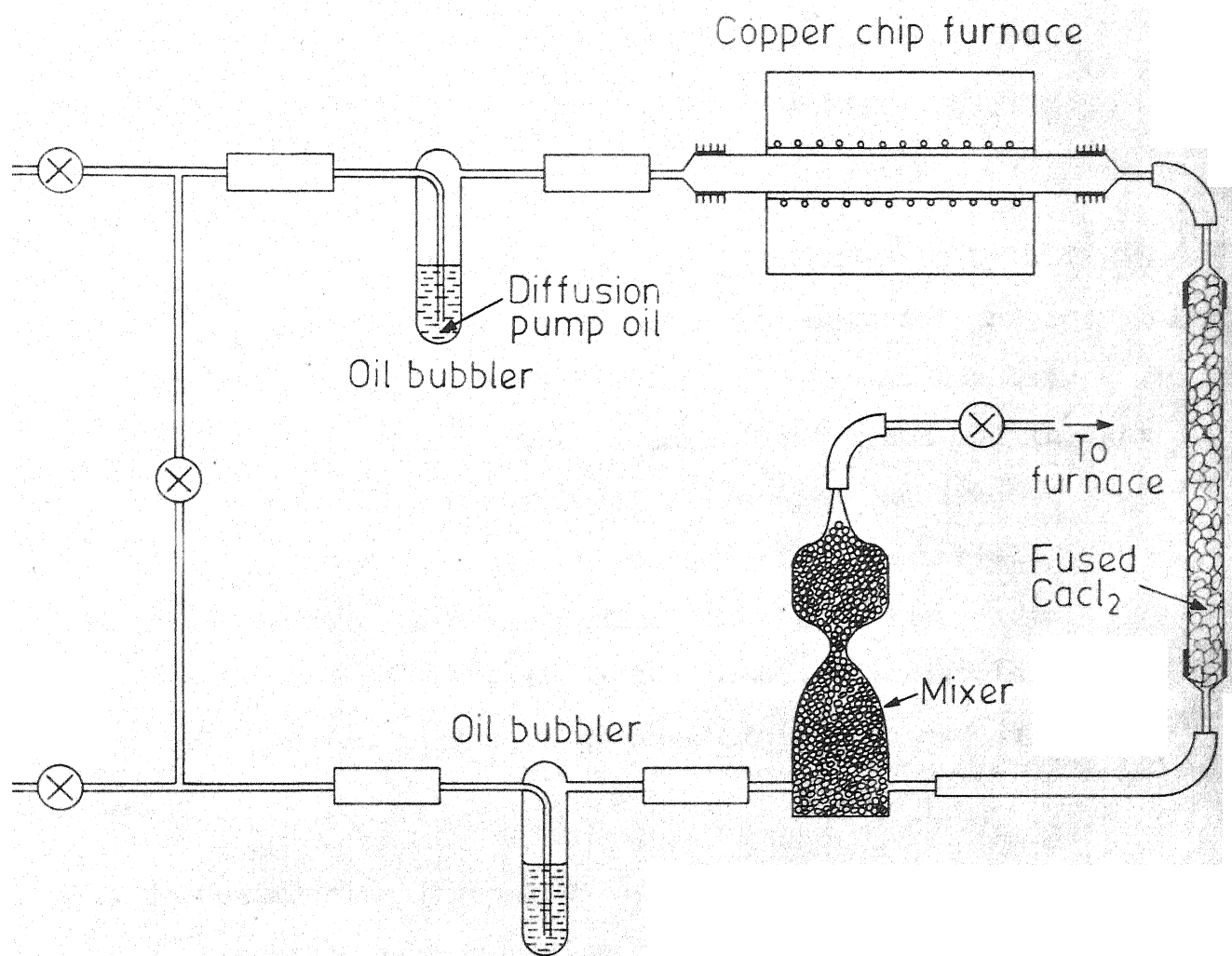


Fig 22

material in which there is a symmetrical harmonically varying induction of a specified maximum value at a specified maximum frequency'. Usually the coreloss test is done with the help of an Epstein test frame.

#### II.4.1 Design consideration

A standard Epstein test frame, as approved by ASTM standards, makes use of a large amount of material and is not suitable for our purpose because there is no facility to produce large melts. Hence a small test frame was thought desirable. Besides the coreloss, it is also required to know the nature of the hysteresis loop of the material. Both these features can be combined in one unit provided we do not need accurate data on B-H loop. The Epstein test frame has been designed to take care of the two requirements.

#### II.4.2 Constructional details

The test frame contains four hollow rectangular arms made of perspex sheet as shown in Fig. 23. The dimension of the arms were 65 mm. x 10 mm. x 10 mm. On these arms, the primary and the secondary windings were made. The details of the design data are given in Appendix III. These four arms were fixed on a perspex base. The specimens needed for the test frame are sheets of size 100 mm x 9.5 mm. The circuit diagram of the test frame is shown in Fig. 24. The test frame has been designed with a view to make loss measurements at flux densities between 10,000 to 20,000 gauss at 50 Hz. With a suitable higher frequency power

supply, it may be used for magnetic tests at say 400 Hz.

#### II.4.3 Testing of Epstein test frame

The Epstein test frame has been tested with 1 mm. thick hot rolled Fe-Si strips supplied by HSL Ranchi. For these sheets, the specific core loss data is known. For testing the equipment, 32 pieces of strips weighing about 200 gms has been accommodated in the four arms of the test frame. The measured characteristics of the test frame are indicated in Figs. 25 to 27. The specific core loss was determined by noting the wattmeter reading and the data is tabulated in Table 3. The loss values quoted and the values determined through the test frame appear to be rather different. The variation could be due to non-compensation of air fluxes. Also the actual magnetic induction in the coil could not be checked for want of an axial probe for a Gaussmeter. Since no other tested material was available, further verification or calibration of equipment could not be done. The B-H loop, for these sheets was traced by an oscilloscope and is shown in Fig. 28.

#### II.5 Magnetic Annealing Furnace and Power Supply

This furnace is required for annealing the already high temperature annealed sample under a constant magnetic field at a desired temperature just below the curie temperature of Fe-Ni alloys. Since it is difficult to produce a magnetic field in an A.C. operated furnace, it was thought appropriate to use a D.C. supply for the furnace so that furnace heating as well as magnetic field generation can

be done at the same time. Since a horizontal tube furnace requiring about 4.5 amp. current to reach  $650^{\circ}\text{C}$  was already available, a suitable power supply was only needed. As the field strength needed was rather low, few hundred Oes only and there is no stringent requirement of fluctuations of the generated magnetic field, a simple power supply was designed with the help of Electrical Engineering Department, I.I.T. Kanpur.

The circuit diagram for the power supply is given in Fig. 29. To avoid large variation in field strength due to voltage fluctuation a three phase A.C. supply for the primary side has been used. Three identical primary transformers with tapplings corresponding to 410 volt, 400 volt, 380 volt and 360 volt at primary side and current carrying capacity of 5.7 amp. has been used. The output voltage (132 volts if primary tapping is at 410 volt) can be controlled to a limited extent by changing the primary tapplings. The minimum voltage obtained was 90 volts when the tapplings of the primary side were at 360 volt. The output voltage and current can be measured by a voltmeter and an ammeter, provided with it. The amount of ripples due to fluctuation in D.C. supply was about 8% in the no load condition and about 6% when connected to a load.

## II.6 Sheet Specimen holder for Laue Technique

Laue technique may have to be used to determine orientation of the individual grains of the fabricated metal sheets. Hence a specimen holder for utilising Laue technique for sheet specimen was thought necessary. The specimen holder



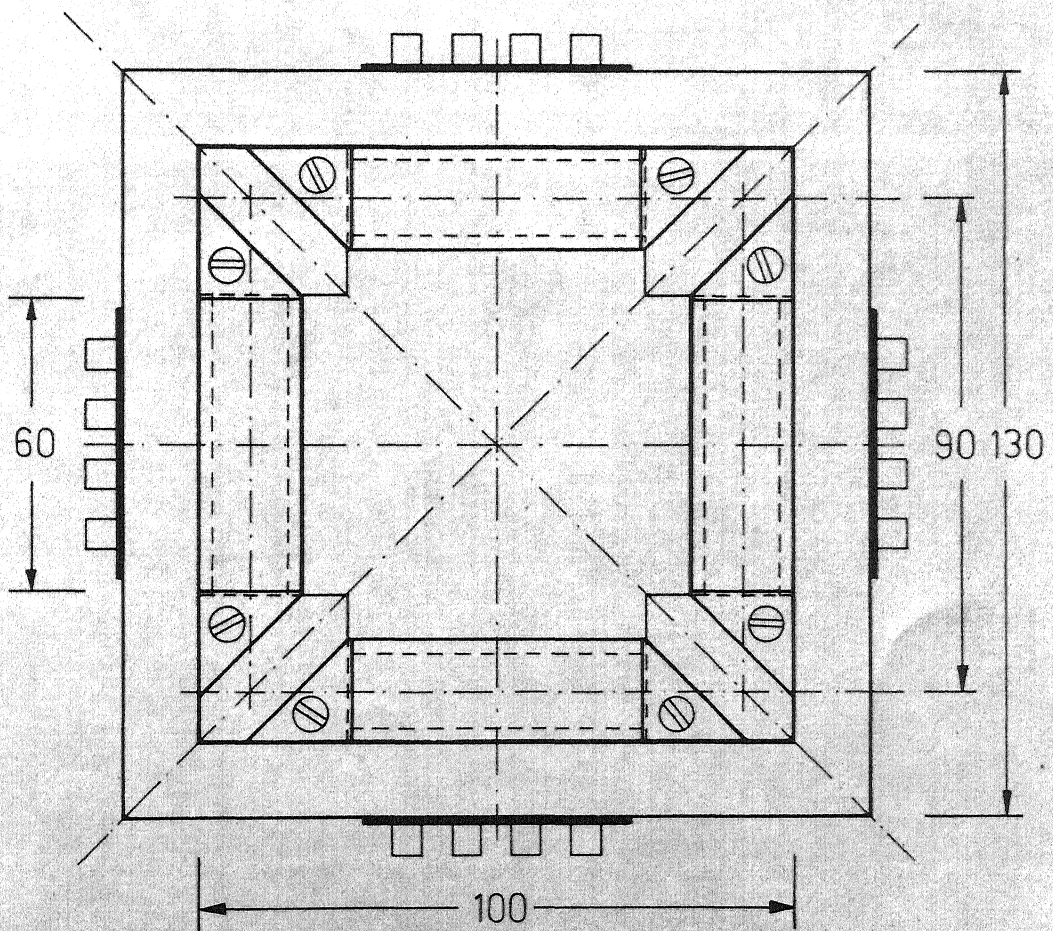
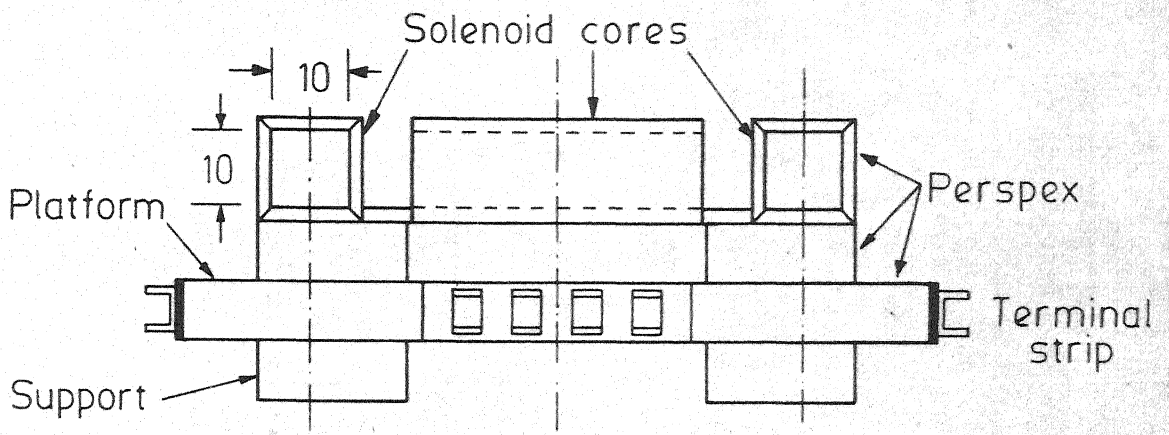
should be such that x-ray exposure can be given throughout the sample without dismantling it from the holder. Since the specimens are at least 1" x 1" and may be of maximum size 3" x 1" sufficient flexibility was needed for bringing any part of the specimen under the x-ray beam.

Detailed drawing of the specimen holder is shown in Fig. 30. The specimen holder is a plate of brass mounted in a slotted vertical brass stand with the help of a brass screw. The holder can slide up and down and can be fixed at any desired position by tightening the screw. The vertical stand alongwith the holder can be moved horizontally on a slotted base and can be fixed at any desired position. The slot sizes are made such that a total vertical travel of about  $3\frac{1}{2}$ " and a horizontal travel of  $1\frac{1}{2}$ " is possible.

For testing purpose, back reflection Laue pattern of a 3" x 1" lithium fluoride single crystal (a monochromater for Fluorescence attachment of diffractometer) was taken at three different points - one bottom most point, one top-most point vertically above the first point and one at a point about  $\frac{3}{4}$ " away in horizontal direction from the second point. <sup>The</sup> ~~As~~ three patterns were found indential indicating that the holder with as large as about 3" vertical motion and  $\frac{3}{4}$ " horizontal motion does not cause any change in orientation. The Laue patterns of the first and second positions are shown in Fig. 31 and Fig. 32. Thus the specimen holder will be ideally suited for finding relative change in orientation from one grain to another.

## FIGURE CAPTIONS

- FIG. 23. Details of Epstein test frame.
- FIG. 24. Circuit diagram of Epstein test frame.
- FIG. 25. Secondary voltage vs. primary current curve obtained for Epstein test frame.
- FIG. 26. Ratio of secondary voltage to current vs. primary current curves for the Epstein test frame.
- FIG. 27. Primary voltage vs. secondary voltage curves for the Epstein test frame.
- FIG. 28. B-H loop obtained for 200 gms of hot rolled Si-Steel Strips.



Dimensions in mm.

Fig. 23

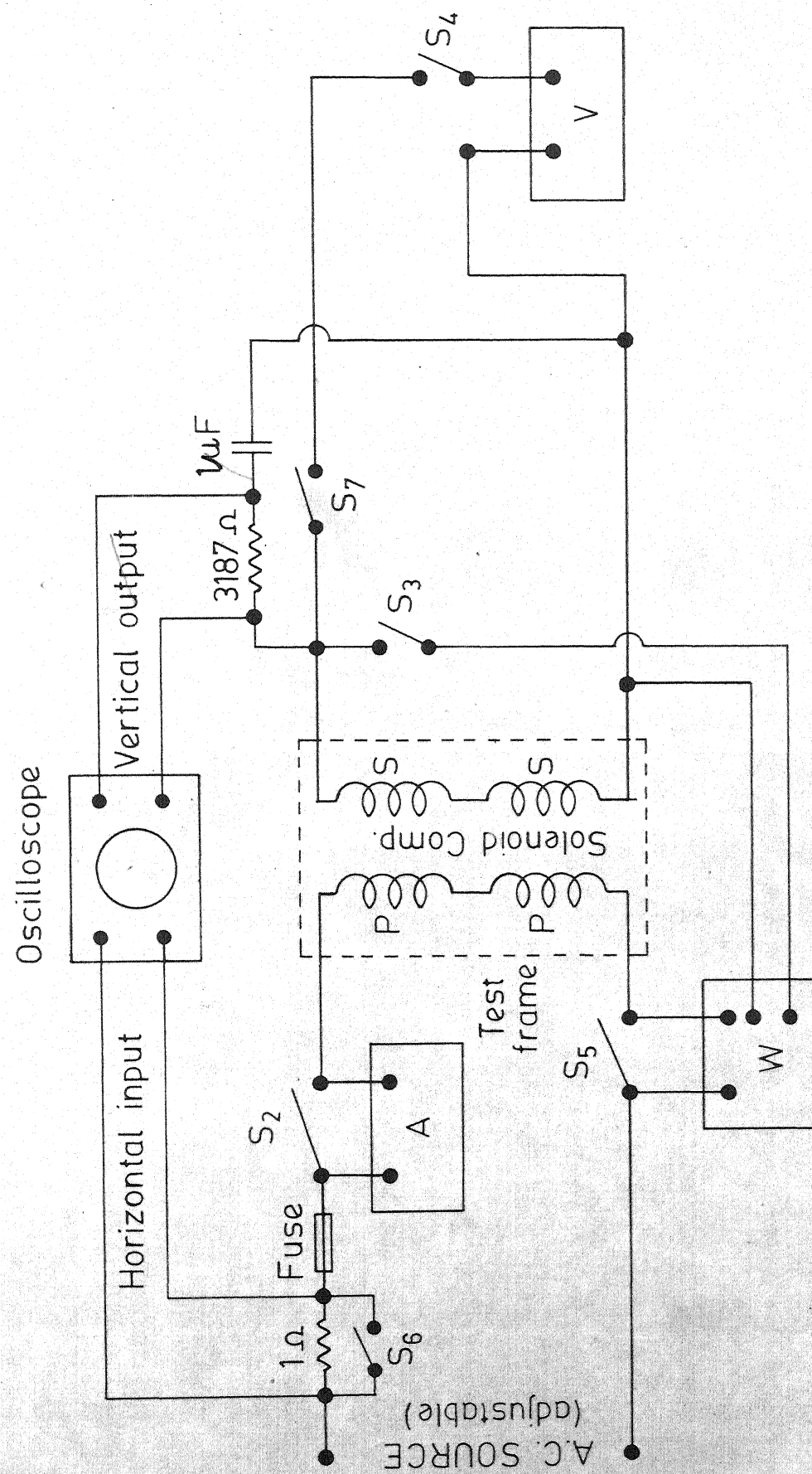


Fig. 24

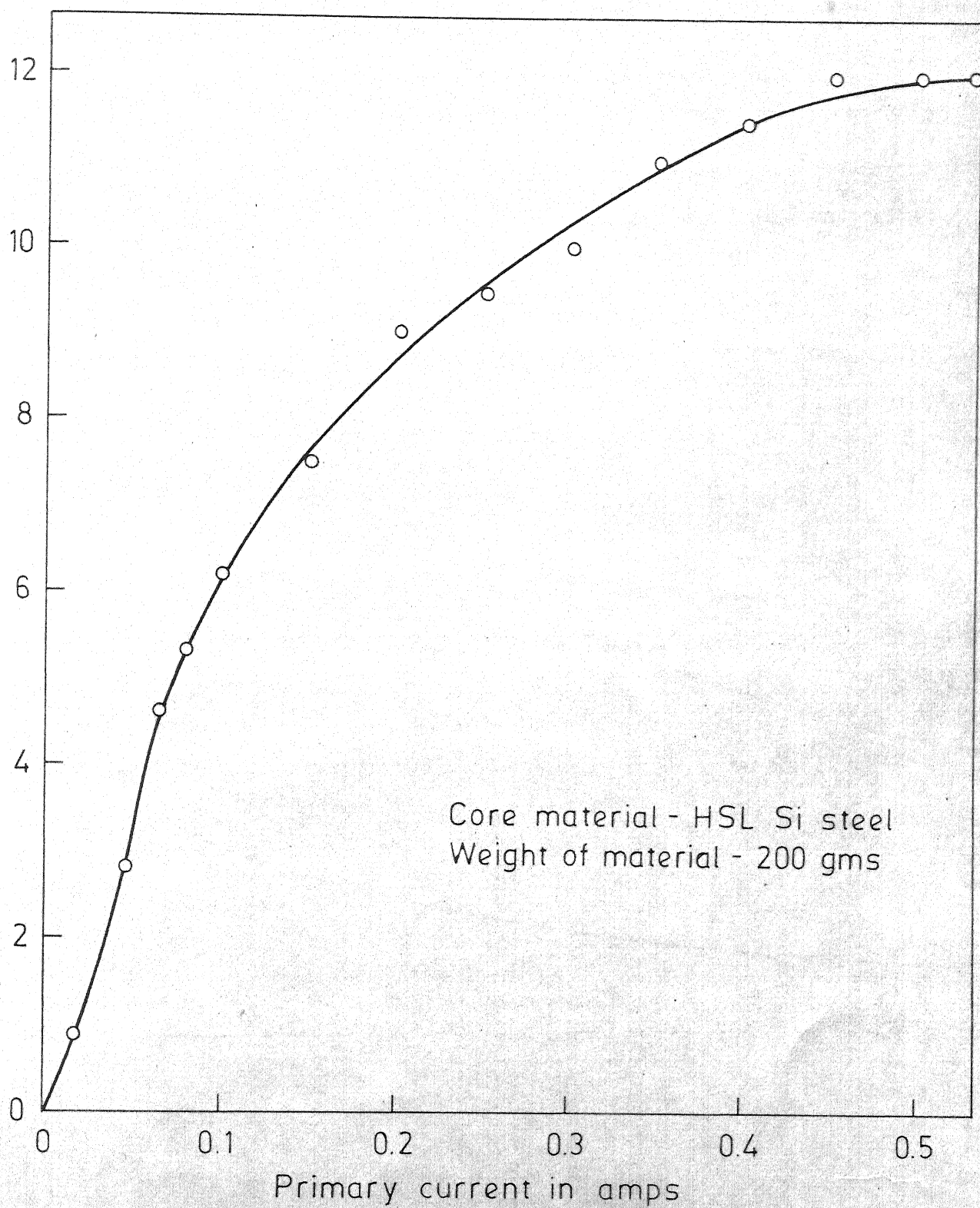


Fig. 25



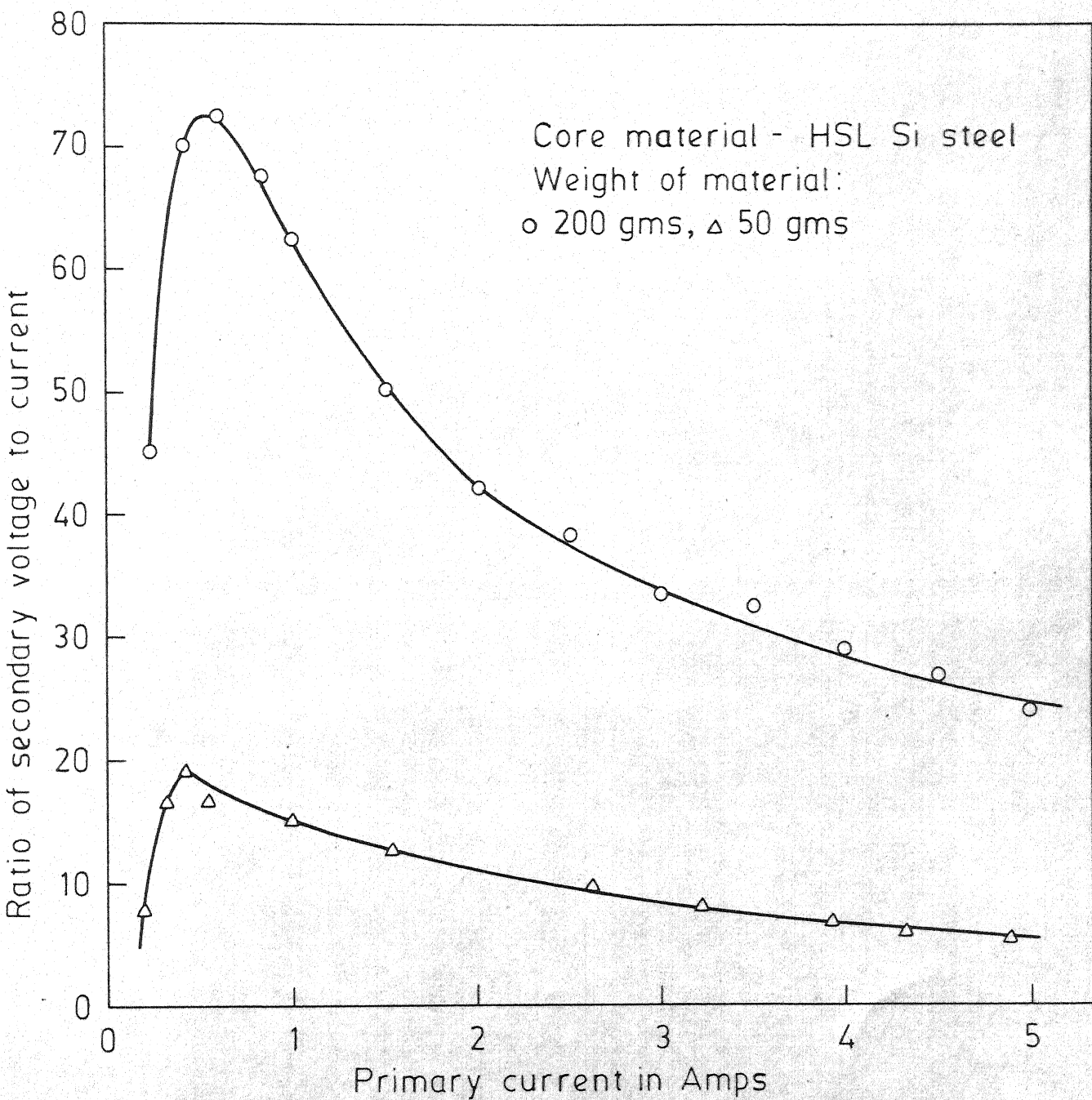


Fig. 26

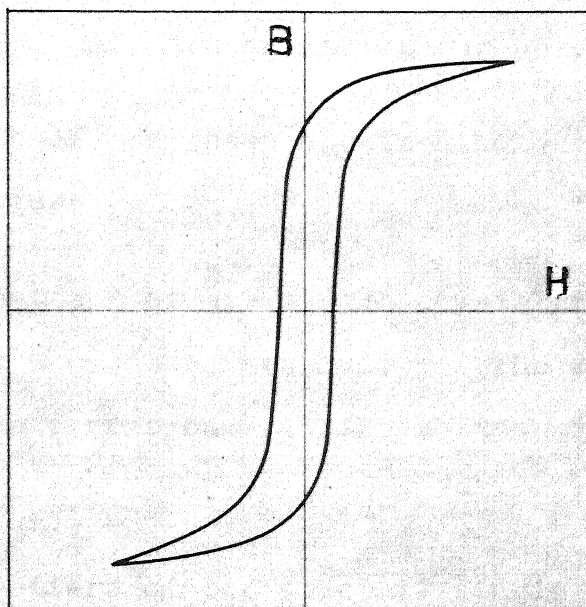


Fig. 28

## FIGURE CAPTIONS

- FIG. 29. Circuit diagram of the D.C. power generation unit for magnetic annealing furnace.
- FIG. 30. Details of the sheet specimen holder for Laue technique.
- FIG. 31. Laue pattern of LiF single crystal fixed to the sheet specimen holder. The diffraction pattern corresponds to the bottom most part of crystal.
- FIG. 32. Laue pattern of the same LiF single crystal fixed to the sheet specimen holder as in Fig. 31. The diffraction pattern corresponds to the top most part of the crystal. The crystal was only displaced vertically with the help of the vertical slide.



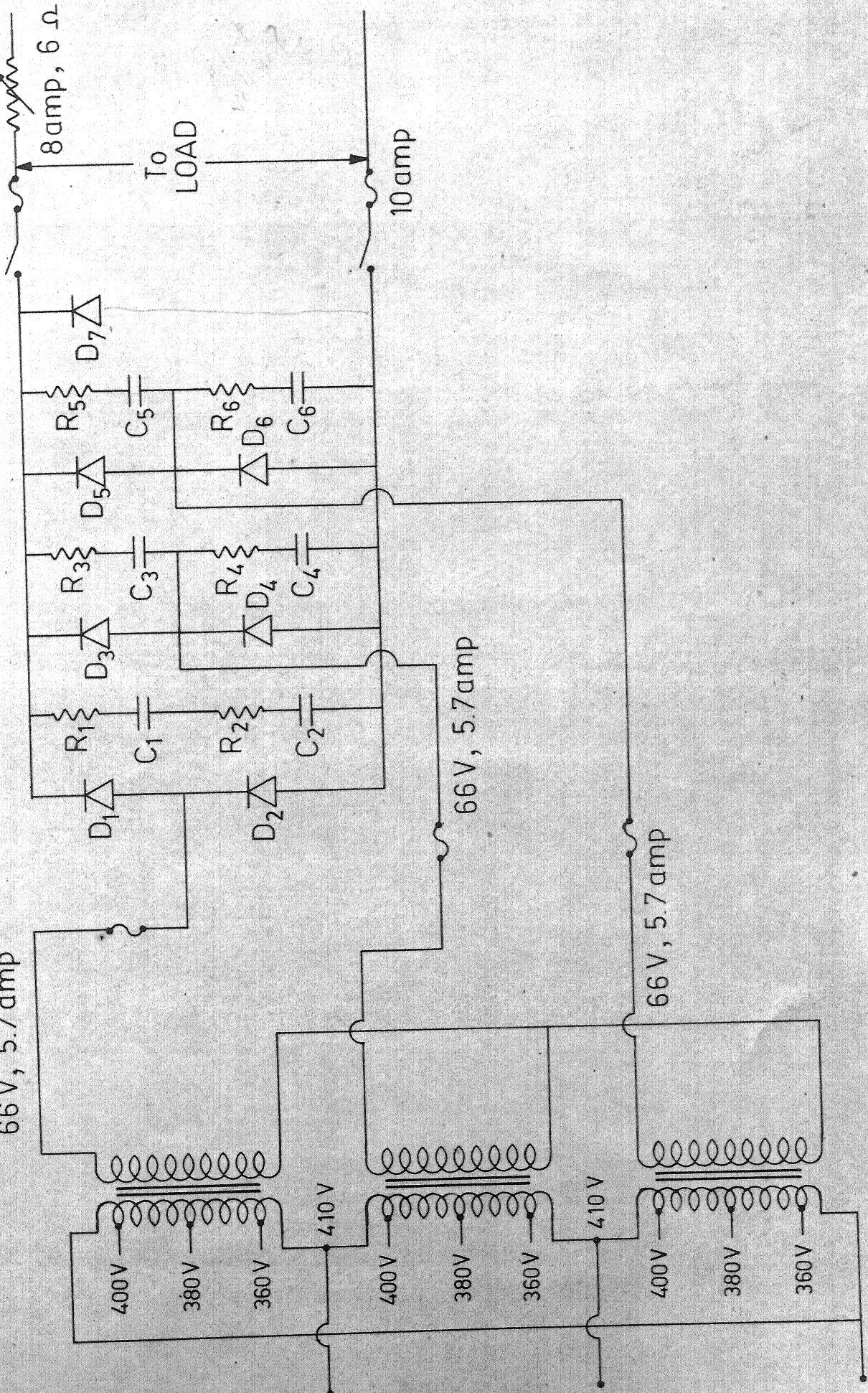
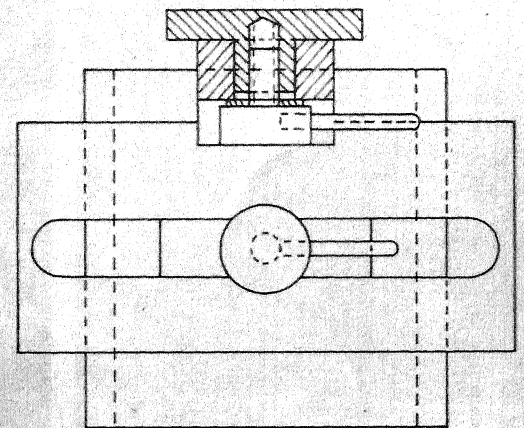
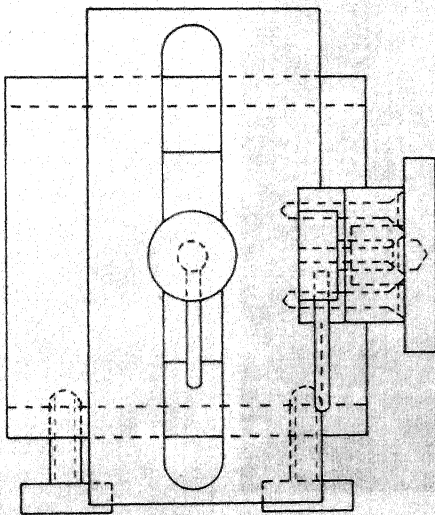
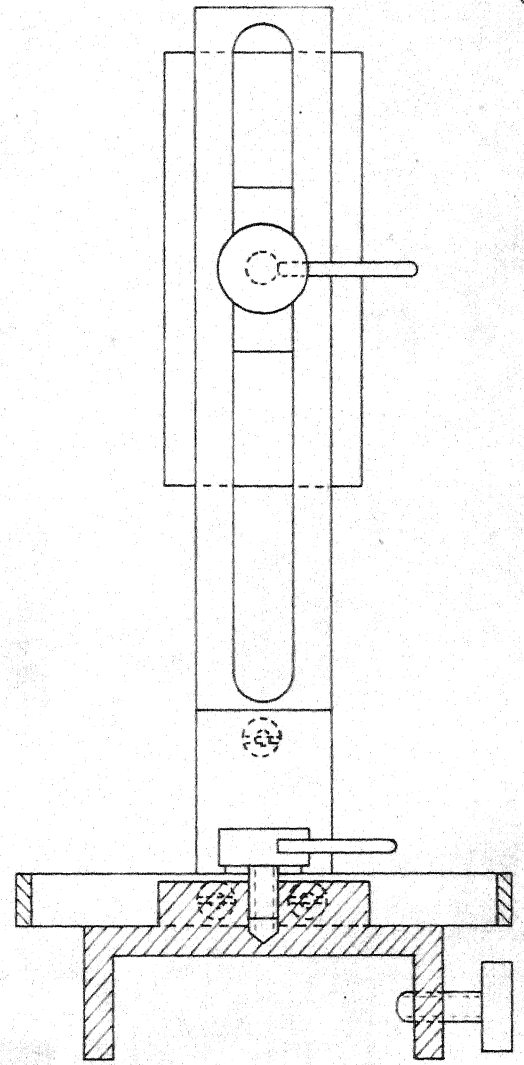
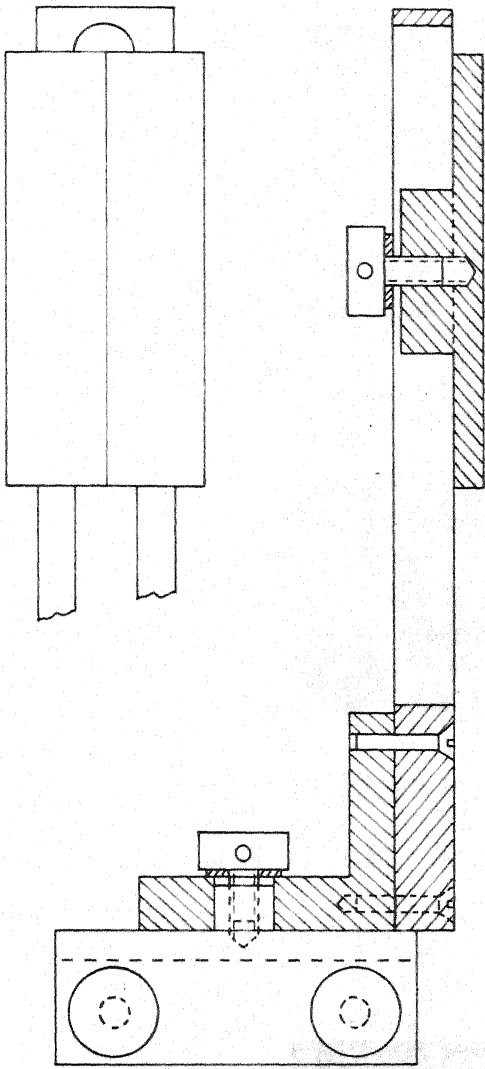


Fig. 29



Scale: 3/4th of actual size

LAUE SPECIMEN HOLDER FOR SHEET MATERIAL OF

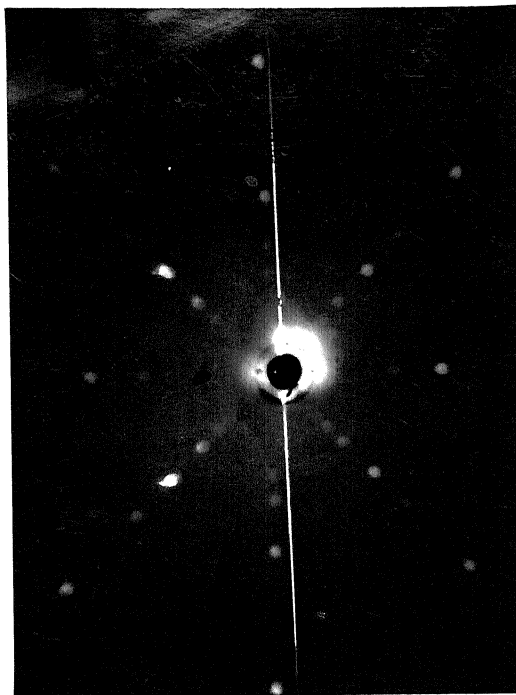


Fig. 31

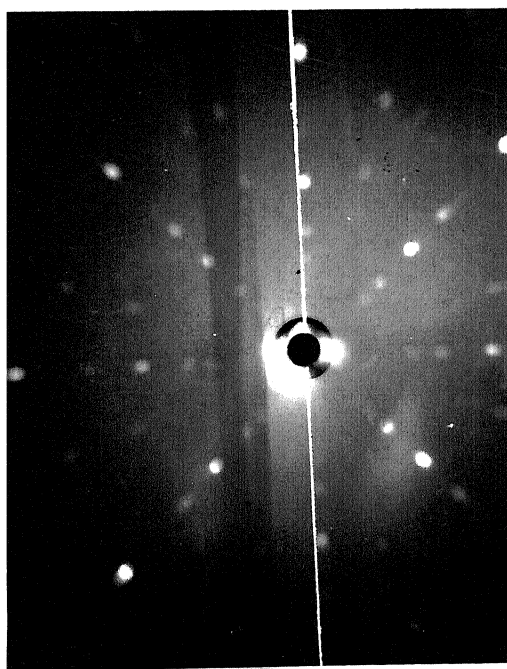


Fig. 32

TABLE III

Epstein Test Frame Data for 200 gms HSL Si Steel Sample

$V_p$ Primary voltage in volts	$V_s$ Secondary voltage in volts	$I_p$ Primary current in mA	Power loss in watt/kg
2.75	9	20	0.06
8.40	2.8	40	0.38
14.00	4.4	60	0.75
17.00	5.4	30	1.13
19.50	6.15	100	1.44
23.50	7.5	150	2.00
26.50	8.3	200	2.31
28.50	9.5	250	2.69
30.00	10.0	300	3.00
32.00	11.0	350	3.25
33.00	11.5	400	3.50
33.50	12	450	3.63
34.00	12	500	3.88

## CHAPTER III

## EXPERIMENTAL PROCEDURE

## CHAPTER III

### EXPERIMENTAL PROCEDURE

The grain orientation study with Fe-Ni alloys was made with alloy composition, namely 48 Ni-Fe. The alloy preparation and characterisation involved the following steps:

- (1) Melting and homogenisation of alloys.
- (2) Hot rolling.
- (3) Cold rolling.
- (4) Annealing under a controlled atmosphere.
- (5) Specimen thinning for x-ray diffraction work.
- (6) Texture determination using x-ray diffraction technique.
- (7) Metallographic investigation.
- (8) Magnetic property study.

#### III.1 Melting and Homogenisation of Alloys

The melting furnace used was a 6 K.W. Ajax induction melting unit fitted with a sealed end quartz tube melting chamber. The available furnace was capable of small melts

100 gms each. Hence to get a reasonable size of melt the cast metal ( $\sim$ 100 gms) was remelted with more material to make a charge of about 200 gms. Depending on the requirements 100 gms or 200 gms ingots were used.

The alloys of different Ni content were prepared by melting 99.9 % pure Ni globules and electrolytic Fe supplied by Semi Elements Inc., New York. Weighed amount of Fe and Ni was melted in argon atmosphere using recrystallised alumina

crucibles. A graphite crucible with a graphite cover was used as the susceptor. Before melting, the furnace chamber was evacuated to a vacuum of about 50 microns of Hg and flushed with argon. This process was repeated twice to remove air. The melting point of all the alloys were near about  $1450^{\circ}\text{C}$ . So the temperature was raised upto  $1500-1550^{\circ}\text{C}$  and was kept at that temperature for five minutes for better mixing by induction stirring. Since there was no provision for casting the alloys under controlled atmosphere, the melt was allowed to solidify in the crucible. The ingots were about 1" dia x  $2\frac{1}{2}$ " long and usually had small blow holes at the surface and some pipe formation. The latter was minimised by allowing the solidification to start at the lower end by lowering the whole quartz tube holding the melt through the induction coil. The surface blowholes were removed by turning operation and the top of an ingot was usually chopped off before further processing. The pure Fe-Ni alloys, however, cracked even when hot rolled at  $1150^{\circ}\text{C}$ . The same sample, when remelted with 0.5% Mn and 0.2% Al, could be rolled successfully. Thus, all the alloys were melted with Mn with or without Al. Since, Mn has high vapour pressure at melting temperature of the alloys, the ingot produced, had lots of blow holes. By trial, a slow solidification procedure was developed. After the alloy was melted and homogenised, the induction furnace power was stepped down to its minimum value ( $\sim 4$  kw), and the furnace tube was lowered very slowly, keeping the induction coil position fixed. In this procedure the top of the melt was kept in molten condition and very slow cooling of melt



started at the bottom. This procedure not only reduced the small blow holes but also reduced the pipe formation quite considerably. After removing the alloys from the induction furnace the ingots were annealed at  $1150^{\circ}\text{C}$  in an open furnace for 1 hour to homogenise them. Then the top part of the ingots were cut to remove the pipe and the surface blow holes were removed by machining. Melting losses in any melt was found to be within  $0.2\%$  to  $0.4\%$ . The homogenised alloys were chemically analysed in one case to determine the change in composition.

### III.2 Hot Rolling

Hot rolling was done to reduce the thickness of the ingots and to break the cast structure. The temperature at which the specimen was heated prior to rolling varied between  $1120^{\circ}$ – $1170^{\circ}\text{C}$ . The ingots were first rolled in transverse direction to increase the width to 1.25" and then rolled along its length. Since the ingots were small, care had to be taken to roll at sufficiently high temperature so that no cracking of specimen occurred. Not more than two passes were possible because the rolling temperature was always kept above about  $1050^{\circ}\text{C}$ . Reduction per pass was 0.020". The final hot rolled thickness was limited by the subsequent percentage of cold rolling desired. The final hot rolled thicknesses of different specimens are shown in Table IV.

### III.3 Cold Rolling

The hot rolled samples were first cleaned on coarse emery papers to remove very thin oxide layer formed during



hot rolling and if any edge cracking was found it was removed by grinding. The cold rolling was carried out on the cleaned samples under two different conditions - (a) rolling at room temperature and (b) rolling at some elevated temperature. A guide for keeping the rolling direction same, was used in both the cases. No intermediate annealing was given to any specimen.

In room temperature cold rolling, the specimen was reduced by 0.005" in each pass. The minimum thickness of the specimen that could be obtained by rolling a single sheet was 0.009" for 48 Nickel-Iron alloys. The useful thickness for the present work was considered to be 0.006". In order to further reduce the thickness, pack rolling was tried. A pack of 3 strips, each 0.009" thick, were rolled together. This process of rolling was found to produce minimum thickness in the range of 0.004" - 0.005" for 48 Ni-Fe alloys. The percent reduction for 48 Ni-Fe alloys, was varied from 90-98%.

Cold rolling of specimens at some elevated temperature was tried for only 48 Ni-Fe alloys. Different temperatures ranging from 100°C to 400°C were used. The specimens were kept in a furnace at a temperature of 100°C (max.) higher than the actual temperature of rolling. The specimen temperature, just before putting it between the rolls, was measured with a thermocouple to ensure that the rolling started at the same temperature. A chromel-Alumel couple

was used for this purpose. Since the specimen temperature in one pass came down quite considerably only one pass was possible each time. Reduction in thickness per pass was kept constant at 0.005''.

#### III.4 Annealing of Alloys Under a Controlled Atmosphere

The cold rolled strip material was cut into pieces of 1.75" long x 1.25" wide so that after annealing pieces of 1.25" long x 1.25" wide specimens could be obtained for x-ray study and the rest could be used for magnetic study and metallography. The fabricated controlled atmosphere annealing furnace was used for this purpose. Since the hydrogen gas purification mixer train was not ready all the annealing work were done in flowing purified argon gas. Annealing temperature was varied between 900°C to 1150°C. The furnace temperature was first raised to the desired value and the temperature was stabilised. The specimens were loaded on the specimen tray of the furnace and kept in the cooler part of the furnace. Then the furnace tube was evacuated to approximately 40 microns of Hg and flushed with purified argon. The process was repeated twice and finally argon gas was allowed to flow through the tube. Initially the gas flow rate was kept around 20 bubbles/minute for 2 minutes and then it was reduced to about 5 bubbles/minute. The bubble rate was measured by a bubbler, connected to the outlet through the special valve. The specimen was then pushed into the hot zone and the annealing was carried out in argon atmosphere for the desired length of time. When the annealing was over, the specimen tray with specimen was

pulled into the cold zone of the furnace and after about 10 minutes, the furnace chamber was opened to remove the annealed specimen. The annealed specimen was found very bright indicating that no oxidation of the specimens took place and that the gas used was sufficiently pure.

The time of annealing was varied in the range of 2 hrs to 16 hrs at a specific temperature. Initially there was indefinite water supply and the water tank was not available. Hence it was not possible to anneal the specimen continuously for 16 hrs. The long annealing of the specimens could be done in four steps - each annealing step was of about 4 hrs duration per day.

### III.5 Specimen Thinning for X-ray Diffraction Work

For accurate determination of texture by transmission method thin specimens, with  $\mu t$  value (where  $\mu$  = linear absorption coefficient and  $t$  is thickness of the sample) approximately around unity<sup>44</sup>, are required. For Fe-Ni alloys  $\mu t \approx 1$  corresponded to specimen thickness of about 0.002" - 0.003". Preparation of specimens of 0.002" thickness, uniform over a whole area of  $1\frac{1}{4}" \times 1\frac{1}{4}"$  is difficult and hence considerable experimentation had to be done.

Careful mechanical polishing was tried first, but the main drawback of this procedure was that it was too time consuming, laborious and to maintain an uniform thickness was not possible. In this procedure the specimen thickness in the same specimen varied from 0.002" - 0.004". For uniform thickness and quicker thinning chemical etching method was considered more suitable.

$\text{HNO}_3$ -water mixture (1:3) was tried at room temperature as well as at about  $50^\circ\text{C}$ . Both turned out to be useless as no reaction occurred. A mixture of  $\text{HNO}_3$ ,  $\text{H}_3\text{PO}_4$ , and acetic anhydride in 1:5:4<sup>45</sup> ratio was tried in the temperature range of  $40^\circ$ - $60^\circ\text{C}$ . A very slow rate of reaction was observed and after keeping it for 25-30 mts. the reaction usually stopped. The specimen obtained had a very good shiny surface but the thinning was practically negligible. Next chemical reagent tried was a mixture of  $\text{HNO}_3$ ,  $\text{H}_2\text{SO}_4$ ,  $\text{H}_3\text{PO}_4$  and  $\text{CH}_3\text{COOH}$  in the ratio of 3:1:1:5<sup>45</sup>. At room temperature, the rate of reaction was negligible but when temp. was raised to  $80^\circ$ - $85^\circ\text{C}$ , the rate of reaction was very fast. If, however, the reaction was allowed to occur for more than five minutes, pits started to form and thinning became non-uniform. If the specimen had any surface defect, non-uniform thinning became more prominent. Hence, the procedure adopted was to mechanically polish specimens on 80 grit and 120 grit emery cloth followed by polishing with 1/0 metallographic emery paper. The polished sheet specimen was then etched in the solution for five minutes. This procedure of alternate mechanical polish followed by chemical thinning was able to produce 0.004" thick specimens. Further chemical thinning was not usually possible as it invariably produced pin holes in the sheets. Thinning down further to 0.002" to 0.003" had to be done by mechanical polishing. The specimen thickness in these cases varied between 0.002" to 0.0025". The process was rather laborious and often produced holes or wrinkles in the specimens, if sufficient care was

not taken. This method, however, was used till an alternative thinning solution could be found.

The best thinning reagent found was a mixture of conc.  $\text{HNO}_3$  and 5% HF in 8:1 ratio<sup>37</sup>. When an annealed sample was kept in the solution at room temperature within ten to fifteen minutes the sample was thinned down to 0.002" to 0.0025". The surface of the sample was very shiny, there was no pit formation and the thickness was very uniform. Most of the specimen thinning was done using this solution.

For easy comparison the chemical composition, working temperature and performance of each of the solutions are listed in Table V.

### III.6 Texture Determination Using X-Ray Diffraction Technique

Texture determination involved:

- (1) Determination of  $\theta_{(hkl)}$ .
- (2) Determination of  $\mu_t$  of each specimen.
- (3) Determination of intensity correction factor.
- (4) Measurement of intensity and plotting the pole figures.

#### III.6.1 Determination of $\theta_{(hkl)}$

Texture determination using a texture goniometer required fixing the radiation counter at the correct Bragg angle.  $\theta_{(hkl)}$  was also needed for calculation of correction factor. Hence, for a given alloy, the Bragg angle of reflection  $\theta_{(hkl)}$ , had to be determined.  $\theta_{(hkl)}$  will have different values depending upon the choice of (hkl) plane

to be used for texture determination. For f.c.c. metals and alloys, usually the (111) and (200) reflections are used. Since the sheet materials have some preferred grain orientation,  $\Theta_{(hkl)}$  cannot be determined with rolled sheets. A random powder specimen has to be used for this purpose. In the present case powder from the annealed alloys was prepared by filing with a Jeweller's file and the powder was then annealed in an evacuated quartz capsule at  $900^{\circ}\text{C}$  for 15 minutes. The powder was used to prepare samples either for Debye-Scherrer pattern or for diffractometry to determine  $\Theta_{(hkl)}$  for (111) and (200) reflections. Since for texture work Mo-radiation was chosen  $\Theta_{(hkl)}$  was determined for the same radiation.

### III.6.2 Determination of $\mu t$

The value of  $\mu t$  for each specimen is required for the evaluation of the intensity correction factor  $R$  (See Section III.6.3).  $\mu t$  of the specimen was determined by using a strong diffracted beam from a parmaquartz (a fine grain polycrystalline quartz) specimen ( $2\theta = 12.15^{\circ}$ ) and measuring the intensity of the diffracted beam with and without the specimen in the path of the diffracted x-ray beam. Then using the general absorption equation,

$$I_t = I_o e^{-\mu t} \quad \dots (4)$$

where  $I_o$  and  $I_t$  are the intensities of incident and transmitted x-rays, respectively, the  $\mu t$  for each specimen was determined.

### III.6.3 Determination of correction factor

In the transmission technique of texture determination, as the specimen is rotated the path length as well as the diffracting volume vary. Therefore, the measured intensity requires correction so that the intensities for the different orientations of the specimen can be compared with each other. Theoretical calculations of the correction factor has been made by Decker, Harker and ~~App~~<sup>46</sup> which is given as

$$I_c = I_m R$$

$$\text{where } R = I_o / I_{\pm\alpha} = \frac{\mu t \exp \left[ -\frac{\mu t \cos \theta}{\cos \theta} \right]}{\cos \theta} \times \frac{[\cos(\theta \pm \alpha) / \cos(\theta \mp \alpha) - 1]}{\exp \left[ -\frac{\mu t}{\cos(\theta \pm \alpha)} \right] - \exp \left[ \frac{-\mu t}{\cos(\theta + \alpha)} \right]} \dots (5)$$

$+\alpha$  is for anticlock wise rotation of specimen from from zero position.

$-\alpha$  is for clockwise rotation of specimen from zero position.

$I_c$  = Corrected intensity

$I_m$  = Measured intensity

$\theta$  = Bragg angle for (hkl) plane used for texture work

$\alpha$  = angle of rotation of specimen around the diffractometer axis

Since the thickness varied from specimen to specimen as well as the composition varied, the values of R had to be determined for different values of  $\mu t$  and  $\theta$ . Using equation (5) the values of R were calculated (shown in Appendix, Table II) with the help of IBM 7044 digital computer for different

$\mu t$ ,  $\alpha$  and  $\theta$ .

#### III.6.4 Measurement of intensity and plotting of pole figures

For a given Fe-Ni sample, the counter was fixed at the correct  $2\theta$  (111) or  $2\theta$  (200) to receive the diffracted beam corresponding to (111) or (200) reflection and the specimen in the goniometer was positioned initially with the rolling direction vertical i.e., coincident with the diffractometer axis, and with the plane of the specimen bisecting the angle between the incident ( $S_0$ ) and diffracted<sup>(S)</sup> beams (Figure 33). This corresponded to  $\alpha = 0^\circ$  and  $\phi = 0^\circ$ , (Rotation of specimen around the sheet normal is the rotation angle  $\phi$ ). The diffractometer conditions used for measurement of intensity of diffracted beam is given in Table VI.

For integration over the whole specimen, the specimen was oscillated with a 1 r.p.m. motor. In 100 seconds counting time 6 to 7 oscillations of the specimen could be given. Since the intensity data collection had to be done manually, only a quarter of a pole figure was determined in each case. To explore a quarter of a pole figure specimens were surveyed usually at  $5^\circ$  intervals of  $-\alpha$  upto  $50^\circ$  (for fixed  $\phi$ ) and at  $5^\circ$  intervals of  $+\phi$  upto  $90^\circ$  (for fixed  $-\alpha$ ). In the regions of high intensity or drastic changes of intensity over smaller angular region, intensity data at smaller angular intervals were taken. The data collected in terms of counts/sec were corrected making use of the respective  $\mu t$ ,  $\alpha$ , and  $\theta$  and the correction table of Appendix (Table II). The corrected intensity data



were used to draw the pole figures on a polar stereographic net drawn at  $2^\circ$  intervals.

To plot the intensity data in a polar net it is evident that when  $\alpha = \phi = 0^\circ$  the pole position coincides with the left cross direction for the initial setting. A rotation of the specimen by  $+\phi$  degrees in its own plane then moves the pole of the reflecting plane  $\phi$  degrees around the circumference of the pole figure and a rotation of  $-\alpha$  about the diffractometer axis moves it  $-\alpha$  degrees from the circumference along a radius (Figure 34). In this way all the corrected intensity data were plotted at the proper pole locations on the pole figures. Contour lines passing through equiintensity points were then drawn to indicate pole densities. The pole figures were interpreted with the help of available standard projections for cubic crystals.

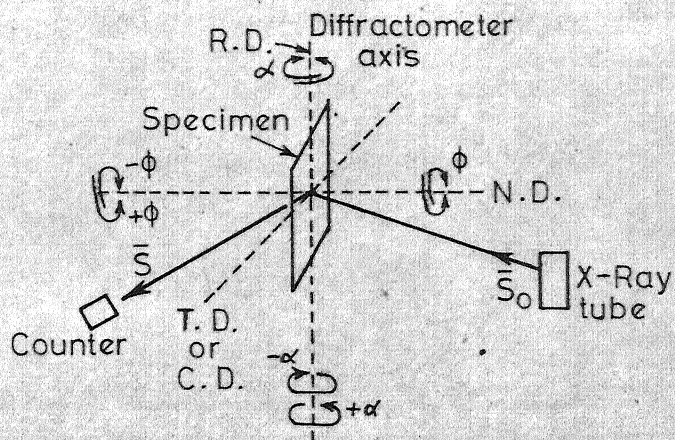
### III.7 Metallographic Investigation

Metallography of the annealed specimens was done to reveal the grain structure of the specimen. Specimens were first mounted on lucite followed by polishing on emery papers (1/0 through 4/0) and then polishing on cloth using alumina powder as abrasive. The well polished, scratch free, specimens were then treated with chemical and electrochemical etching solution (as listed below to develop the microstructure. The different etching solution tried were

- (1) 60 ml ethanol, 15 ml hydrochloric acid, 5 gms anhydrous ferric chloride<sup>47</sup>.

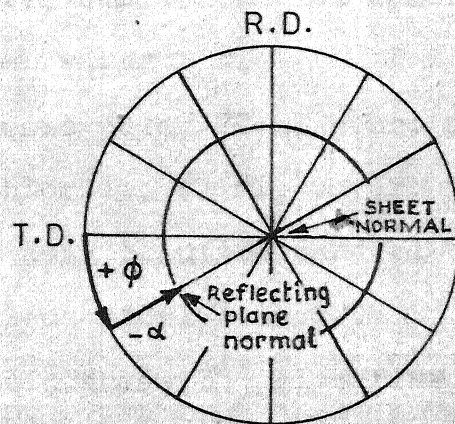
## FIGURE CAPTIONS

- FIG. 33.     Diffractometer geometry for transmission technique.
- FIG. 34.     Use of a polar net to plot the diffracted beam intensity measured in the transmission technique of texture determination.



Diffractometer geometry for transmission technique. The positions of rolling direction (R D) Transverse or cross direction (T.D. or C D) and normal direction (N D) correspond to  $\alpha = 0$  and  $\phi = 0$

Fig. 33



Angular relationships in the transmission pole figure method on the stereographic projection  
 (On the projection the position of the reflecting plane normal is shown for  $\phi = 30^\circ$  and  $\alpha = -30^\circ$ )

Fig. 34

- (2) 2% Nital
- (3) 5 gms anhydrous ferric chloride, 40 ml ethyl alcohol, 60 ml water.
- (4) 5 gms anhydrous ferric chloride, 2 ml conc. hydrochloric acid, 99 ml ethyl alcohol.
- (5) 10 ml conc. hydrochloric acid, 2 ml. conc. nitric acid
- (6) 20 gms copper sulfate, 10 ml conc. hydrochloric acid, 100 ml water
- (7) 3 gms. chromic acid, 20 ml conc. nitric acid, 3 gms ammonium chloride, 40 ml. water.
- (8) 10% oxalic acid solution used electrolytically<sup>49</sup> with stainless steel cathode.
- (9) 33% sulphuric acid, 33% glycerine, 34% water used electrolytically with Pt cathode at 35°C to 60°C<sup>48</sup>.

### III.8 Magnetic Measurements

Magnetic measurements are required to know the total power loss of the textured material and to trace the shape of the hysteresis loop. An Epstein test frame was fabricated for this purpose. For loss measurements using the test frame about 200 gms of material is required. Hence, for each heat treatment it was not possible to test the magnetic losses. So it was decided that only after developing a reasonably good textured material, one whole melt may be used for this test. Since a Princeton Applied Research vibrating sample magnetometer (Model 155) was available (it uses very small specimen about 0.02 to 0.03 gm) the annealed alloys sheet specimens were tested with it to determine their

magnetic characteristics.

If a material is placed in a uniform magnetic field, a dipole moment proportional to the product of the sample susceptibility times the applied field is induced in the sample. If the sample is made to undergo sinusoidal motion as well, an electrical signal can be induced in suitably located stationary pick up coils. This AC signal at the vibration frequency is proportional to the magnitude of the moment induced in the sample. However, it is also proportional to the vibration amplitude and frequency of vibration. This being the case, moment readings taken simply by measuring the amplitude of the signal are subject to errors resulting from variations in the amplitude and frequency of vibration. To overcome this problem, a model 155 magnetometer incorporates a nulling technique to obtain moment readings which are free of these sources of error. By this technique, the effects of vibration amplitude and frequency shifts are cancelled and readings are obtained which vary only with moments, the quantity of interest. The corresponding field strength can be measured by a Gaussmeter. This is the working principle of the vibrating sample magnetometer.

The specimen holder of the magnetometer is very small and maximum size of the sample is restricted to a sheet size of  $\frac{3}{16}$ " x  $\frac{1}{8}$ ". If the grain size of the test material is large, then the magnetic property may vary from sample to sample for the same material because the sample will have few grains and their orientation may be different in different samples.

The placement of specimens in the magnetometer is rather important since the sheets are to be magnetised along the rolling direction the small sheet specimens are to be cut along the rolling direction. For this reason the specimens were cut slightly long in length compared to its width so that there was no error in their placement in the sample holder. The specimens were placed in the specimen holder such that the rolling direction was in the direction of the applied field direction. After turning the magnet power supply, the field strength was slowly increased (till it reached to 10K Oe. field) and its value was noted through a sensitive gaussmeter. The corresponding magnetization in emu was read from the direct digital display of the magnetometer. The values of  $M$  vs  $H$  was plotted in graph paper to get the idea of the magnetic characteristics of the sample. To know approximately the coercive force of the sample, the magnetic field was decreased slowly from saturation value ( $\sim 10K$  Oe) to zero and the corresponding magnetization was noted. It was plotted on a graph paper and the demagnetization curve was extrapolated to  $M = 0$ , to get the coercive force.

Processing data for 48 permalloys.

Speci- men No.	Intended alloy composition in wt					Details of Mechanical forming					Annealing in	
	Ni	Fe	Mn	Al		Hot Rolling Temp in °C	Final size in inches	Tem. of rolling in °C	Cold Rolling Final size in inches	reduc- tion in thick- ness	Argon atmosphere Temp. in °C	Time in hour
1	2	3	4	5	6	7	8	9	10	11	12	
1	48.2	51.1	0.5	0.2	1050-1150	0.092	room temp.	8-9	90	1058	4	
1(a)	48.2	51.1	0.5	0.2	1050-1150	0.092	room temp.	5	92	1058	4	
2	48.2	51.1	0.5	0.2	1050-1150	0.134	room temp.	8	94	900 950 1000 1058 1058 1058 1058 1100	4 4 4 1 2 2½ 4 7½ 2	
2(a)	48.2	51.1	0.5	0.2	1050-1150	0.134	room temp.	5	96	1058 1058 1058 1120 1120 1120 1120	1 8 16 4 6 8 10	



Table IV (Contd.)

1	2	3	4	5	6	7	8	9	10	11	12
3	48.2	51.1	0.5	0.2	1050-1150	0.265	room temp.	7-8	97	1058 1058	2 4
3(a)	48.2	51.1	0.5	0.2	1050-1150	0.265	room temp.	5-6	97.7	1058 1058 1058 1120 1120 1120 1120	4 8 16 4 6 8 10
4(a)	48.2	51.1	0.5	0.2	1050-1150	0.150	room temp.	5-6	96	1058	4
4(b)	48.2	51.1	0.5	0.2	1050-1150	0.150	200	5-6	96	1058	4
4(c)	48.2	51.1	0.5	0.2	1050-1150	0.150	400	5-6	96	1058	4
5(a)	48.2	50.5	1.2	-	1050-1150	0.150	room temp.	5-6	96	1058	4
5(b)	48.2	50.5	1.2	-	1050-1150	0.150	150	5-6	96	1058	4
5(c)	48.2	50.5	1.2	-	1050-1150	0.150	250	5-6	96	1058	4
6(a)	48.2	51.3	0.5	-	1050-1150	0.150	150	5-6	96	1058	4
6(b)	48.2	51.3	0.5	-	1050-1150	0.150	250	5-6	96	1058	4

TABLE V

## Chemical Thinning Solutions for Fe-Ni Alloys

No.	Chemical composition	Working Temp. and time	Performance of the solution
1.	$\text{HNO}_3$ - 25 ml $\text{H}_2\text{O}$ - 75 ml	Room temp.	No reaction could be detected.
2.	$\text{HNO}_3$ - 10 ml $\text{H}_3\text{PO}_4$ - 50 ml $(\text{CH}_3\text{CO})_2\text{O}$ - 40 ml	$40^\circ$ to $60^\circ\text{C}$ 25 to 30 mts	Reaction rate was very slow. Gave very good shinny surface. May be used for chemical polishing for metallography.
3.	$\text{HNO}_3$ - 30 ml $\text{H}_2\text{SO}_4$ - 10 ml $\text{H}_3\text{PO}_4$ - 10 ml $\text{CH}_3\text{COOH}$ - 50 ml	$80^\circ$ - $85^\circ\text{C}$ 4 to 5 minutes at a time	Reaction rate was very fast. Dissolution was not very uniform and produced etch pits. The rate of reaction could be controlled to some extent by controlling bath temperature. The chemical etching along with mechanical polishing gave reasonable thinning.
4.	$\text{HNO}_3$ (conc) - 80 ml HF (5%) - 10 ml	Room temp. 10-15 minutes	Reaction rate is not very fast. Surface was shinny. Thinning was uniform down to 0.002" thickness of specimen. No pit formation. The best of all the chemical thinning reagent.

TABLE VI  
Diffractometer Conditions used for Texture Determination

Radiation	- $\text{MoK}_{\alpha}$
Counter	- Scintillation Counter
Voltage	- 45 kV
Ampere	- 15 mA
Slit system at the source	- $3^{\circ}$ MR Sollar slit
Slit system at the counter	- MR sollar slit with $0.2^{\circ}$ receiving slit
Scaler counting time	- 100 sec.

## CHAPTER IV

### RESULTS

## CHAPTER IV

## RESULTS

Ni-Fe alloys of compositions 48 p.c.t. Nickel were prepared by controlled atmosphere induction melting and then processed through hot rolling and cold rolling followed by annealing in a controlled atmosphere. Details of forming treatment have been presented in an earlier chapter. The experimental results obtained through x-ray diffraction and magnetic measurements have been described in the following sections.

## IV.1 X-Ray Study

## IV.1.1 Bragg Angle Determination

The necessity of Bragg angle determination has been discussed earlier. Since the texture study needed reasonable amount of material and our melt size was small, several alloys of same nominal composition had to be melted. So x-ray diffraction technique needed determination of Bragg angles for each alloy. Annealed fillings from the bulk alloy was used as random specimen and the Bragg angle ( $\theta$ ) for the two prominent reflections, (111) and (200), were determined for each alloy. The results are presented in Table VII. As seen from the data, the variation in  $\theta$  is not large. Hence, for the same nominal composition, the true alloy compositions are expected to be quite close to each other.

#### IV.1.2 Texture Determination

Texture was determined by using a transmission texture goniometer. Since texture determination was done by measuring the diffracted beam intensity for each angular setting of the texture goniometer (done manually), only one quarter of the pole figure was determined. Usually the cold rolled texture for each specimen was determined for variation in cold reduction and rolling temperature. Cold rolled texture of some of the specimen are shown in Figs. 35 to 42. Since there was practically no change in texture if the difference in the percent reduction was small, some of the cold rolled pole figures are not shown here. For comparison, the (111) and (200) pole figures of cold rolled Cu, obtained by Goodman and Hu<sup>50</sup> are shown in Fig. 12 and Fig. 13.

Cold rolled Ni-Fe alloys were annealed at various temperatures and for various lengths of time to determine the most suitable temperature to produce the desired texture, the texture data obtained has been presented here in two ways - (1) in the pole figures showing the actual distribution of intensity of (111) reflection and (2) in tabular form summarising the peak intensities obtained at different locations of the pole figures. The pole figures are presented in Fig. 43 to 73 and the intensity data is tabulated in Table VIII. Since in all the pole figures, the back-ground intensities were rather low, only about 100 cps (out of which counter noise was about 30-40 cps) the intensity of peaks are presented relative to the

lowest background observed ( $\sim 100$  cps). Blank areas in the pole figure represent relative intensities less than 4, usually between 1 and 3. All the annealed textures showed essentially the same locations of peak intensities (see pole figures in Figs. 43 to 73). The peak intensity positions have been identified as poles 1 through 8. In tabulating the intensity data the relative peak intensities corresponding to these pole locations have been used. For each alloy the process variables are mentioned in the table and for ease of identification of pole figures, the figure numbers are also mentioned. Here also for a few cases the pole densities (the relative intensities of the (111) reflection at the appropriate pole locations) were rather low and for these cases the pole figures have not been determined in detail and hence not shown. The relative intensity<sup>of</sup>/peak positions corresponding to the poles 1 through 8 were, however, determined. Since only one quarter of pole figure was determined, for proper texture identification it was necessary to determine the (200) pole figure for one specimen besides its (111) pole figure. The (200) pole figure for specimen 6(b), annealed at  $1058^{\circ}\text{C}$  for 4 hrs has been shown in Fig. 72. A composite pole figure showing the (111) and (200) peak pole locations for this specimen is shown in Fig. 74.

#### IV.2 Magnetic Measurements

Since the melt size was small and magnetic loss measurement required large amount of specimen and the fact that the Epstein test frame could not be calibrated within

the limited time, power loss measurement was not possible. Using <sup>the</sup>available Princeton Applied Research Model 155 magnetometer, some magnetic tests were performed with small pieces of annealed sheet specimens. All the specimens, however, could not be tested because of the breakdown of the magnet. The results obtained through the magnetometer are shown in Fig. 74 to 75 as plots of  $M$  vs.  $H$  in the first quadrant. In one case, the coercive field  $H_c$  was determined by extrapolation of the demagnetisation curve obtained in the first quadrant.



## FIGURE CAPTIONS

- FIG. 35. (111) pole figure of sample 1(a), 90% cold rolled at room temperature.
- FIG. 36. (111) pole figure of sample 2, 94% cold rolled at room temperature.
- FIG. 37. (111) pole figure of sample 2(a), 96% cold rolled at room temperature.
- FIG. 38. (111) pole figure of sample 3, 97% cold rolled at room temperature.
- FIG. 39. (111) pole figure of sample 4(b), 96% cold rolled at 200°C.
- FIG. 40. (111) pole figure of sample 4(c), 96% cold rolled at 400°C.
- FIG. 41. (111) pole figure of sample 5(b), 96% cold rolled at 150°C.
- FIG. 42. (111) pole figure of sample 5(c), 96% cold rolled at 250°C.

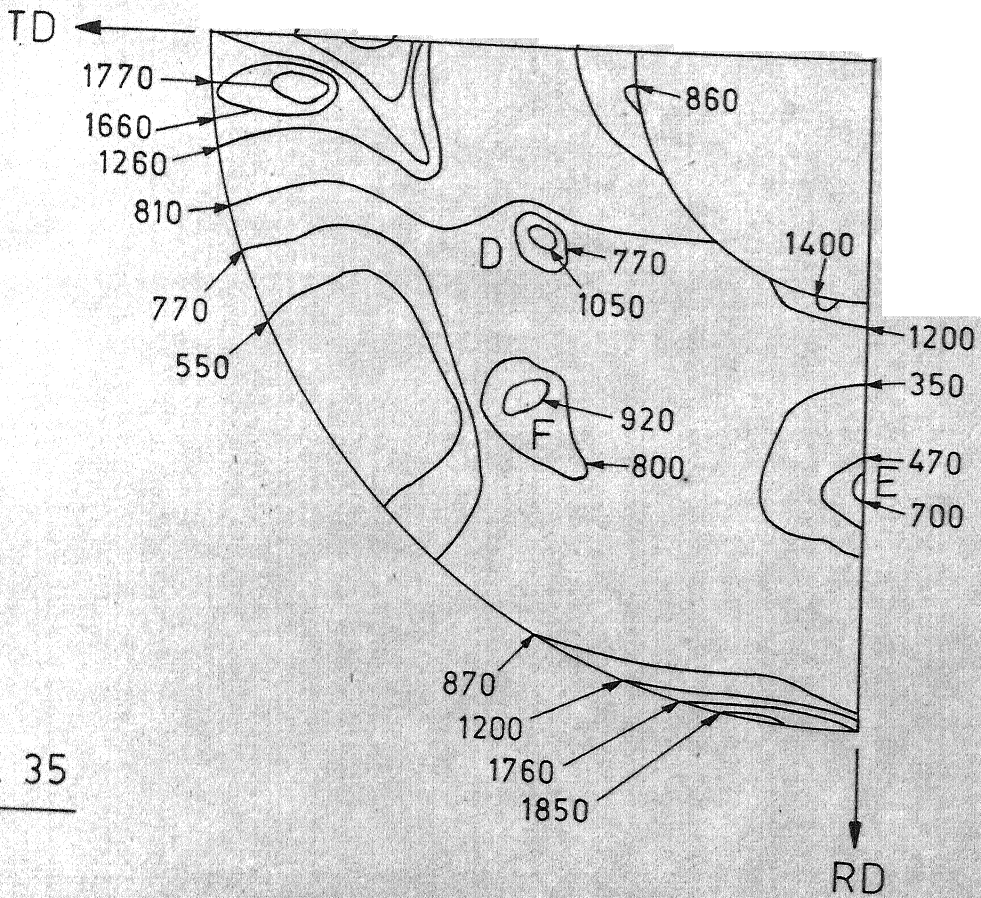


Fig. 35

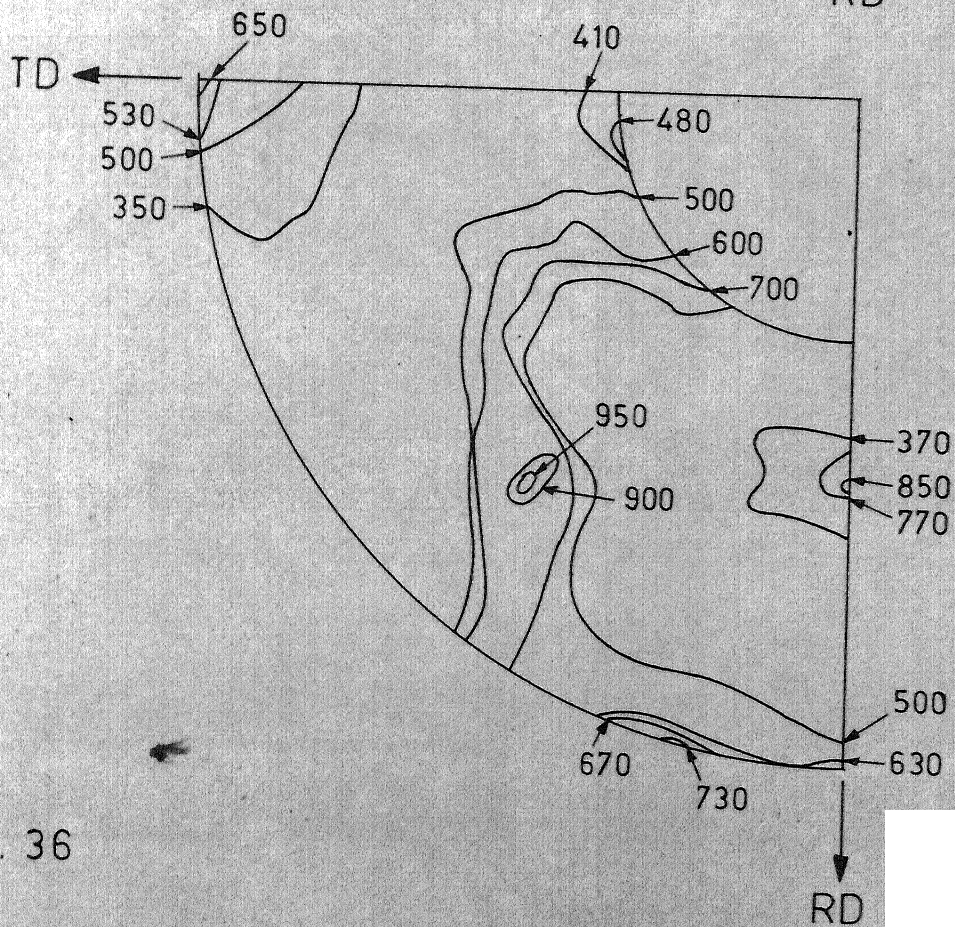


Fig. 36

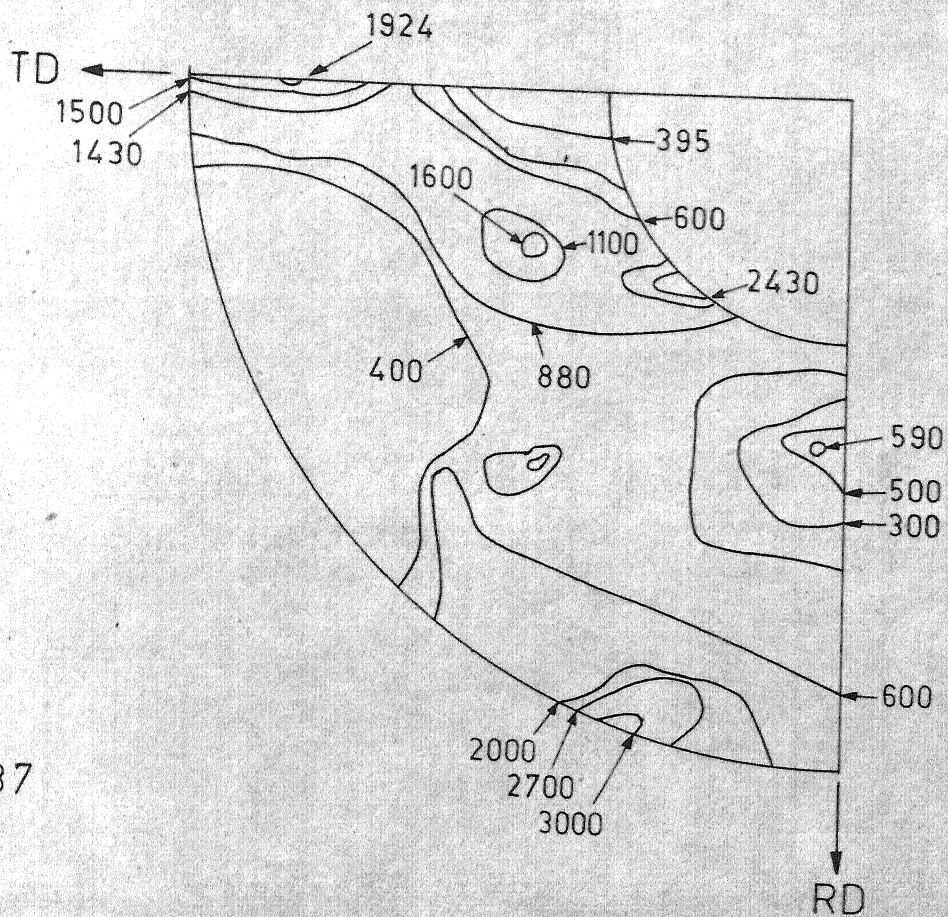


Fig. 37

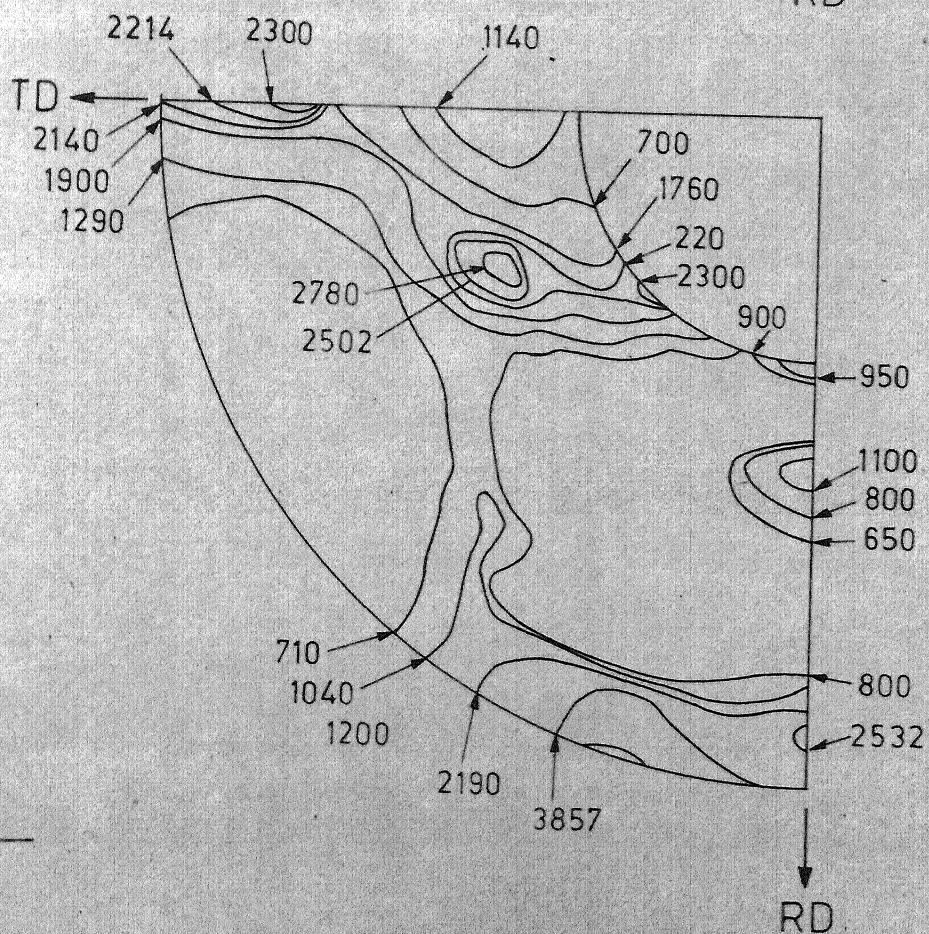


Fig. 38



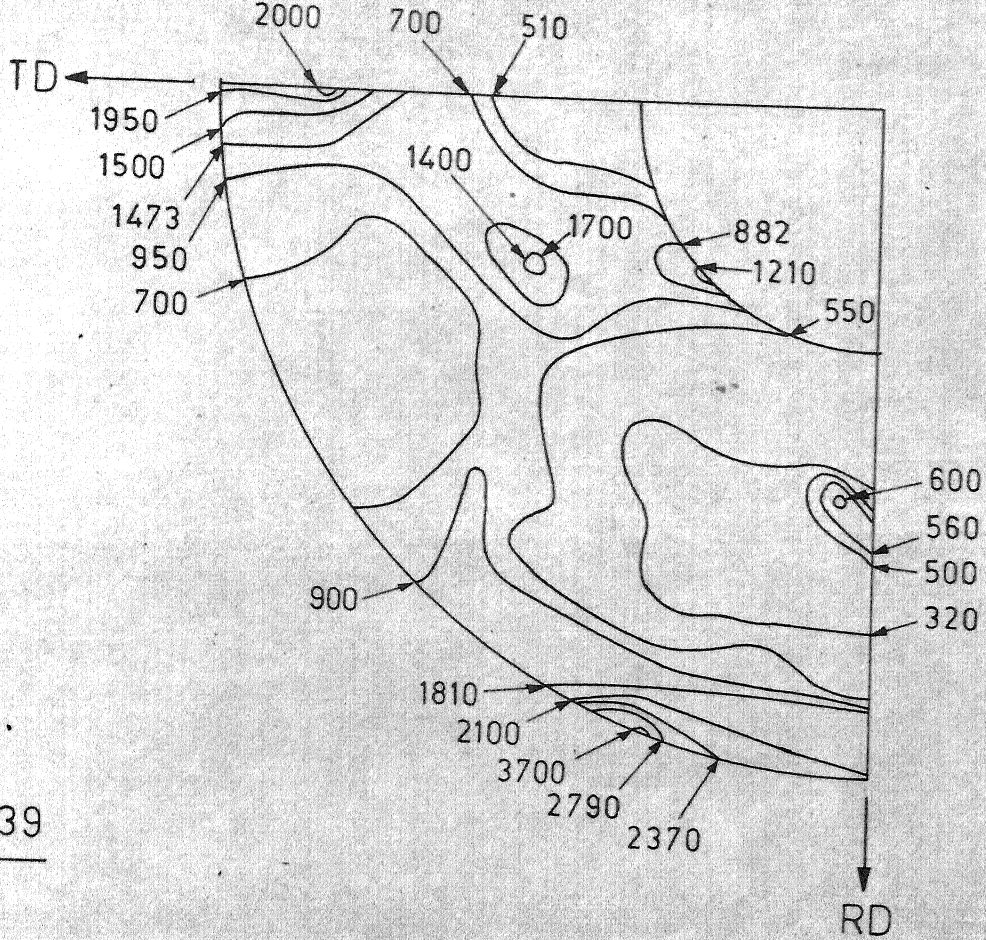


Fig. 39

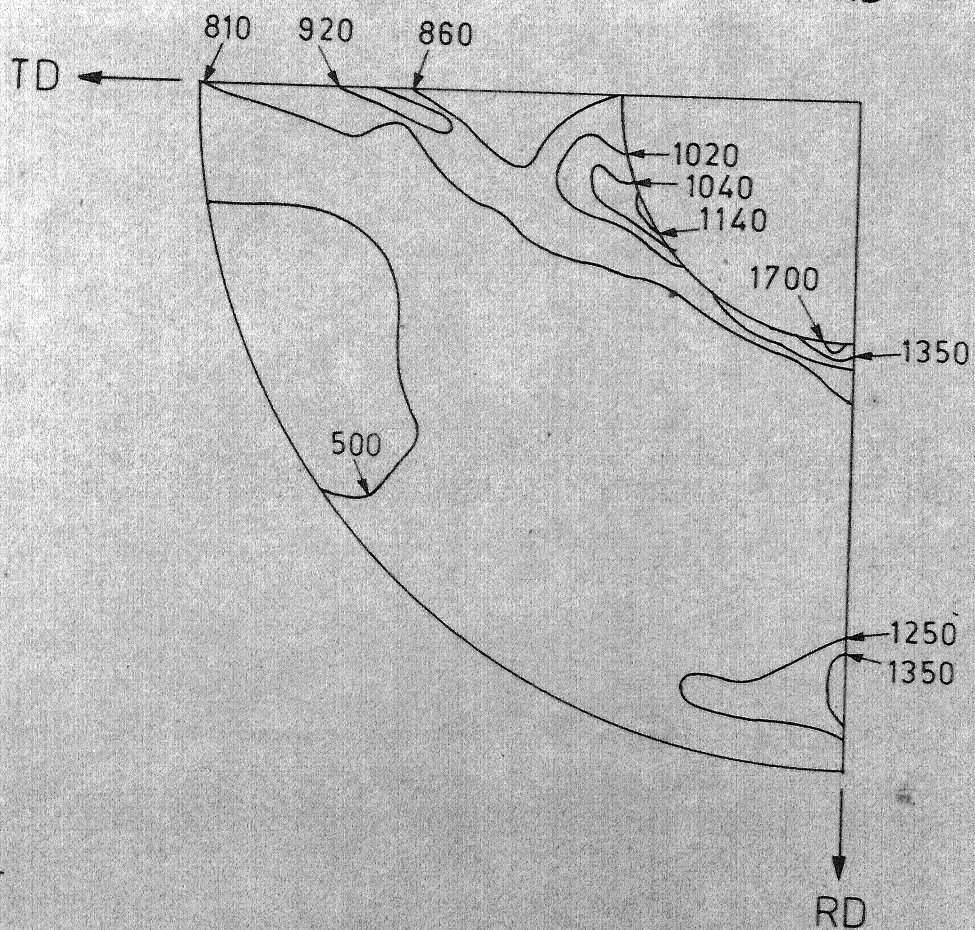


Fig. 40

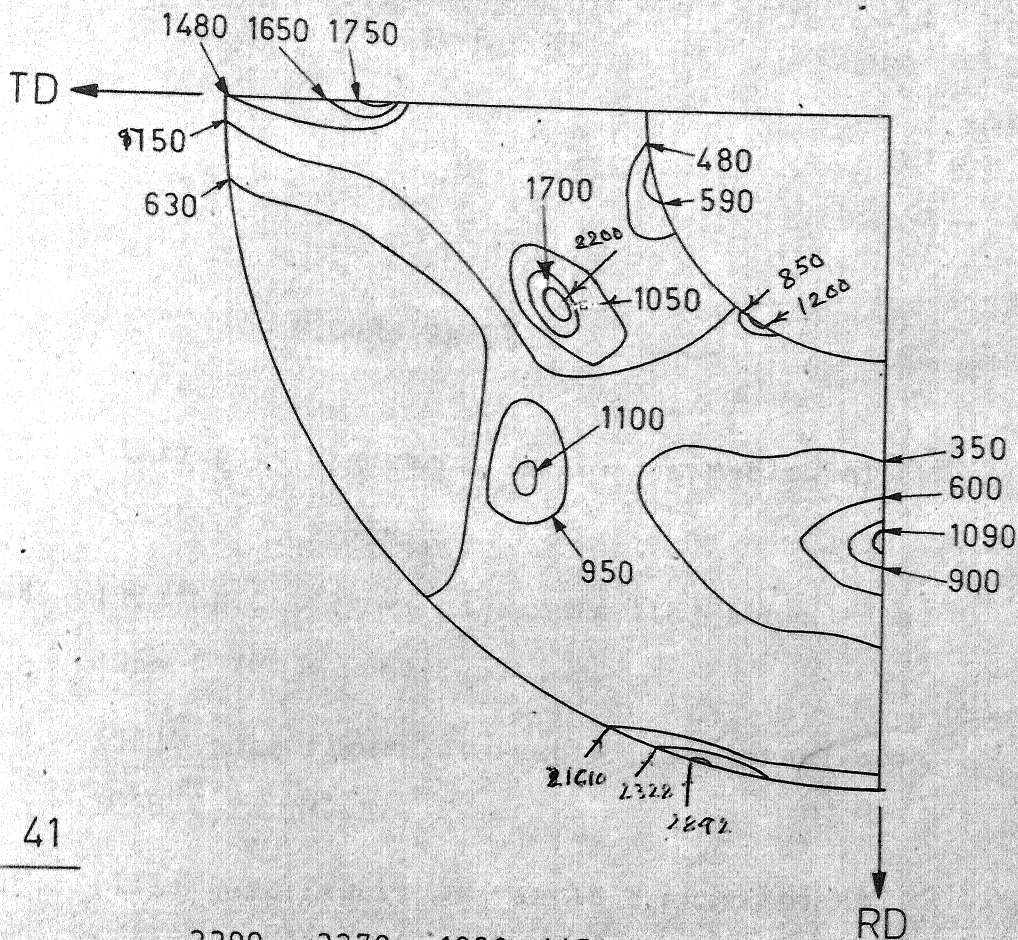


Fig. 41

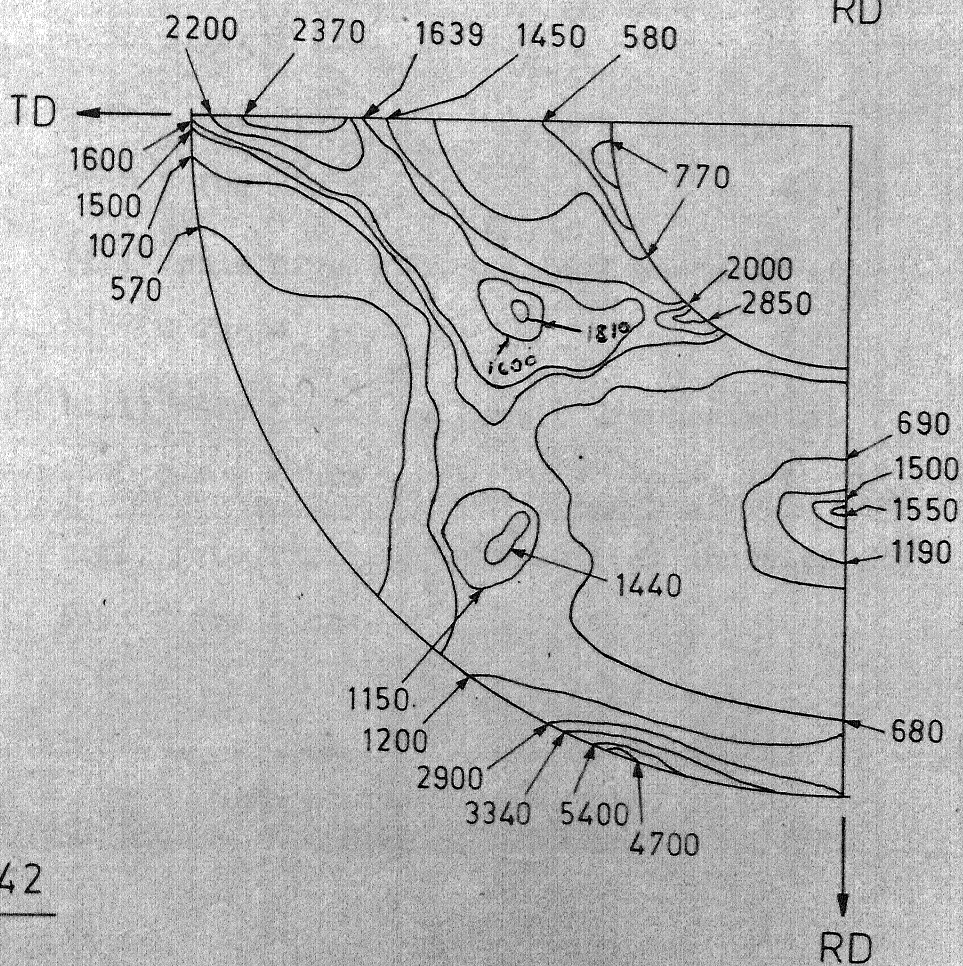


Fig. 42



## FIGURE CAPTIONS

- FIG. 43. (111) pole figure of sample 1 annealed at  $1058^{\circ}\text{C}$  for 4 hrs.
- FIG. 44. (111) pole figure of sample 1(a) annealed at  $1058^{\circ}\text{C}$  for 4 hrs.
- FIG. 45. (111) pole figure of sample 1(a) annealed at  $1058^{\circ}\text{C}$  for  $7\frac{1}{2}$  hrs.
- FIG. 46. (111) pole figure of sample 2 annealed at  $1058^{\circ}\text{C}$  for 1 hrs.
- FIG. 47. (111) pole figure of sample 2 annealed at  $1058^{\circ}\text{C}$  for 2 hrs.
- FIG. 48. (111) pole figure of sample 2 annealed at  $1058^{\circ}\text{C}$  for 4 hrs.
- FIG. 49. (111) pole figure of sample 2 annealed at  $1100^{\circ}\text{C}$  for 4 hrs.
- FIG. 50. (111) pole figure of sample 2(a) annealed at  $1058^{\circ}\text{C}$  for 4 hrs.

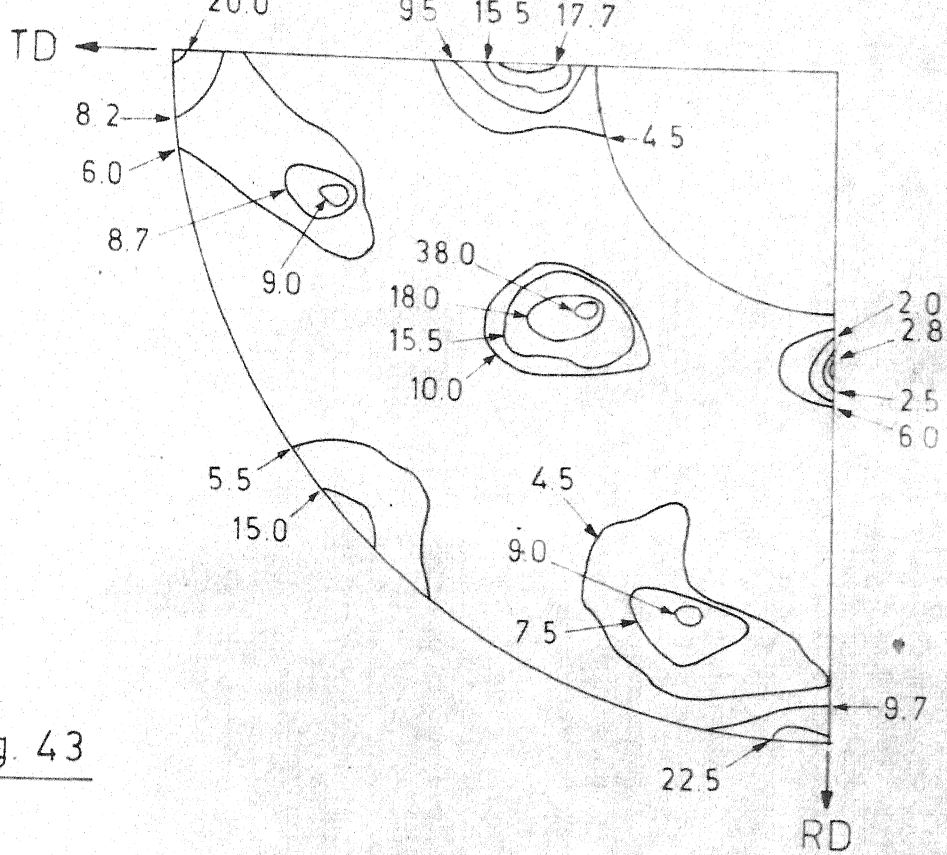


Fig. 43

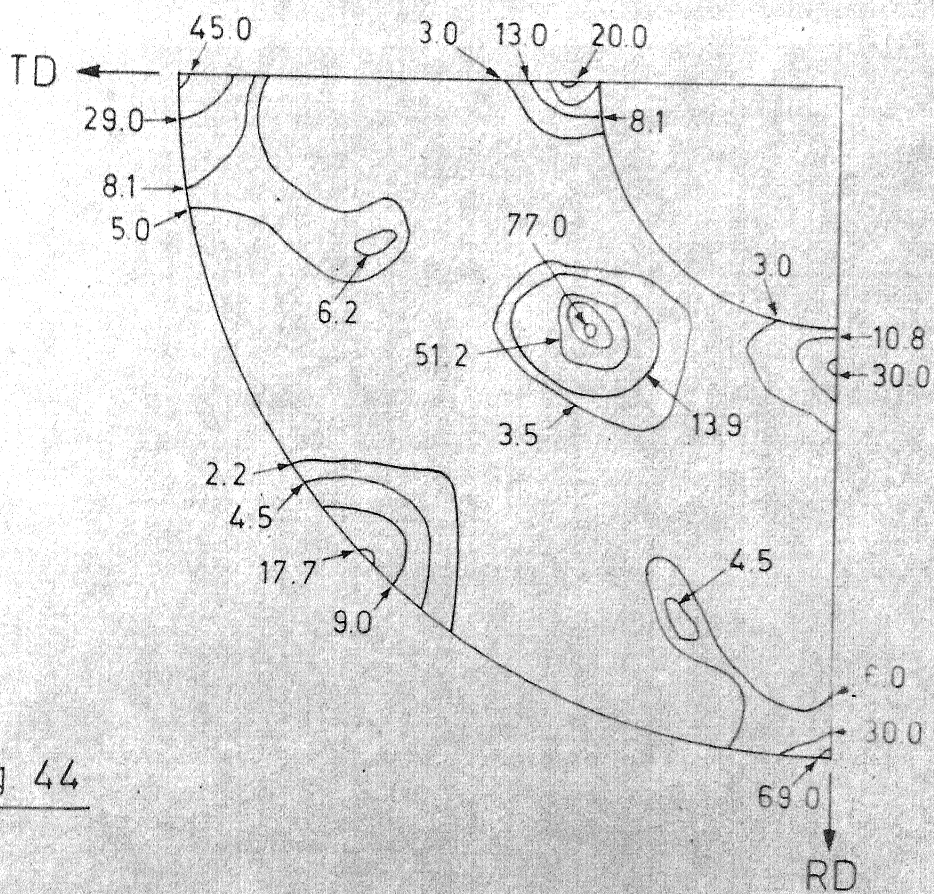


Fig 44

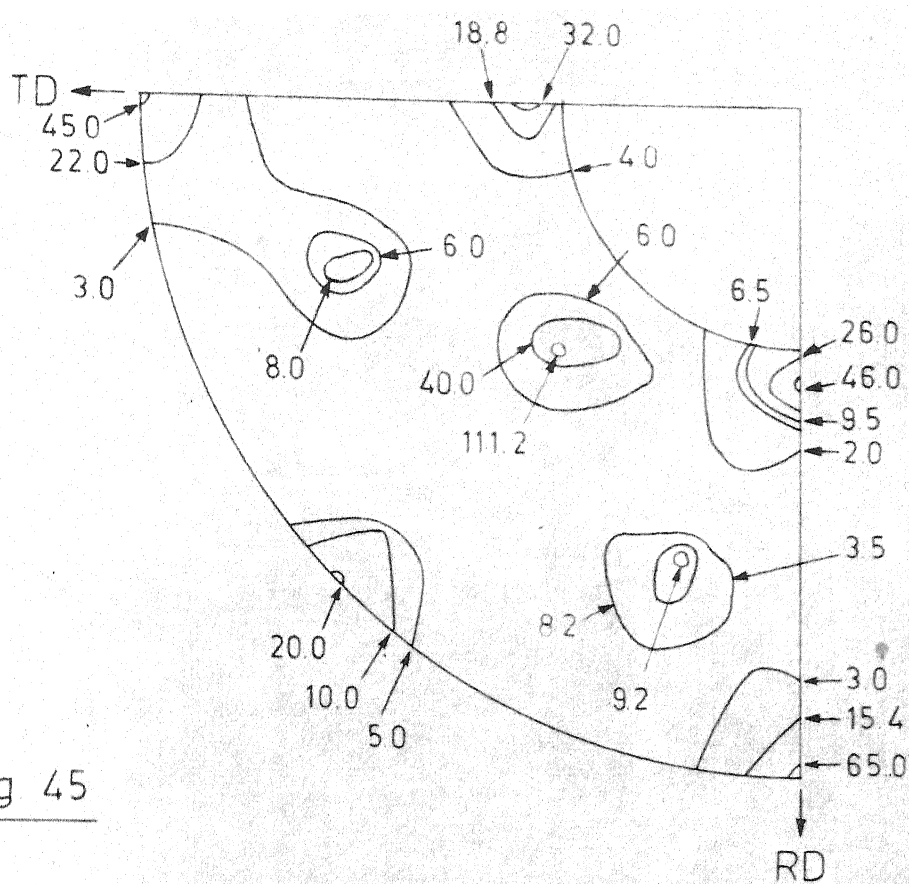


Fig. 45

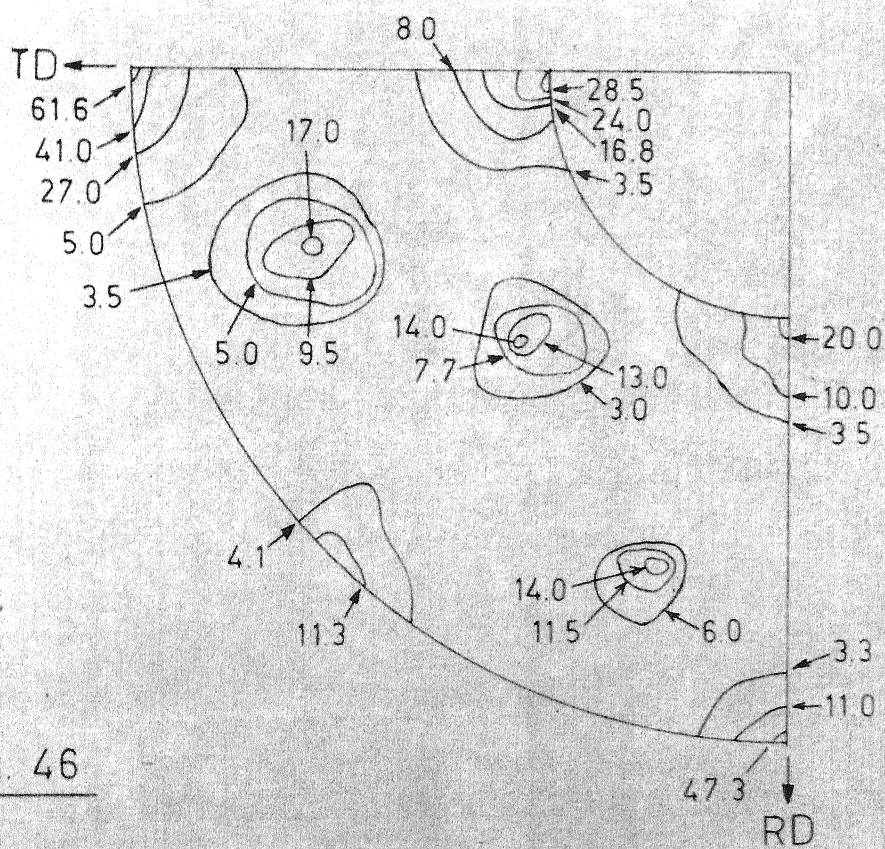


Fig. 46



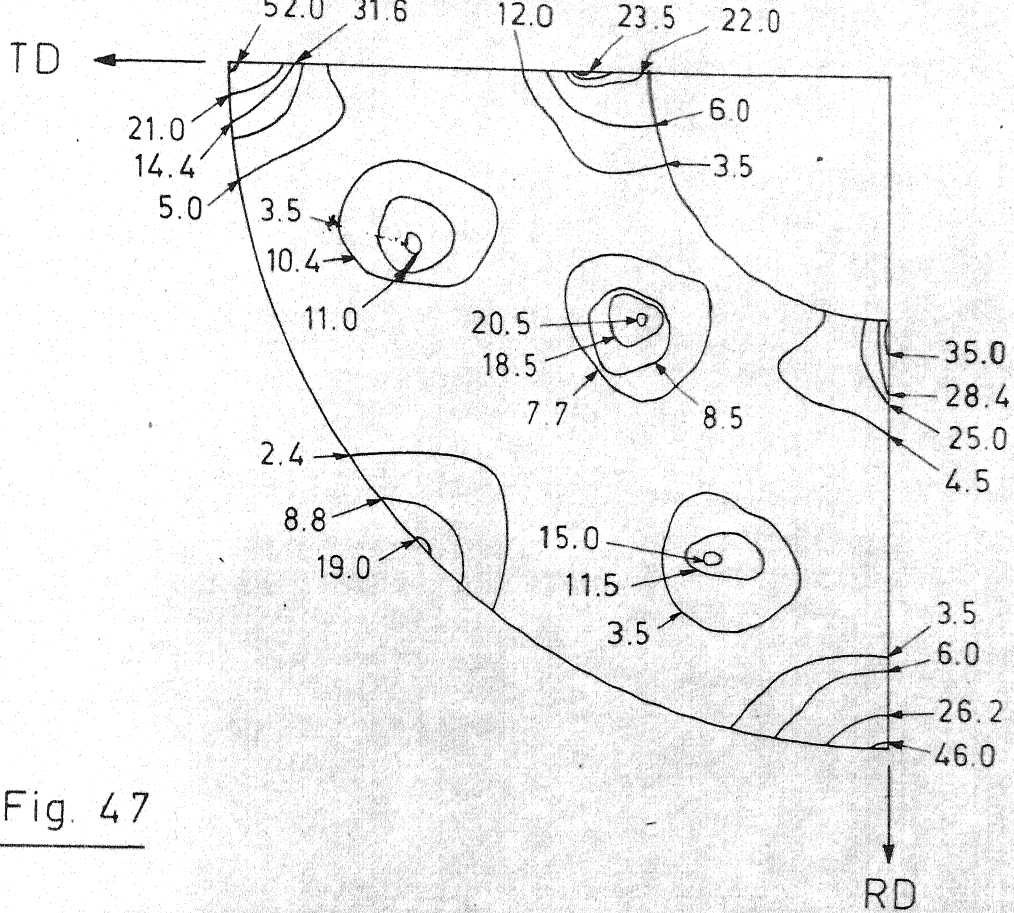


Fig. 47

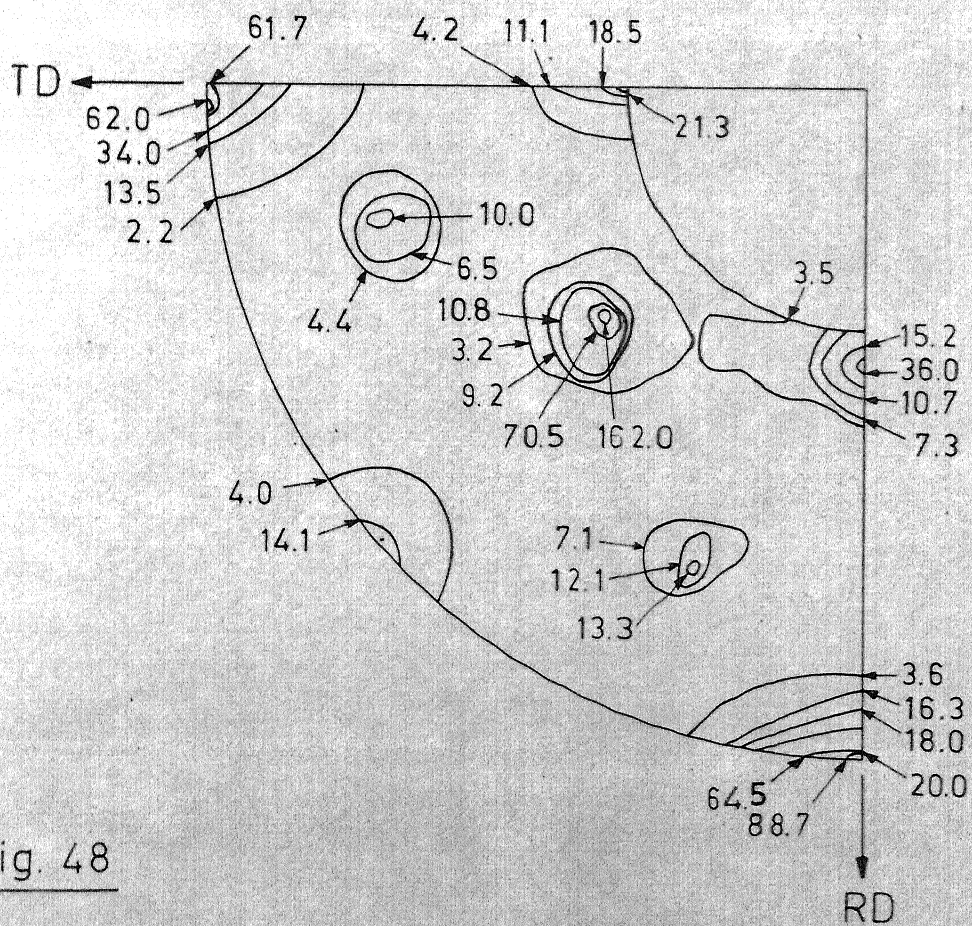


Fig. 48

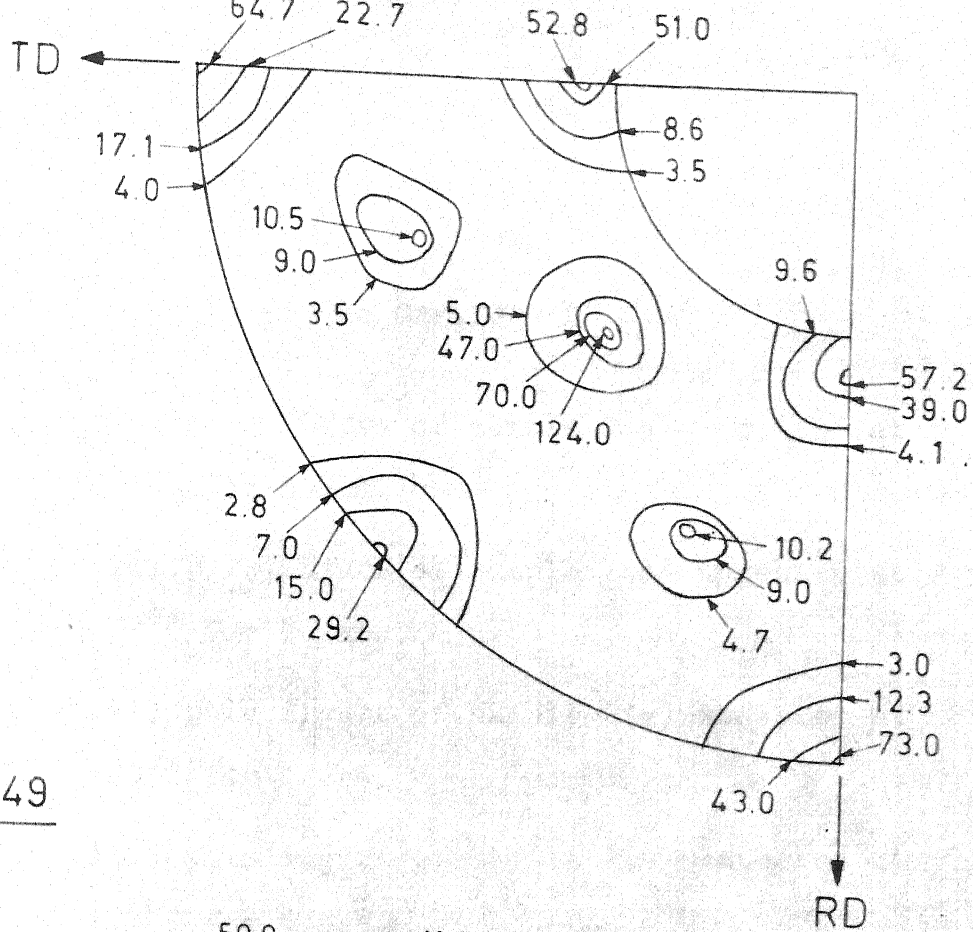


Fig 49

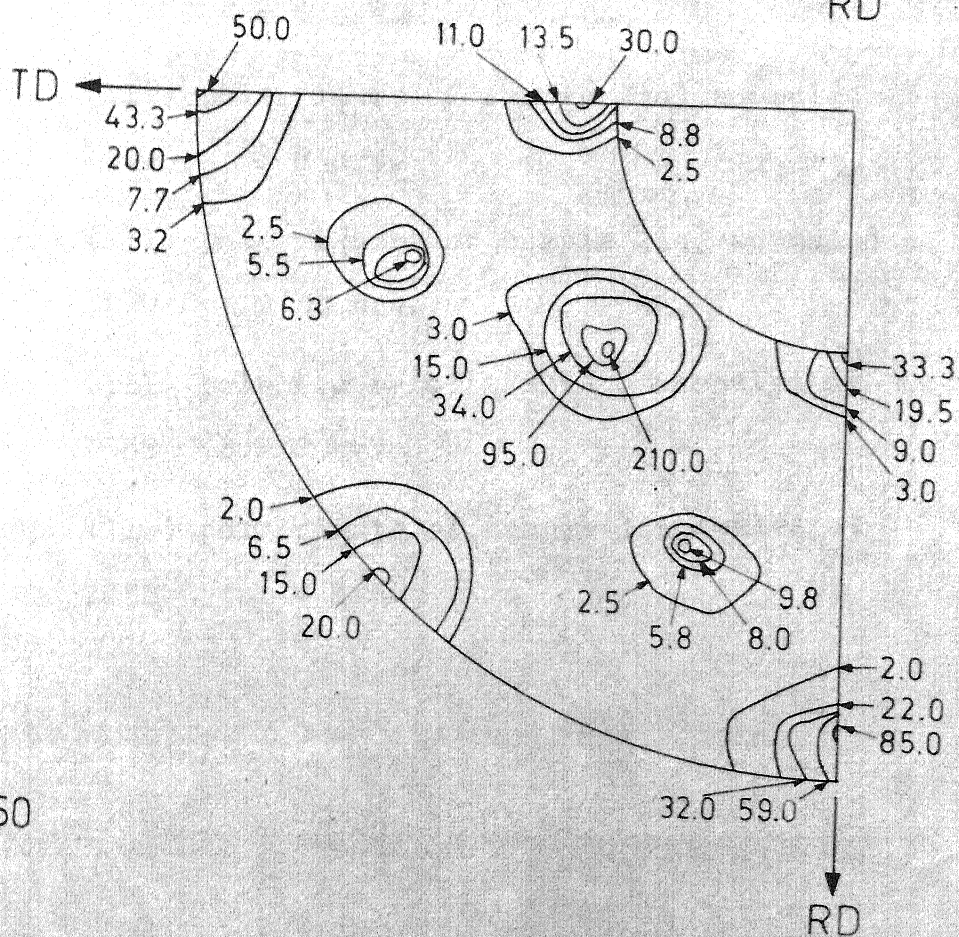


Fig. 50

## FIGURE CAPTIONS

- FIG. 51. (111) pole figure of sample 2(a) annealed at 1058°C for 8 hrs.
- FIG. 52. (111) pole figure of sample 2(a) annealed at 1058°C for 16 hrs.
- FIG. 53. (111) pole figure of sample 2(a) annealed at 1120°C for 4 hrs.
- FIG. 54. (111) pole figure of sample 2(a) annealed at 1120°C for 6 hrs.
- FIG. 55. (111) pole figure of sample 2(a) annealed at 1120°C for 8 hrs.
- FIG. 56. (111) pole figures of sample 2(a) annealed at 1120°C for 10 hrs.
- FIG. 57. (111) pole figure of sample 3 annealed at 1058°C for 2 hrs.
- FIG. 58. (111) pole figure of sample 3 annealed at 1058°C for 4 hrs.



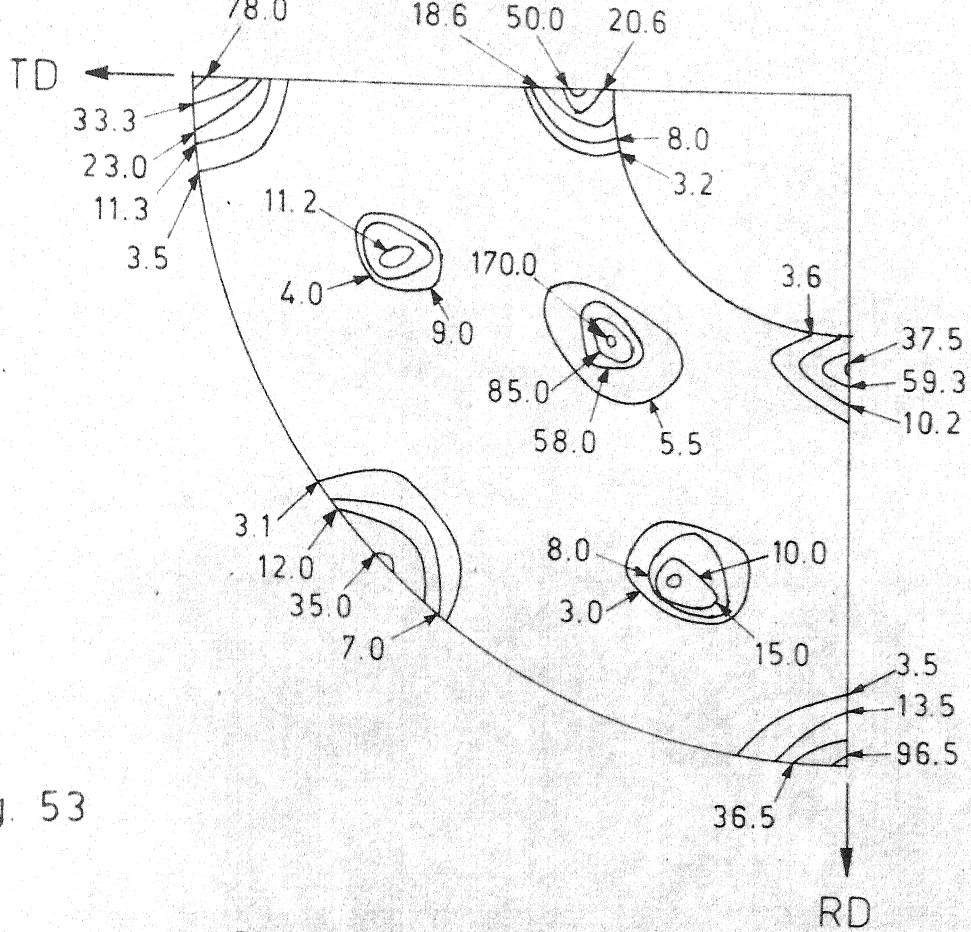


Fig. 53

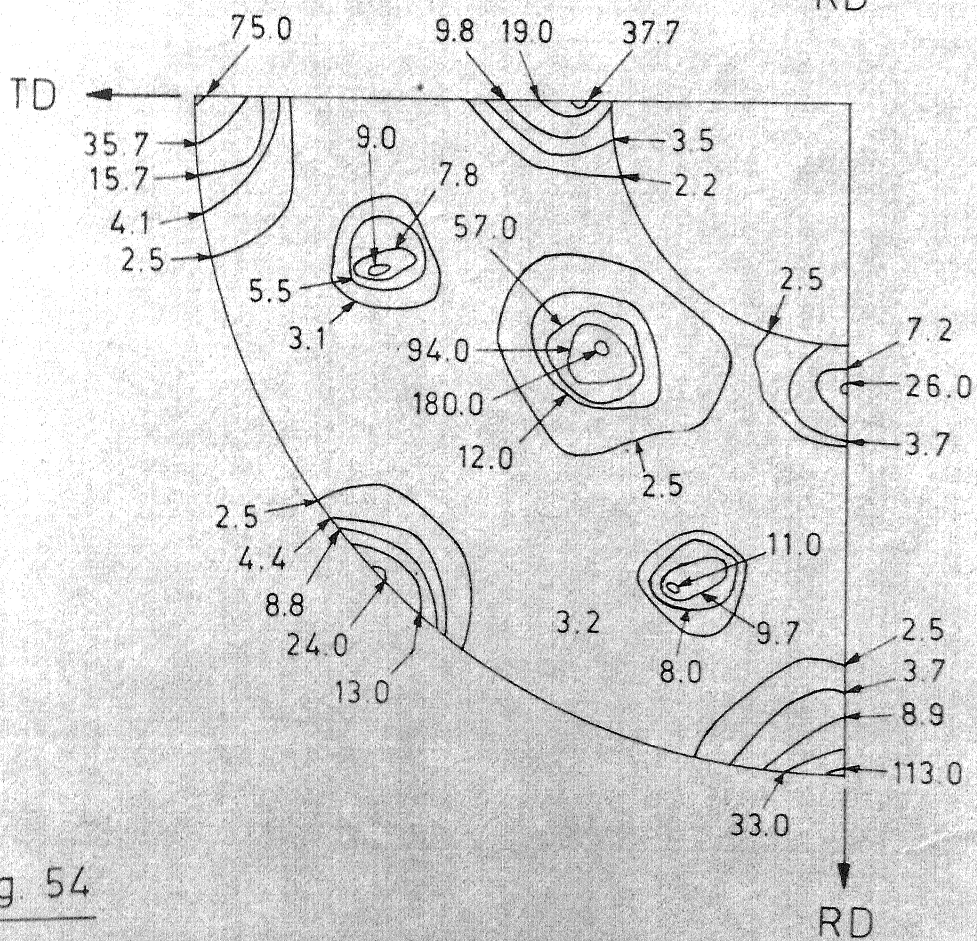


Fig. 54

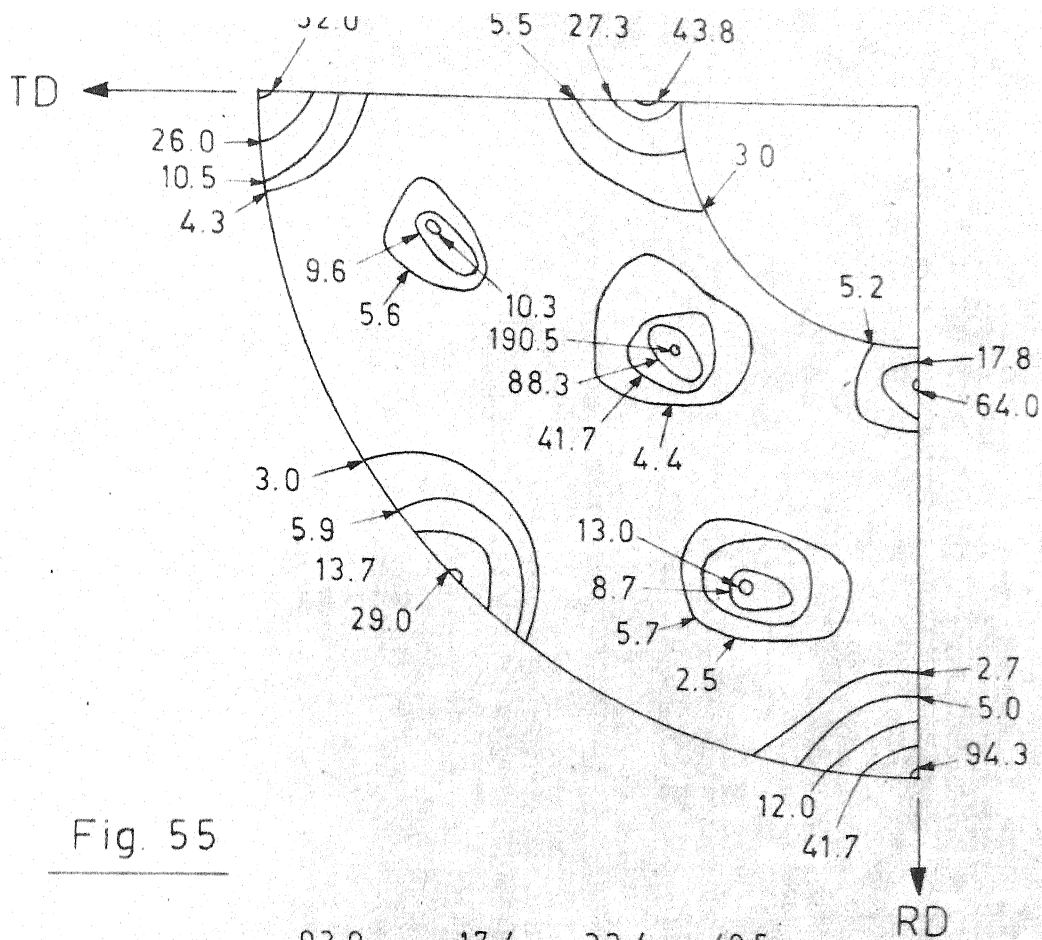


Fig. 55

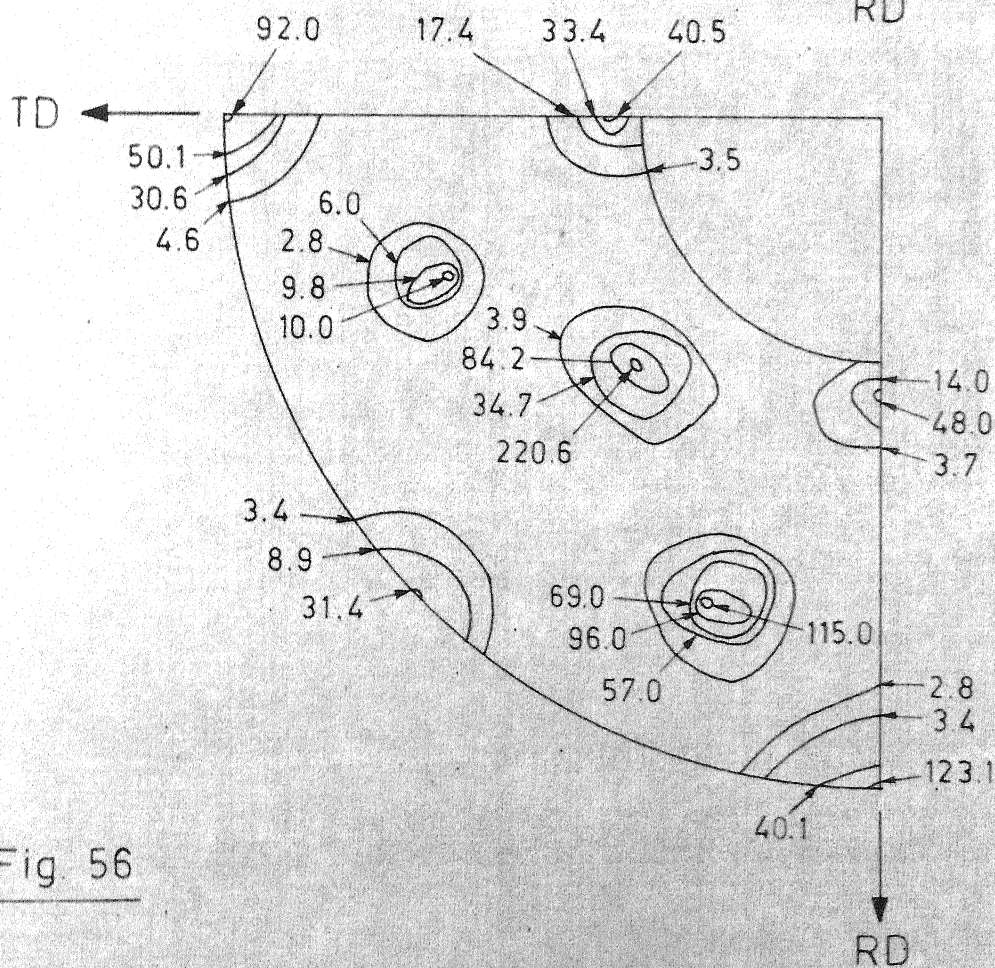


Fig. 56

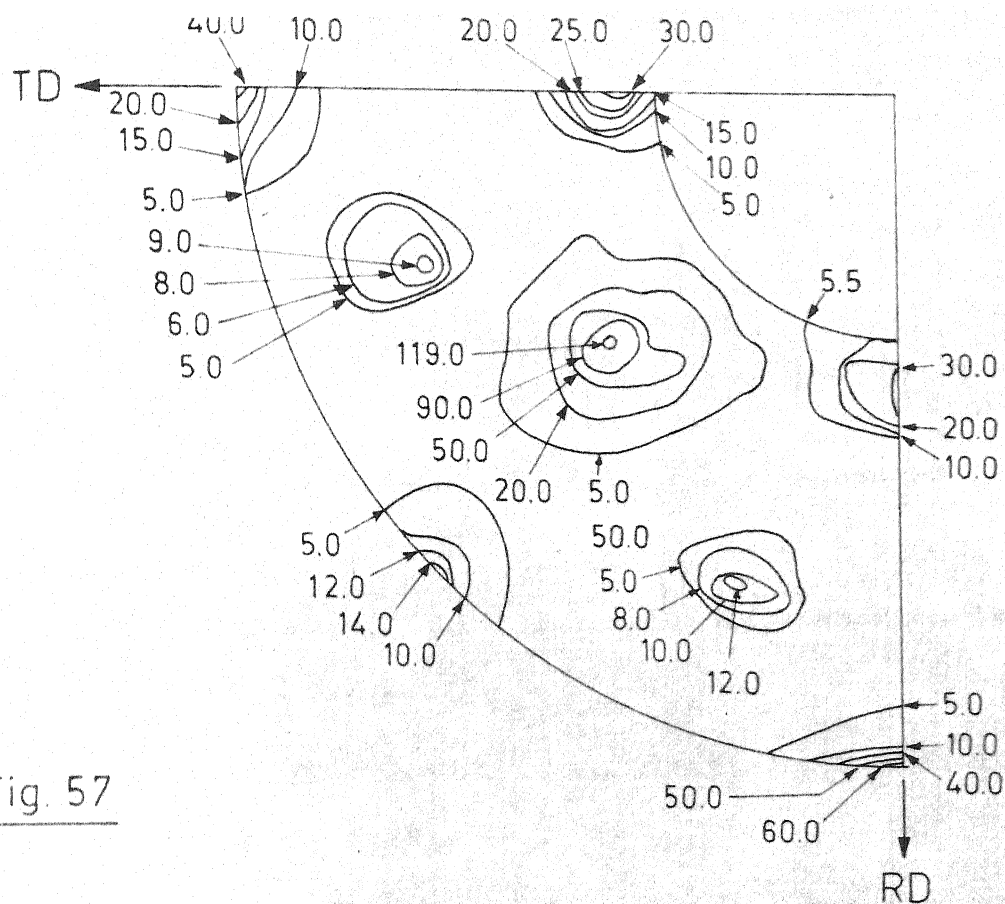


Fig. 57

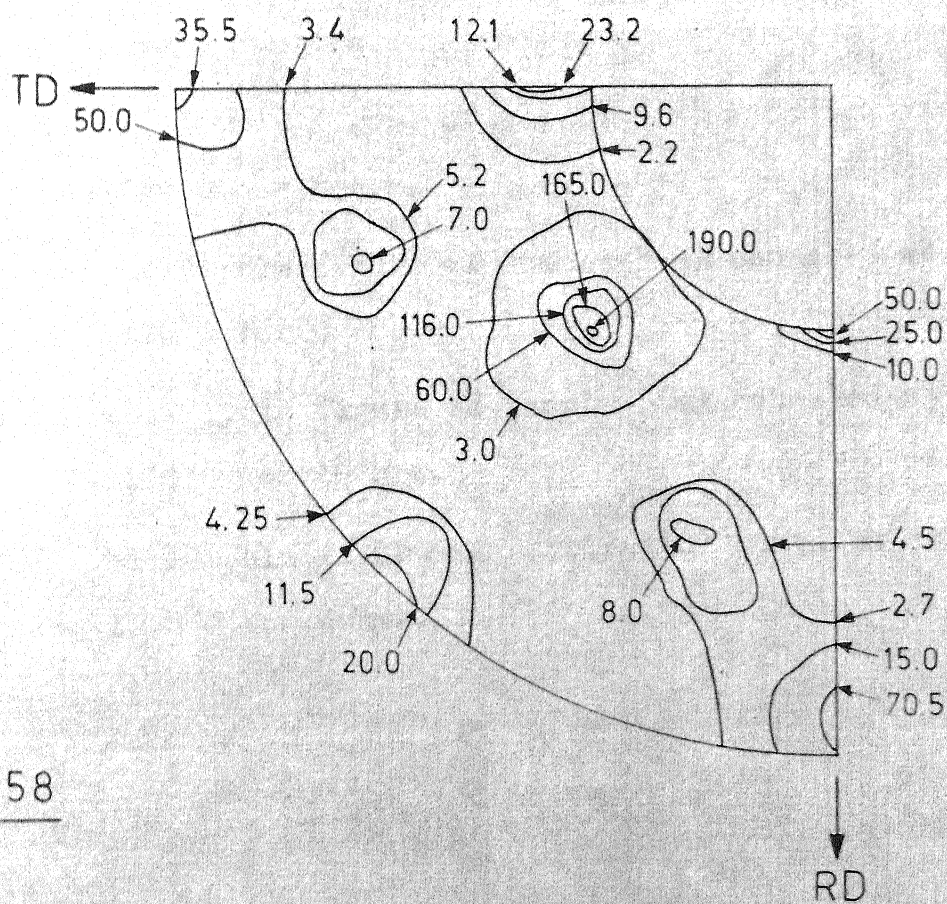


Fig. 58

## FIGURE CAPTIONS

- FIG. 59. (111) pole figure of sample 3(a) annealed at  $1058^{\circ}\text{C}$  for 4 hrs.
- FIG. 60. (111) pole figure of sample 3(a) annealed at  $1058^{\circ}\text{C}$  for 8 hrs.
- FIG. 61. (111) pole figure of sample 3(a) annealed at  $1058^{\circ}\text{C}$  for 16 hrs.
- FIG. 62. (111) pole figure of sample 3(a) annealed at  $1120^{\circ}\text{C}$  for 4 hrs.
- FIG. 63. (111) pole figure of sample 3(a) annealed at  $1120^{\circ}\text{C}$  for 6 hrs.
- FIG. 64. (111) pole figure of sample 3(a) annealed at  $1120^{\circ}\text{C}$  for 8 hrs.
- FIG. 65. (111) pole figure of sample 3(a) annealed at  $1120^{\circ}\text{C}$  for 10 hrs.
- FIG. 66. (111) pole figure of sample 4(b) annealed at  $1058^{\circ}\text{C}$  for 4 hrs.



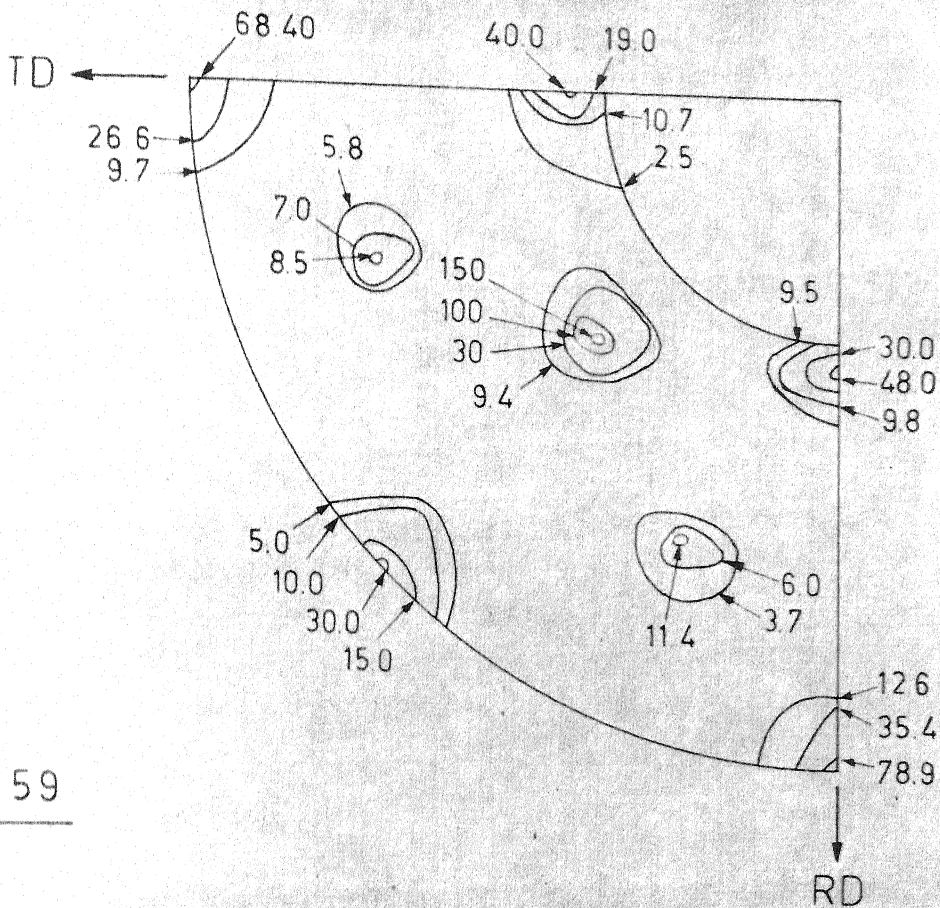


Fig 59

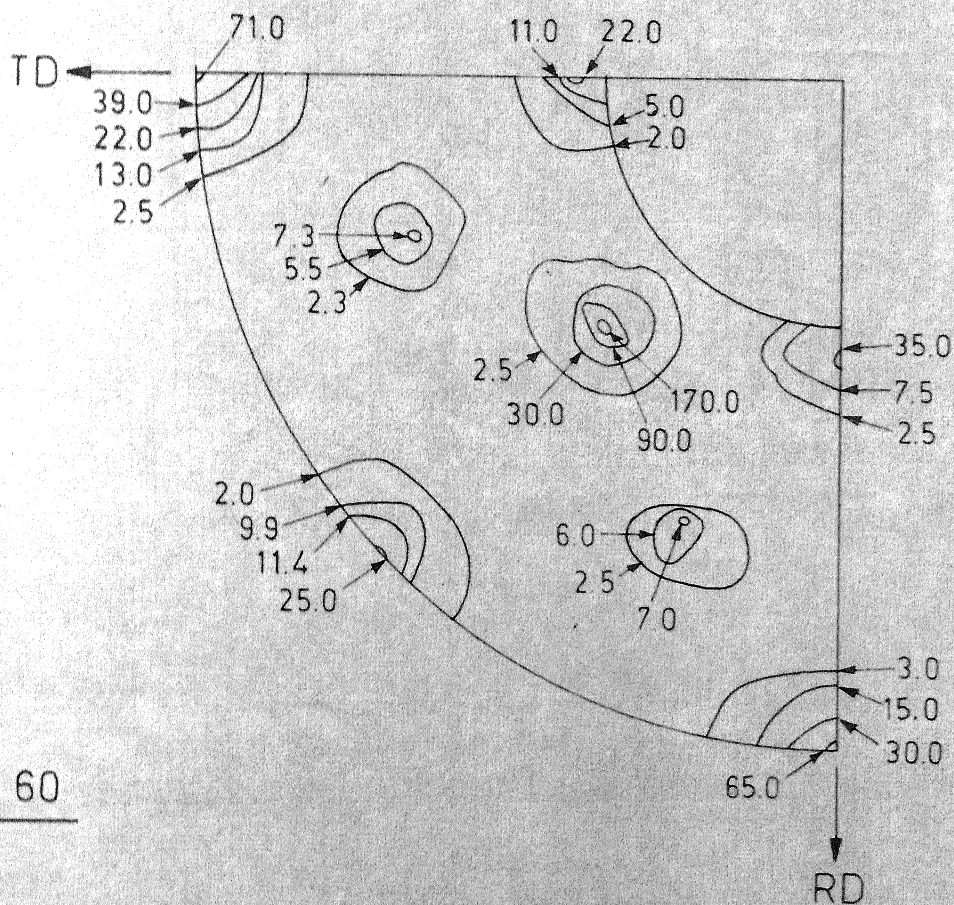


Fig. 60



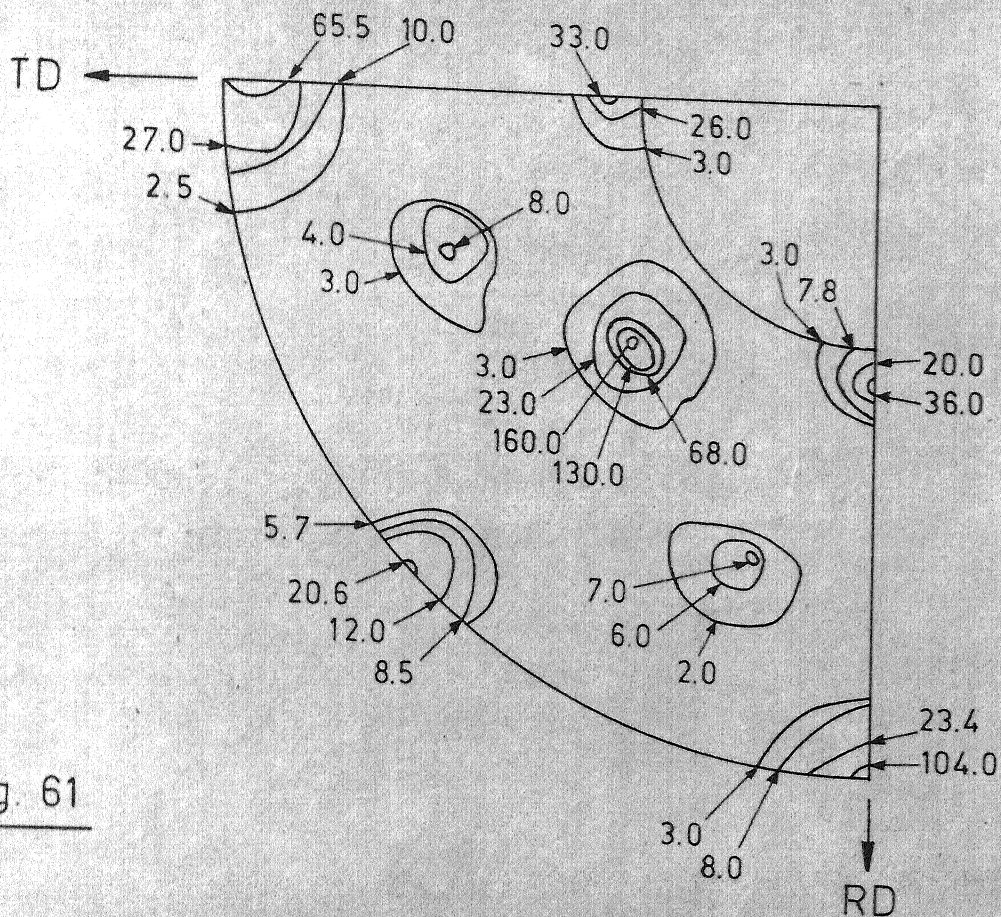


Fig. 61

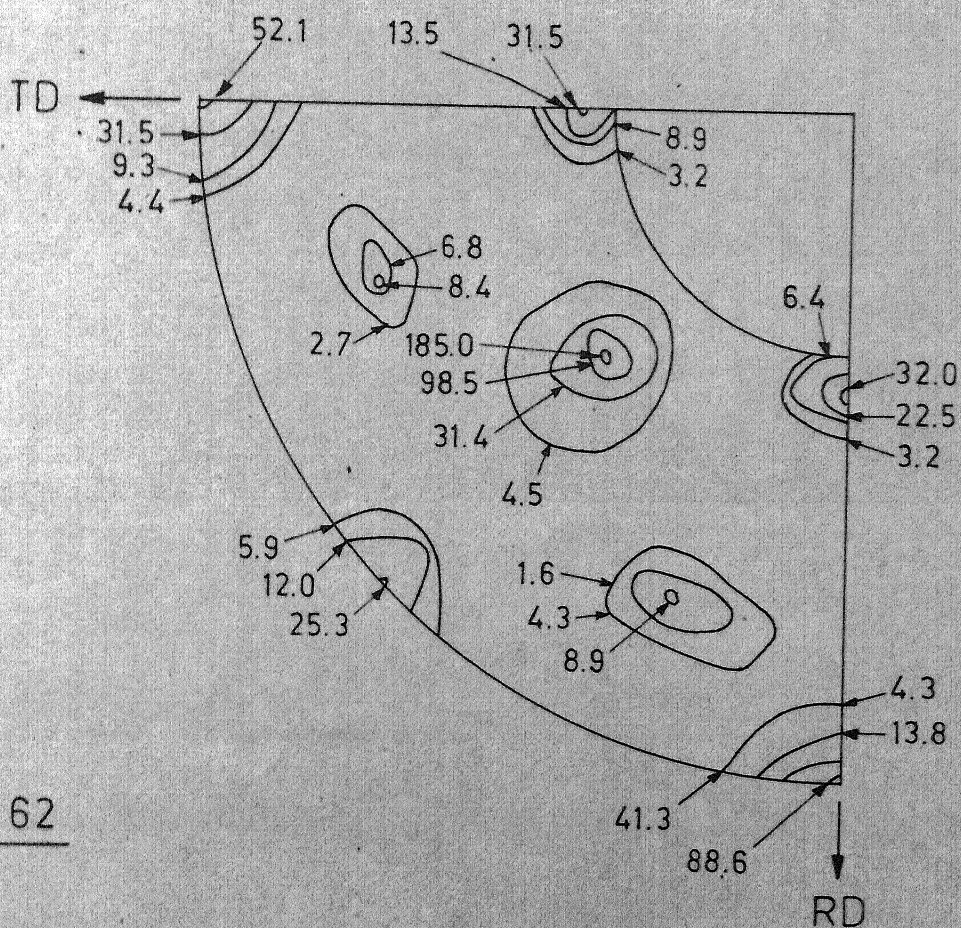


Fig. 62



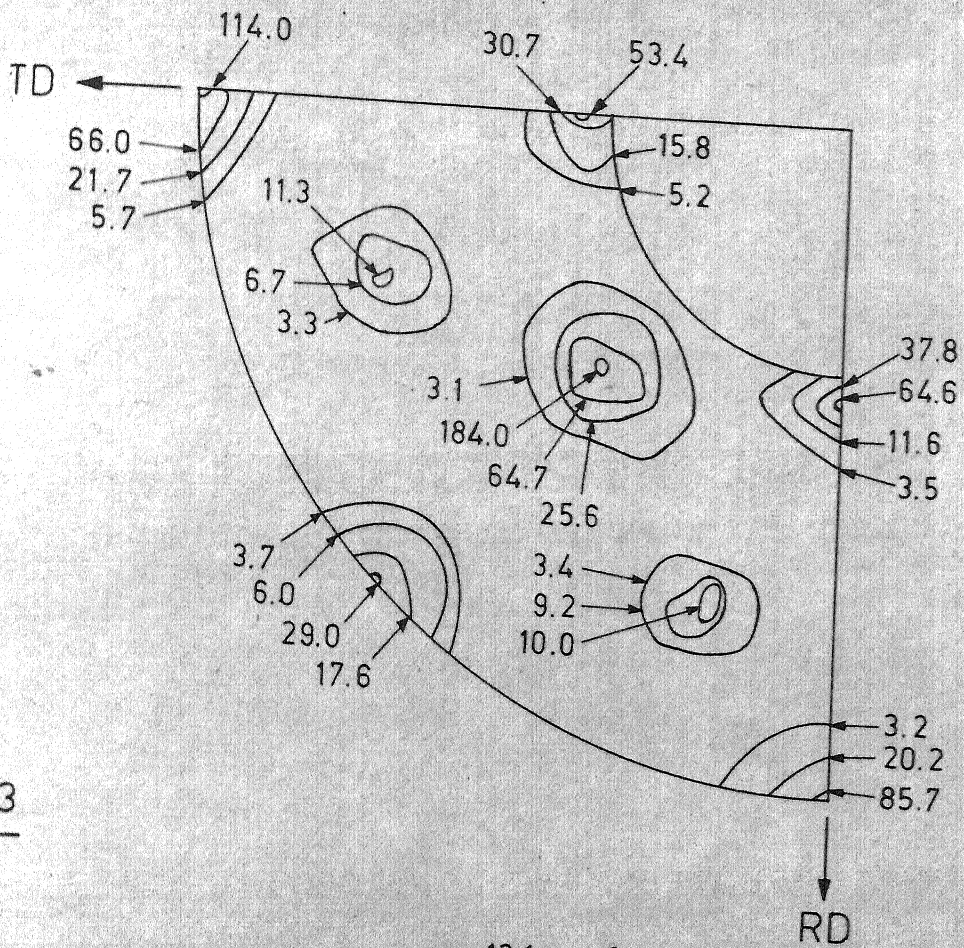


Fig. 63

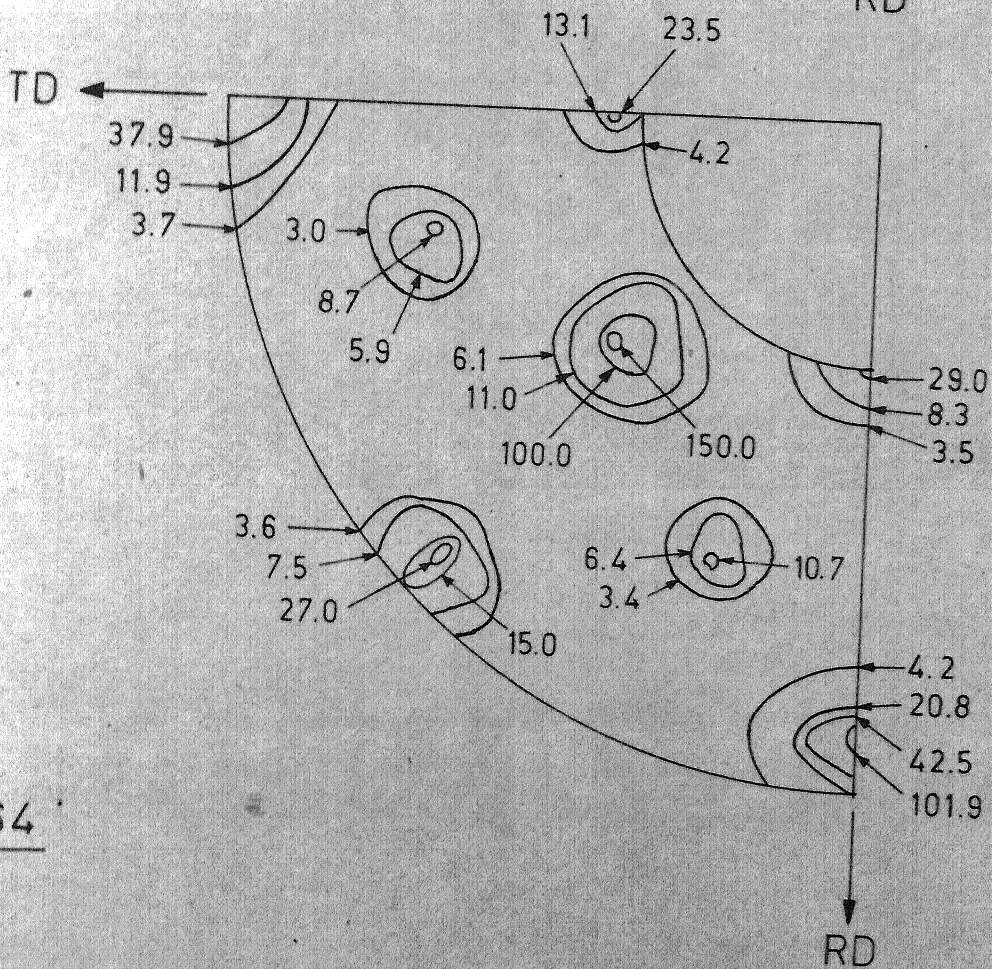


Fig. 64



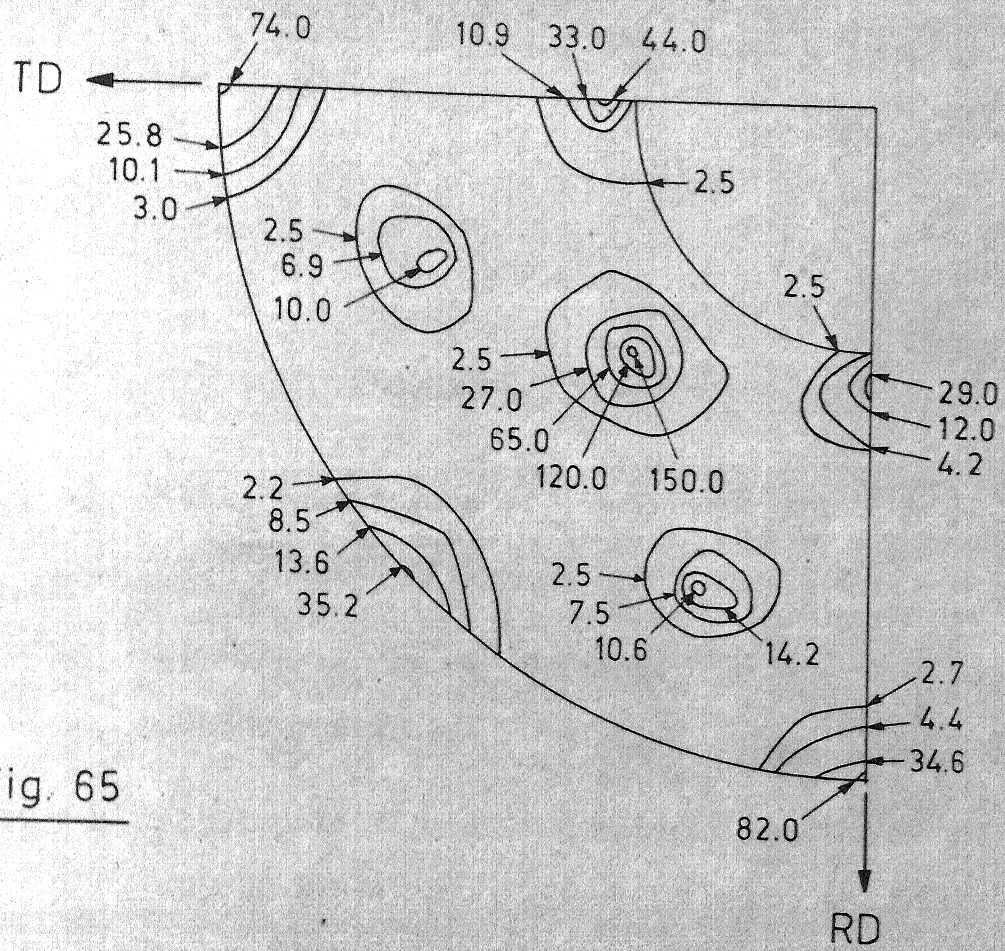


Fig. 65

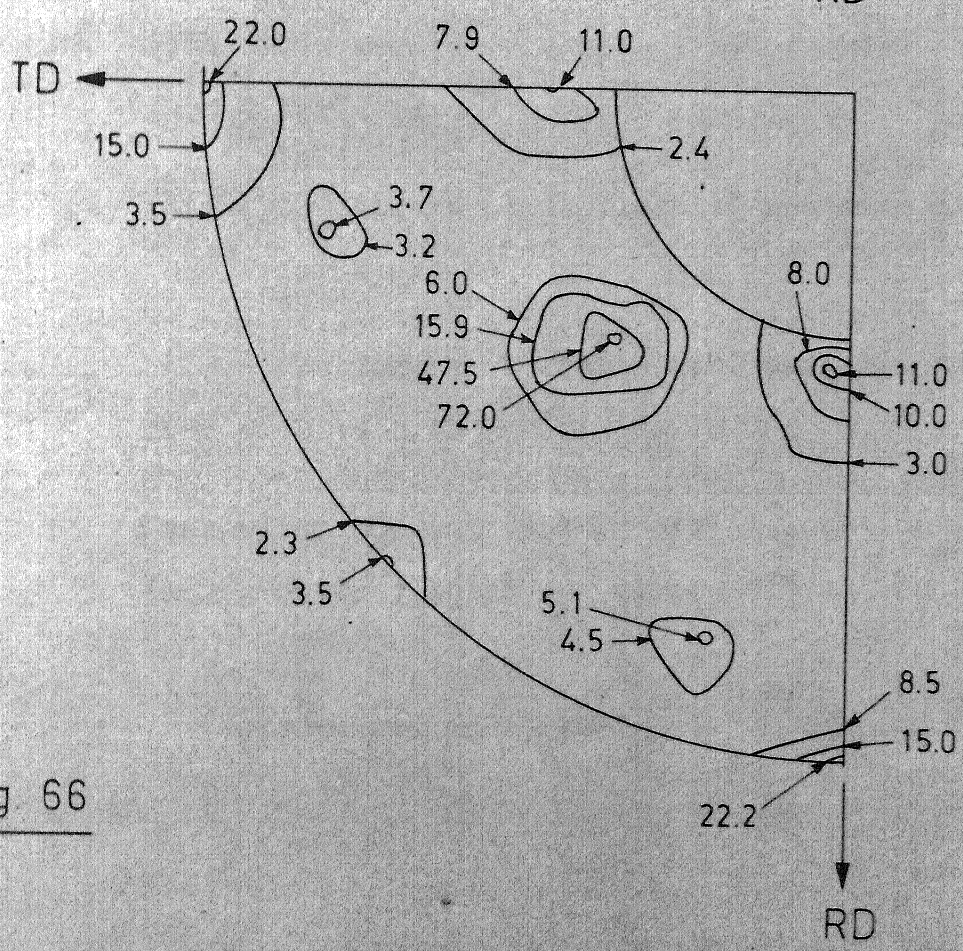


Fig. 66

## FIGURE CAPTIONS

- FIG. 67. (111) pole figure of sample 4(c) annealed at  $1058^{\circ}\text{C}$  for 4 hrs.
- FIG. 68. (111) pole figure of sample 5(a) annealed at  $1058^{\circ}\text{C}$  for 4 hrs.
- FIG. 69. (111) pole figure of sample 5(b) annealed at  $1058^{\circ}\text{C}$  for 4 hrs.
- FIG. 70. (111) pole figure of sample 5(c) annealed at  $1058^{\circ}\text{C}$  for 4 hrs.
- FIG. 71. (111) pole figure of sample 6(b) annealed at  $1058^{\circ}\text{C}$  for 4 hrs.
- FIG. 72. (200) pole figure of sample 6(b) annealed at  $1058^{\circ}\text{C}$  for 4 hrs.
- FIG. 73. Stereogram showing peak intensity locations of (1H) and (200) poles for sample 6(b).

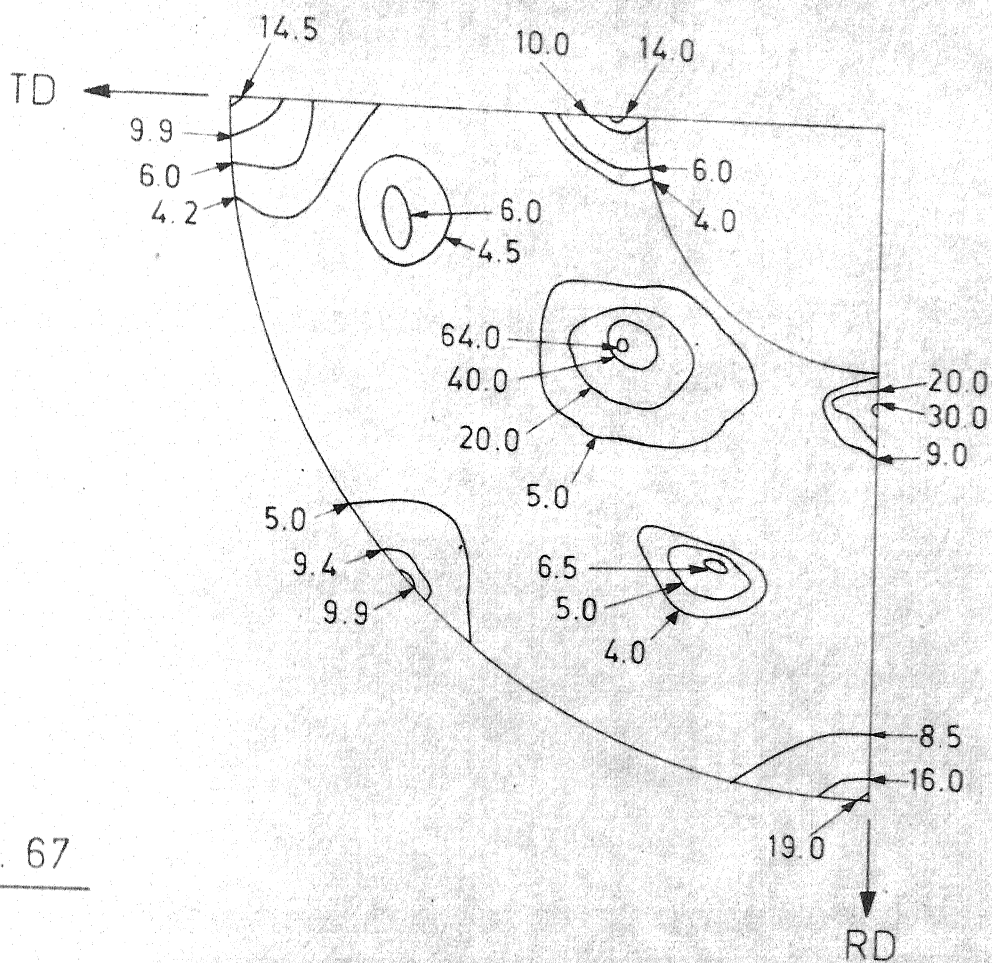


Fig. 67

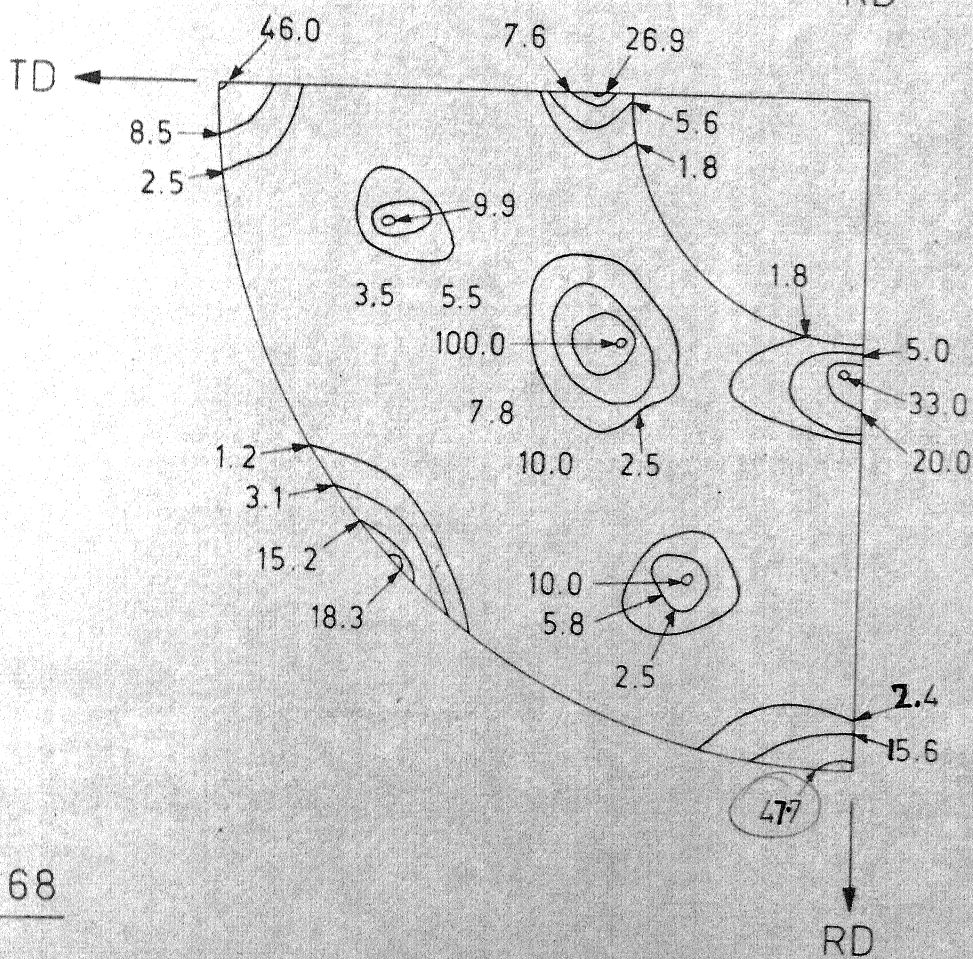


Fig. 68

2.65  
47.7



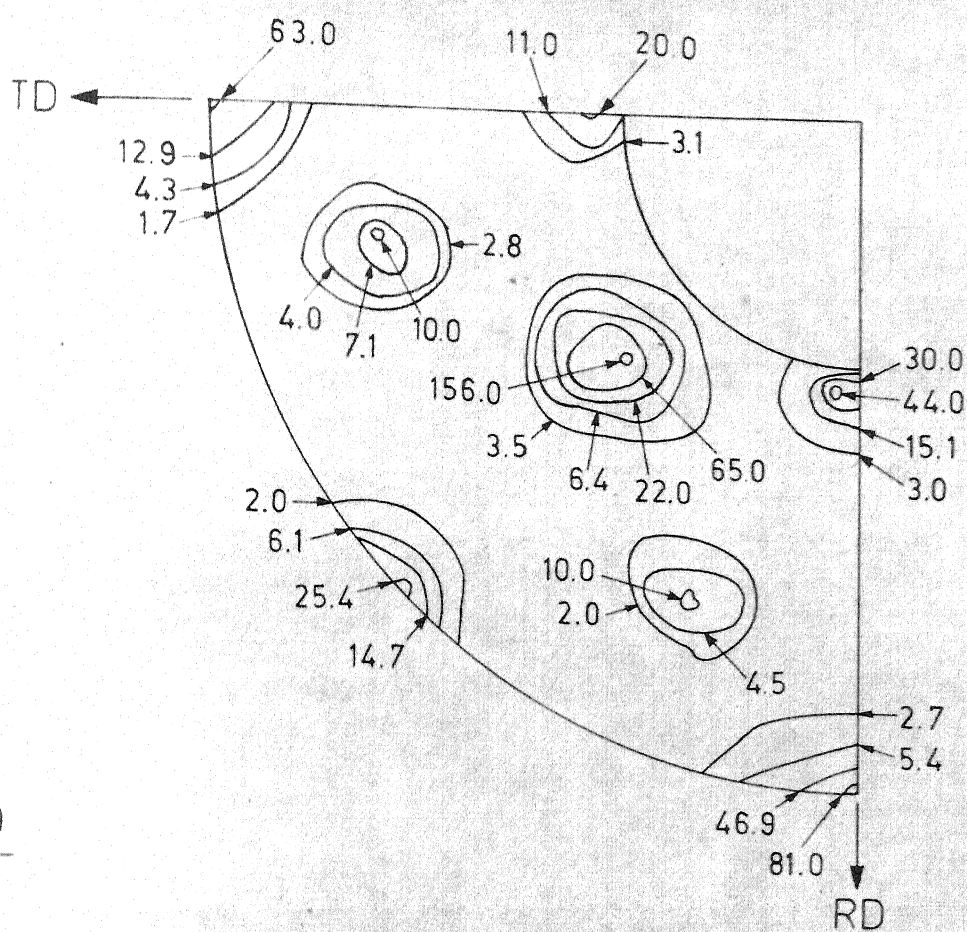


Fig. 69

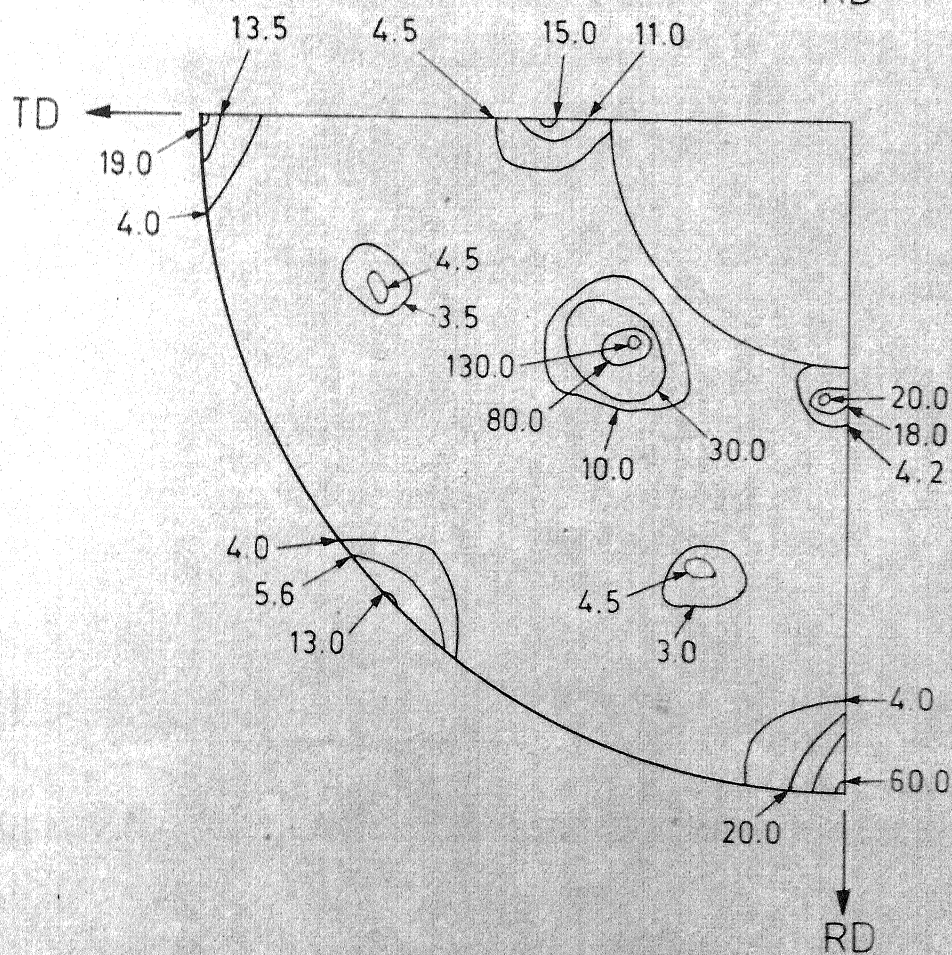


Fig. 70

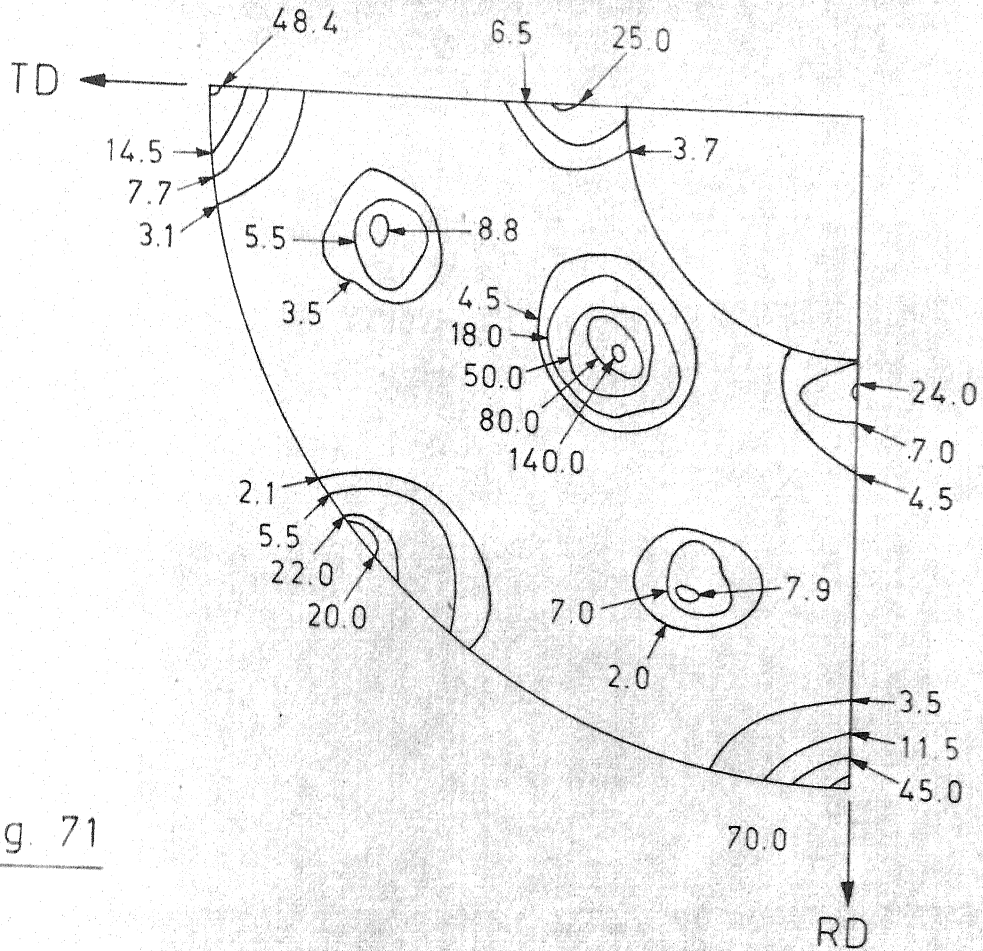


Fig. 71

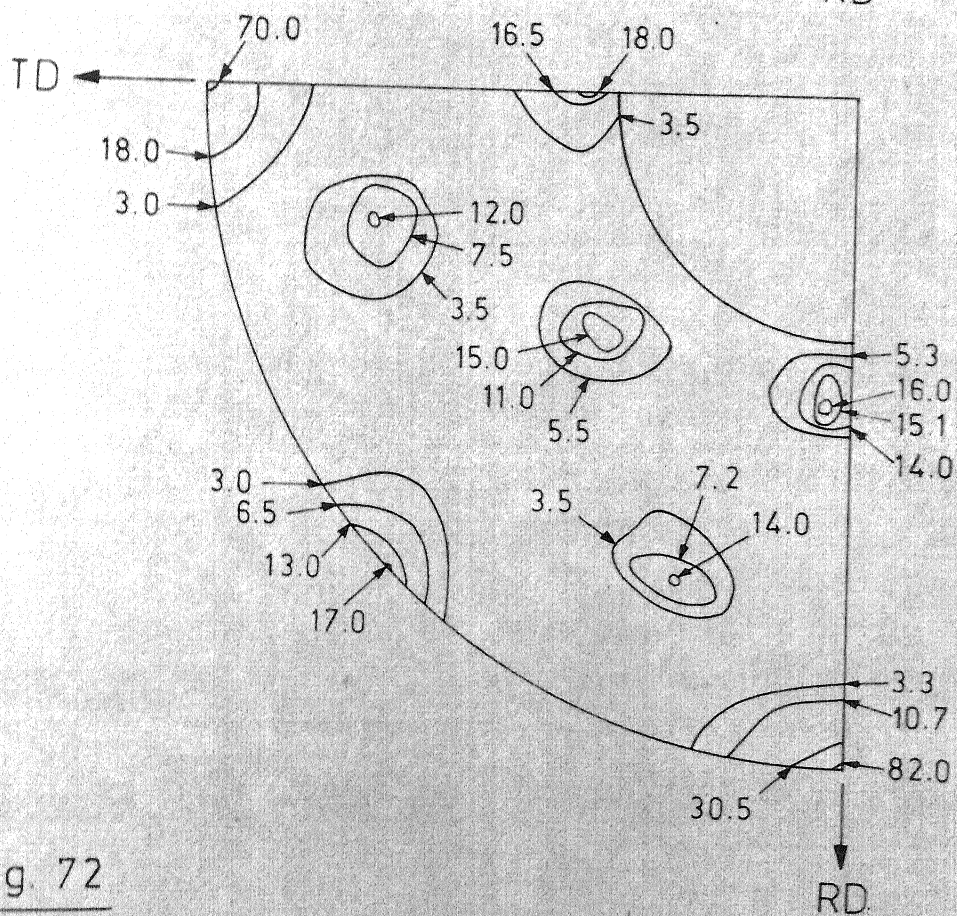
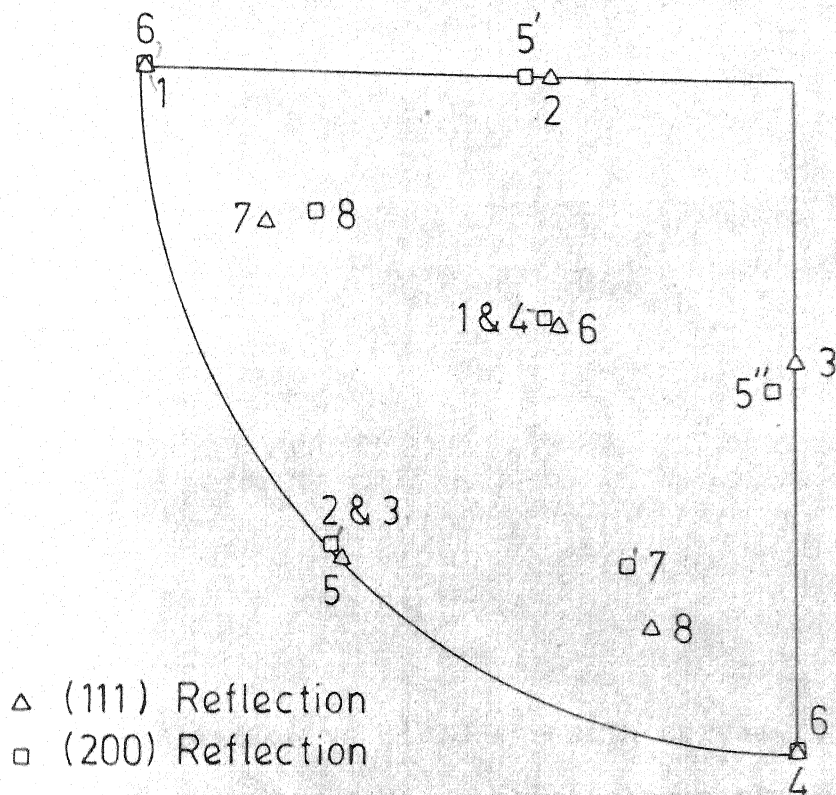


Fig. 72





Pole No.	Texture Description	Remarks
1	$(321)[hkl]$	$[hkl] \perp [\bar{1}\bar{1}\bar{1}]$ or $[11\bar{1}]$
2	$(130)[3\bar{1}3]$	Twin of pole 2
3	$(130)[hkl]$	
4	$(321)[\bar{1}\bar{1}\bar{1}]$	May arise due to texture of 8
5'		
5''		
5-5'	$(011)[\bar{7}1\bar{1}]$	
5-5''	$(011)[\bar{1}33]$	
6	$(001)[100]$	90° to each other or twin of each other <b>cube orientation texture</b>
7	$(122)[\bar{2}10]$	
8	$(122)[\bar{1}22]$	

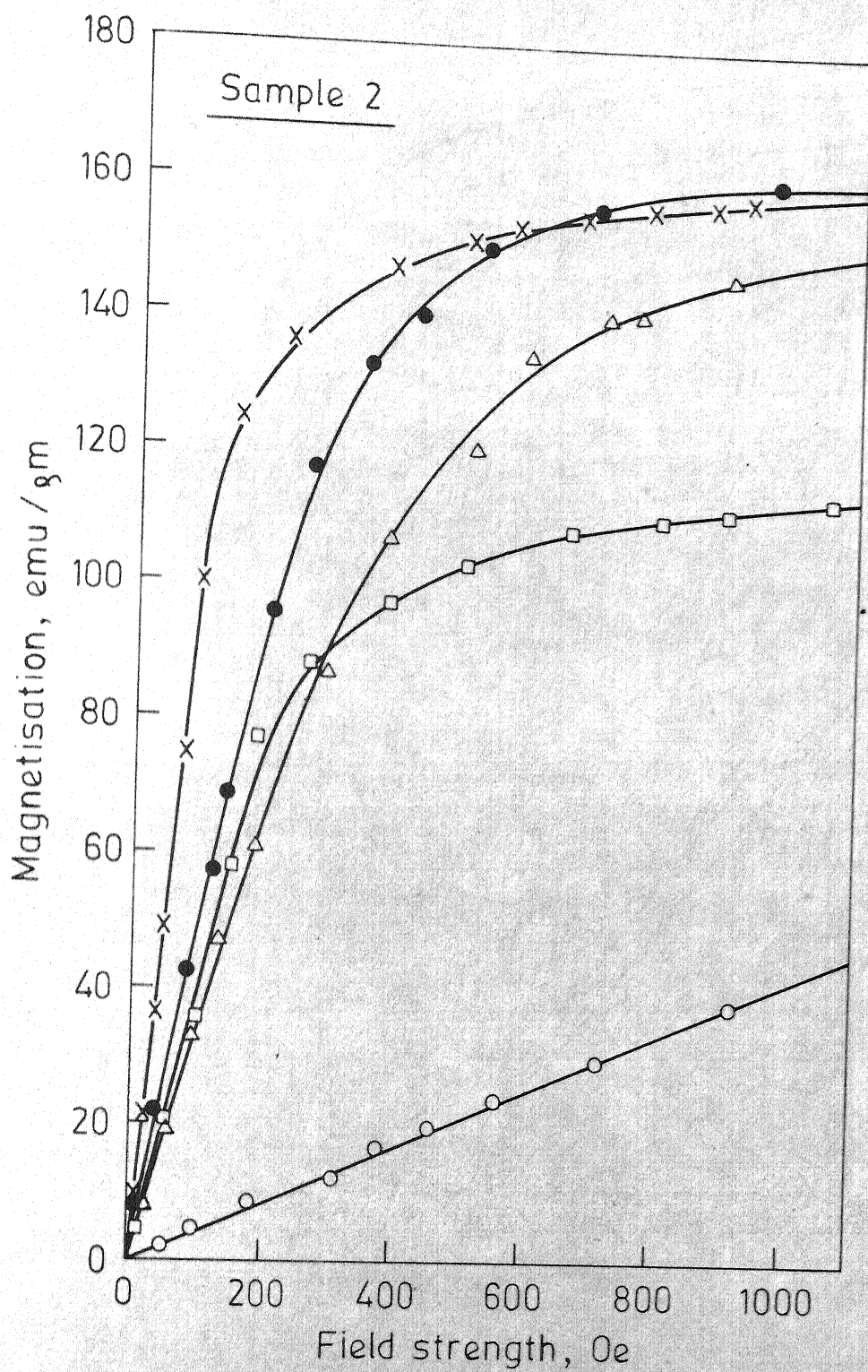
Fig. 73



## FIGURE CAPTIONS

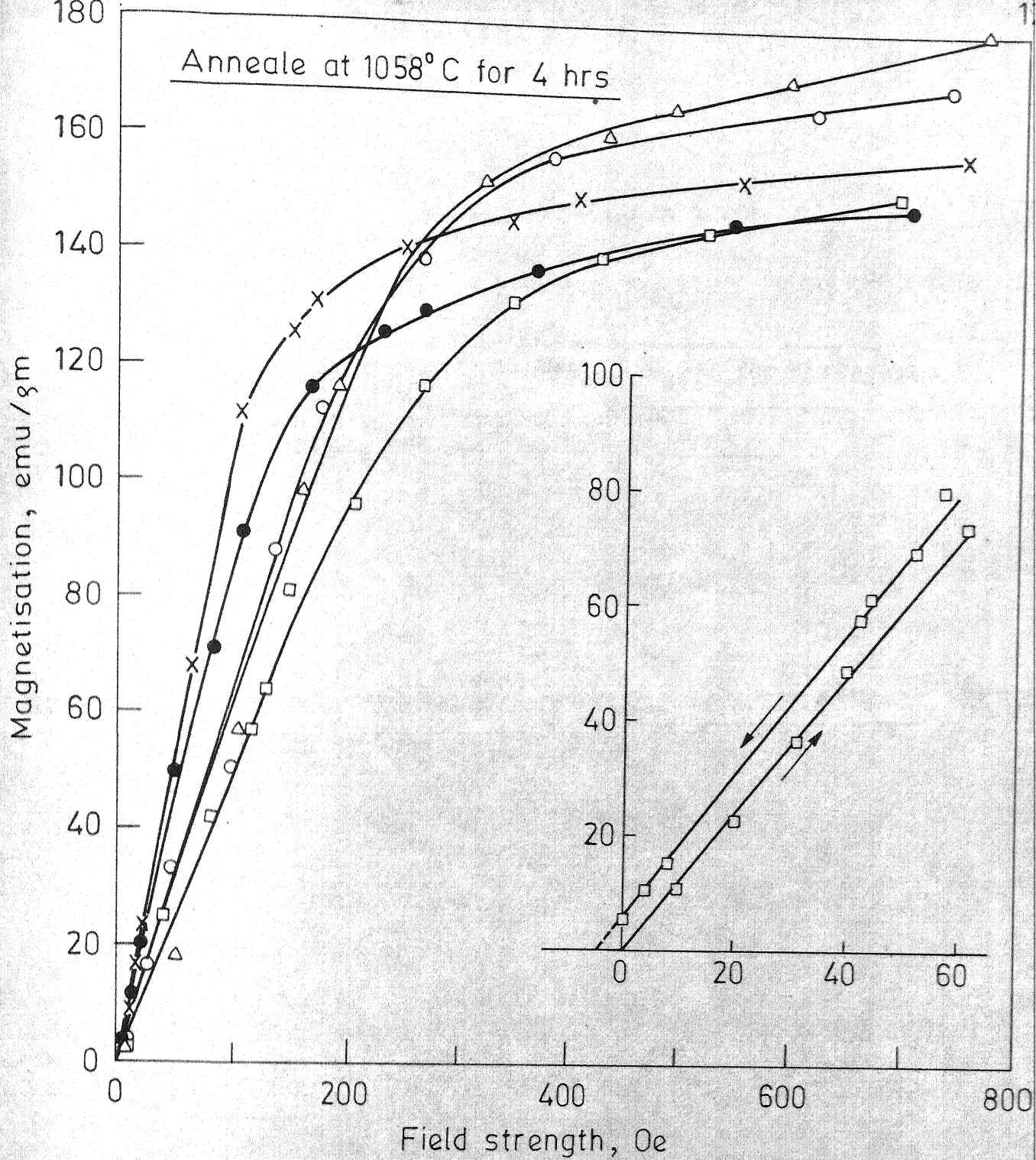
FIG. 74. Magnetisation vs field strength curves for sample 2 after various processing stages.

FIG. 75. Magnetisation vs. field strength curves for 48 permalloy specimens annealed at  $1058^{\circ}\text{C}$  for 4 hrs.



- As cast
- △ Cold rolled
- Annealed at 645°C for 2 hrs
- x Annealed at 1058°C for 4 hrs
- Annealed at 1058°C for 4 hrs

Fig. 74



- x Sample 1
- o Sample 2a
- Δ Sample 3a
- Sample 2
- Sample 3

Fig. 75

TABLE VII

Bragg angle of reflection ( $\theta_{hkl}$  in terms of  $2\theta_{hkl}$ ) for different samples

Sample No.	Bragg angle of reflection ( $2\theta_{hkl}$ ) for different plane of projection	
	$2\theta_{(111)}$	$2\theta_{(200)}$
1 and 3	19.55	22.6
2 and 5	19.6	22.62
4 and 6	19.58	22.61

TABLE VIII

Relative Peak Intensity at Different Pole Locations of Different Heat Treated Samples

Description of the sample	Relative intensity of (111) reflection in pole fig.										Figure N
	1	2	3	4	5	6	7	8	9	10	
1, 90 C.R. annealed at 1058°C for 4 hrs.	20.2	22.0	28.3	28.5	15.2	58.3	9.8	9.2	43		
1(a), 92 C.R. annealed at 1058°C for 4 hrs.	46.5	21.9	30.6	69.3	17.7	127.2	6.4	6.03	44		
1(a), 92 C.R. annealed at 1058°C for 7½ hrs.	45.0	32.1	46.6	65.0	20.6	110.2	8.68	9.21	45		
2, 94 C.R. annealed at 900°C for 4 hrs	20.1	18.5	22.6	21.1	16.0	30.1	7.1	6.3	-		
2, 94 C.R. annealed at 950°C for 4 hrs	12.0	22.8	28.6	22.8	18.9	31.2	5.4	7.4	-		
2, 94 C.R. annealed at 1000°C for 4 hrs	25.2	26.2	23.6	41.2	14.0	62.2	7.7	5.0	-		
2, 94 C.R. annealed at 1058°C for 1 hr	61.6	28.9	31.9	47.3	14.3	14.6	10.8	12.5	46		
2, 94 C.R. annealed at 1058°C for 2 hrs.	52.0	23.5	35.0	46.0	19.0	20.7	11.7	11.6	47		
2, 94 C.R. annealed at 1058°C for 4 hrs.	62.2	22.2	31.2	78.7	15.5	162.9	10.5	13.2	48		
2, 94 C.R. annealed at 1100°C for 4 hrs.	64.7	57.0	57.2	73.3	29.2	124.0	10.4	10.2	49		

Table VIII (Contd.)

1	2	3	4	5	6	7	8	9	10
2(a), 96 C.R. annealed at 1058°C for 4 hrs.	50.5	31.0	34.6	85.1	20.2	212.7	6.3	6.8	50
2(a), 96 C.R. annealed at 1058°C for 8 hrs.	80.3	27.7	23.4	80.8	10.5	148.0	7.6	11.2	51
2(a), 96 C.R. annealed at 1058°C for 16 hrs.	93.6	42.7	33.1	73.4	26.0	210.6	9.4	13.0	52
2(a), 96 C.R. annealed at 1120°C for 4 hrs.	78.7	50.7	55.3	96.5	35.7	173.8	11.4	15.4	53
2(a) 96 C.R. annealed at 1120°C for 6 hrs.	75.0	32.7	26.3	113.1	24.2	181.7	9.2	11.5	54
2(a) 96 C.R. annealed at 1120°C for 8 hrs.	52.5	43.4	64.4	94.3	29.1	190.5	10.3	13.5	55
2(a), 96 C.R. annealed at 1120°C for 10 hrs.	92.4	40.5	48.9	123.1	31.4	220.6	10.2	11.5	56
2(a), 96 C.R. annealed at 1058°C for 2 hrs.	40.8	30.5	30.1	64.0	14.0	119.0	12.0	9.0	57
3, 97 C.R. annealed at 1058°C, for 4 hrs.	61.1	26.1	51.2	70.4	30.2	190.9	8.3	7.5	58
3(a), 97.8 C.R. annealed at 1058°C for 4 hrs.	68.4	41.5	43.6	78.9	30.1	151.1	8.5	11.4	59
3(a), 97.8 C.R. annealed at 1058°C for 8 hrs	71.0	28.3	36.4	65.9	26.4	174.7	7.8	7.7	60



Table VIII (Contd)

1	2	3	4	5	6	7	8	9	10
3(a), 97.8 C.R. annealed at 1058°C for 16 hrs.	65.0	33.9	36.9	104.8	20.5	164.4	8.6	7.3	61
3(a), 97.8 C.R. annealed at 1120°C for 4 hrs.	52.1	31.5	32.6	88.7	45.3	135.5	8.4	8.9	62
3(a), 97.8 C.R. annealed at 1120°C for 6 hrs.	114.3	53.5	69.6	85.7	15.0	164.1	11.4	10.1	63
3(a), 97.8 C.R. annealed at 1120°C for 8 hrs.	84.6	23.5	29.4	101.9	35.2	156.0	8.1	10.7	64
4(a), 97.7 C.R. annealed at 1120°C for 10 hrs.	74.1	44.3	29.1	82.6	35.2	156	10.7	14.2	65
4(b), 96 C.R. at 200°C annealed at 1058°C for 4 hrs	22.0	11.4	11.5	22.2	3.5	72.2	3.8	5.7	66
4(c), 96 C.R. at 400°C annealed at 1058°C for 4 hrs.	14.5	13.0	30.2	19.2	9.4	64.2	6.3	6.7	67
5(a), 96 C.R. annealed at 1058°C for 4 hrs.	46.6	26.9	25.1	47.7	18.3	100.7	10.1	5.8	68
5(b), 96 C.R. at 150°C annealed at 1058°C for 4 hrs.	63.2	29.9	43.5	81.9	25.4	156	10.0	10.4	69

Table VIII (Contd.)

1	2	3	4	5	6	7	8	9	10
5(c), 96 C.R. at 250°C annealed at 1058°C for 4 hrs.	19.4	15.6	20.1	63.8	13.6	119.7	4.6	3.3	70
6(a), 96 C.R. at 250°C annealed at 1058°C for 4 hrs.	48.4	25.9	24.1	72.0	22.8	145	8.8	7.9	71



## CHAPTER V

### DISCUSSION

In the present study an attempt has been made to develop cube texture in 48 permalloy. From the previous discussions it is clear that the development of cube texture in permalloys requires very high cold deformation followed by a high temperature annealing. The temperature and time of annealing depends upon the specific composition of the alloy. The process variables for developing cube texture are the percent cold reduction, time and temperature of annealing and the composition of the alloy.

The developed texture is usually studied through x-ray diffraction technique employing a suitable goniometer or using Laue diffraction technique. The choice between the two techniques depends on the grain size of the specimen to be studied. If the grain size is sufficiently large ( $\geq 1$  mm dia), the orientation of each individual grain can be determined through the use of Laue technique. On the other hand, if the grain size is small, the overall texture of the sample can be determined using a texture goniometer. In order to choose between the two available techniques, an estimate of grain size of annealed sheet specimens was tried through standard metallographic technique. High Ni alloys are difficult to etch. Hence, for Fe-Ni sheets, several etching solutions, both chemical etching and electrochemical etching solutions, were tried. Even though in some available literature<sup>47,48</sup> etching of

grain boundaries, in Fe-Ni base alloys has been claimed, the present specimens could not be etched with any of the suggested etching solutions. The solutions were found to produce only etchpits (Fig. 76). Since the metallographic technique failed to reveal the grain structure, x-ray diffraction technique was employed to determine whether Laue technique was suitable for the texture study. Back reflection Laue pattern was taken using one of the annealed sheet specimen and a 1 mm. dia x-ray beam collimator. The diffraction pattern did not produce the usual Laue spot pattern but showed some spotty lines indicating that the specimens were of reasonably small grain size and were not suitable for texture study through Laue technique. Hence, the texture study of all specimens was done with the available transmission type texture goniometer. The limitation of this type of goniometer is that the maximum angle of rotation of specimen around the diffractometer axis ( $\alpha$ ) is  $45^\circ$  to  $50^\circ$ . Because of this it was not possible to determine a complete pole figure; the central part of a pole figure could not be studied.

The cube texture  $(100)[001]$ , being developed in Ni-Fe alloys, is an annealing texture. Hence, as such the study of deformation texture, obtained by cold rolling may not be considered so important. FCC metals, when cold rolled, however, does not produce only one type of texture. Basically, two different textures are produced

as (123)  $[\bar{4} \bar{1} 2]$  and (146)  $[\bar{2} \bar{1} 1]$  (see Fig. 12 and Fig. 13) and (2) brass type texture, which is essentially (110)  $[\bar{1} \bar{1} 2]$ . In the development of cube texture in f.c.c. metals and alloys, it has been found that cube texture and its perfection depend on whether cold rolling produces in the material a sharp copper type texture. Brass type texture is known not to favour cube texture formation. Hence, it was considered necessary to study the cold rolled texture of a few Ni-Fe alloys to determine whether or not the cold rolled texture was close to copper type texture. Because of the limitation of available goniometer, it was not possible to study the complete cold rolled texture. The partial pole figures determined were compared with the features of well developed copper type texture (Fig. 12 and Fig. 13) to find qualitatively the nature of cold rolled texture produced.

#### V.1 Study of Cold Rolled Texture

The (111) cold rolled pole figures for copper (Fig. 12) indicate essentially peak intensities at three locations in the pole figure - pole A at  $\phi = 0$  and  $\alpha \approx 5^\circ$  to  $10^\circ$ , pole B at  $\phi = 70^\circ$  and  $\alpha = 0^\circ$ , and pole C at  $\phi = 90^\circ$  and  $\alpha \approx 70^\circ$ . Using the present goniometer study around the location of pole C could not be done. However, it was possible to see the peculiar intensity variations around pole C. The (111) cold rolled pole figures for a few Fe-Ni alloys are shown in Figs. 35 to 42.

48 permalloy was given different cold deformation varying between 90% to 98% reduction in thickness to determine the minimum amount of deformation needed to produce sharp copper type texture. For 90% cold reduction (Fig. 35) it is clear that the peaks corresponding to A and B are present but there is no indication of a sharp increase in intensity near  $\alpha = 50^\circ$ ,  $\phi = 70^\circ$ , as will be expected if a sharp cube texture developed. (It should be noted here that the intensity of pole C is much higher than the poles A and B (Fig. 12)). Thus it appears that 90% cold reduction produced Cu-type texture but it may not be quite sharp. In the pole figure (Fig. 35) it is also found that besides the peaks corresponding to A and B there are a few other peaks present of which pole D at  $\phi = 30^\circ$ ,  $-\alpha = 35-40^\circ$  is rather prominent. Pole E and F at  $\phi = 90^\circ$ ,  $-\alpha = 30$  to  $35^\circ$  and  $\phi = 40$  to  $45^\circ$  and  $-\alpha = 10^\circ$  to  $35^\circ$  respectively are somewhat low intensity peaks. No attempt was made in this study to identify the cold rolled textures produced. Thus, unlike copper, 48 permalloy appears to have some other secondary textures besides the copper type texture. Cold rolled textures of Ni-Fe alloys are usually not published in literature and hence it is not possible to compare the present textures with those produced by others. Very early texture study of 95% cold reduced 36 Ni-Fe permalloy by Sachs et al<sup>51</sup> (possibly used the less accurate photographic method) indicate the presence of an imperfect copper type texture (details of cold rolling is not available) but does not show secondary

48 permalloy was given different cold deformation varying between 90% to 98% reduction in thickness to determine the minimum amount of deformation needed to produce sharp copper type texture. For 90% cold reduction (Fig. 35) it is clear that the peaks corresponding to A and B are present but there is no indication of a sharp increase in intensity near  $\alpha = 50^\circ$ ,  $\phi = 70^\circ$ , as will be expected if a sharp cube texture developed. (It should be noted here that the intensity of pole C is much higher than the poles A and B (Fig. 12)). Thus it appears that 90% cold reduction produced Cu-type texture but it may not be quite sharp. In the pole figure (Fig. 35) it is also found that besides the peaks corresponding to A and B there are a few other peaks present of which pole D at  $\phi = 30^\circ$ ,  $-\alpha = 35-40^\circ$  is rather prominent. Pole E and F at  $\phi = 90^\circ$ ,  $-\alpha = 30$  to  $35^\circ$  and  $\phi = 40$  to  $45^\circ$  and  $-\alpha = 10^\circ$  to  $35^\circ$  respectively are somewhat low intensity peaks. No attempt was made in this study to identify the cold rolled textures produced. Thus, unlike copper, 48 permalloy appears to have some other secondary textures besides the copper type texture. Cold rolled textures of Ni-Fe alloys are usually not published in literature and hence it is not possible to compare the present textures with those produced by others. Very early texture study of 95% cold reduced 36 Ni-Fe permalloy by Sachs et al<sup>51</sup> (possibly used the less accurate photographic method) indicate the presence of an imperfect copper type texture (details of cold rolling is not available) but does not show secondary

peaks corresponding to D, E and F poles.

When the percent reduction in thickness was increased to 94%, the cold rolled texture (Fig. 36) was essentially the same as the specimen with 90% reduction in thickness except for a minor shift of pole locations. Comparison of Fig. 35 and Fig. 36 reveals that not much improvement in texture was obtained when percent reduction in thickness increased from 90% to 94%. At and above 96% cold reduction, however, the pole figures (Fig. 37 and Fig. 38) indicate peak intensities corresponding to pole A and B as well as an increasing trend in intensity as  $\alpha$  increased from  $45^\circ$  to  $50^\circ$  at  $\phi \sim 70^\circ$ . It is, however, noticeable that the secondary peaks D, E, F also become rather prominent with increase in percent reduction in thickness. Thus it appears that in order to produce sharp copper type texture in 48 permalloy at least about 96% cold reduction is necessary.

## V.2 Study of Annealed Texture of 48 Permalloy with Small Amount of Mn

Success of development of sharp and perfect cube texture depends on process variables. In the first phase of present study, the process variables tried were percent cold reduction, temperature and time of annealing. Hence, at first, variation in these parameters in producing cube texture in 48 permalloy was investigated. The cube texture pole figures for copper are shown in Fig. 77 and Fig. 78. The (111) pole locations indicate ideal (111) pole location at  $\phi = 45^\circ$ ,  $-\alpha = 35^\circ$  corresponding to the

## FIGURE CAPTIONS

FIG. 76. Microstructure of 48 permalloy sample after annealing.

FIG. 77. (111) pole figures for annealed copper with cube texture.

FIG. 78. (200) pole figure for annealed copper with cube texture.



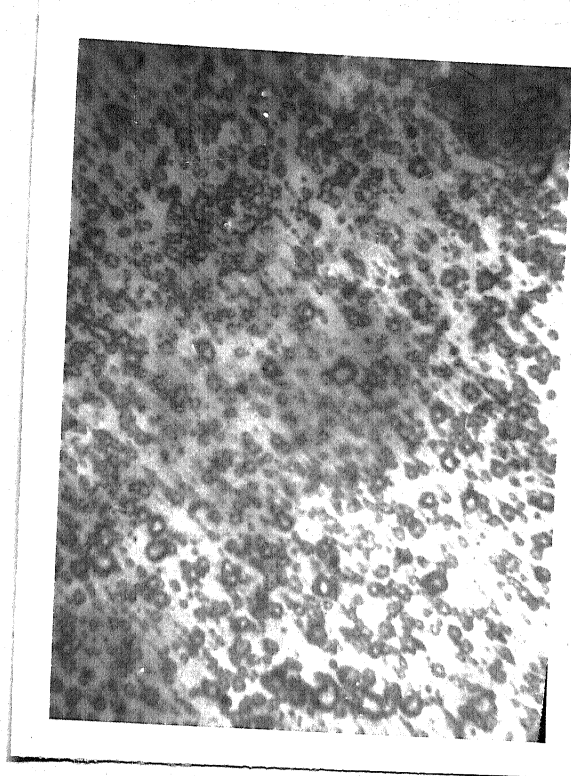
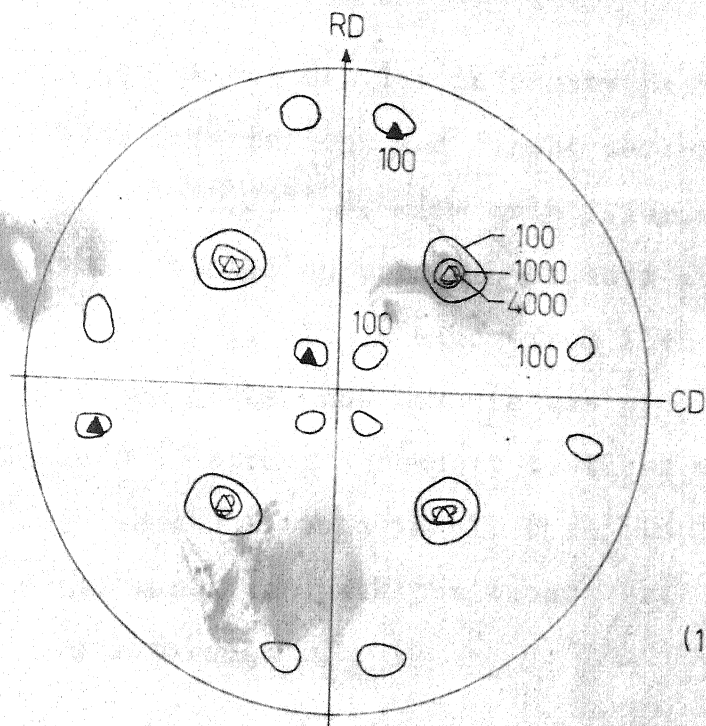


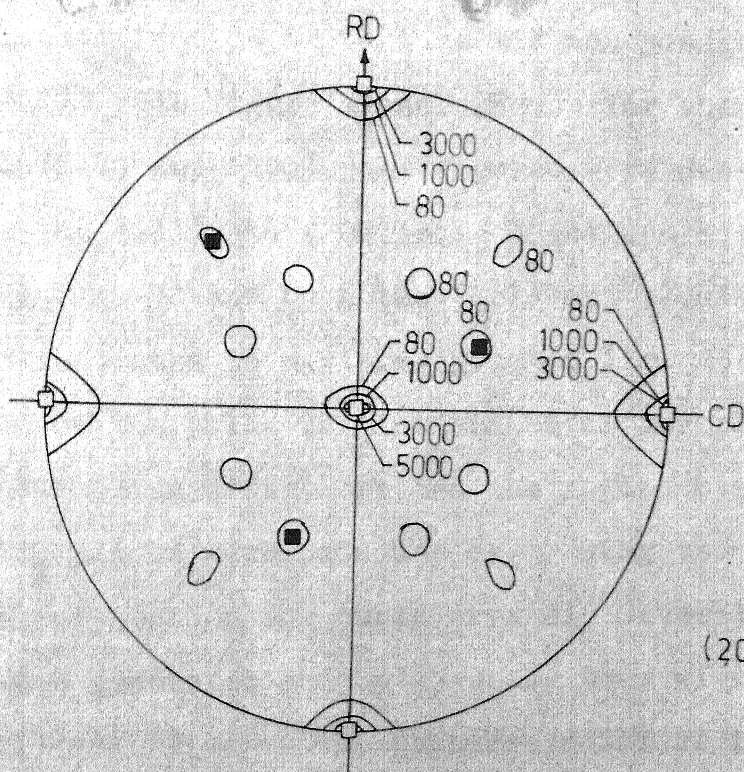
Fig. 76

Mag x 1000



(111) pole figure

Fig. 77



(200) pole figure

Fig. 78

(100)[001] texture and three more low intensity peaks which are due to twin orientations and can be described in terms of a texture  $\{122\}\langle 21\bar{2}\rangle$ . The pole figures corresponding to the annealed 48 permalloy sheets are shown in Fig. 42 to Fig. 71. It is clear from the pole figures that in all the cases cube texture was produced, at the same time several strong secondary textures were present. Since the peak positions in all the pole figures were practically the same, the peak positions were identified as poles 1 through 8.

#### V.2.1 Identification of Peak Positions in Pole Figures

An attempt was made to identify the textures. Since only one quarter of a pole figure was partially determined unambiguous identification of texture was not possible through the (111) pole figure alone. Hence for one specimen both (111) and (200) pole figures were determined. For this case the (111) and (200) pole locations are shown in Fig. 71 and Fig. 72 and both the (111) and (200) pole locations are indicated in a stereogram in Fig. 73. For identification of the poles the invariance of the planes of projection and rolling directions and the angles between  $\{100\}$  and  $\{111\}$  planes were made use of. Using the standard (001) projection for cubic crystals several standard projections were generated and by matching them with the (100) and (111) pole figures the textures could be identified as shown in Fig. 73. It is clear from the figure itself that like the twins for cube orientation, twin

orientations corresponding to the secondary textures are also present because of which so many peaks (1 through 8) appear in the pole figures determined. Stefan et al<sup>37</sup> also found several secondary orientations in their study of 50 permalloy. The secondary textures found by these authors are, however, different from those found in the present investigation.

From the pole figures determined, evaluation of the effect of process variables on the perfection of cube texture cannot be done by taking one set of poles only but we have to consider all the poles together. The comparison will be based on the relative intensities at the peak positions because the spread in intensities around the peak positions were quite similar in practically all the cases. For convenience of discussing the effect of each parameter, the intensity data of Table VIII have been rearranged in several tables, Tables IX to XII, to clearly show the effect of one parameter while the others were essentially kept constant.

#### V.2.2 Effect of Percent Reduction on the Annealed Texture

The relative intensities of cold rolled alloys (90% to 98% reduction in thickness) annealed at 1058°C for 4 hrs<sup>are</sup> shown in Table IX. As indicated earlier, the pole 6 corresponds to the ideal cube orientation. Hence an increase in the intensity of (111) reflection at pole 6 location will indicate that a larger fraction of crystallites are with cube orientation. A perfection of texture,

however, will be indicated also by a simultaneous considerable decrease in intensity of all other secondary textures. Since the relative intensity data of Table IX does not indicate such a behaviour, identification of best percent cold reduction was done somewhat differently. The texture corresponding to pole 4 has been described as  $\{123\}\langle 111 \rangle$  type. Since the idea of developing cube texture in the material was to have an easy direction of magnetisation (in this case  $\langle 001 \rangle$ ) of all grains to align themselves parallel to the rolling direction, the grains with  $\langle 111 \rangle$  aligned parallel to the rolling direction may be viewed as a favourable one <sup>because</sup> for fcc crystals  $\langle 111 \rangle$  direction is the easiest direction of magnetisation. Therefore the analysis of data has been made with this assumption that the particular value of a parameter for which the two textures  $(100)\langle 001 \rangle$  and  $(123)\langle 111 \rangle$  become prominent, was the best condition for developing possibly the best magnetic property (but possibly not the best condition for developing the most prominent single texture with cube orientation of grains). If we assume this, then we find that 96% cold reduction produced the best texture. It is clear from the Table IX that poles 1,2,3,7 and 8 are not very sensitive to percent cold reduction if it is greater than 90%. The intensity of pole 5, however, appears to increase with increasing cold reduction. The data of Table IX also supports the earlier conclusion (drawn for cold rolled textures) that the percent reduction near about 96% is necessary to develop reasonably prominent

cube texture. The intensity data for 97% and 98% cold reduction also supports the findings<sup>23,27</sup> that excessive cold rolling may be detrimental to the production of cube texture. The present data indicates that the percent cold reduction to be given to the material to produce sharp cube texture is rather critical.

#### V.2.3 Effect of Annealing Temperature on Annealed Texture

The effect of annealing temperature was studied with an alloy cold reduced by 94%. Specimens were annealed at 900°C, 950°C, 1000°C, 1058°C and 1100°C for the same length of time (4 hrs). The relative intensity data are tabulated in Table X. It is clear from the table that annealing at 1058°C produced the best result in this alloy. Since 96% cold reduction was found to give the best texture in 48 permalloy, a check was made by annealing 96% cold reduced alloy at 1058°C and 1120°C (Table X). The tabulated data again shows that 1058°C annealing produced better texture than that produced by higher annealing temperature. For want of specimen, no study of 96% cold rolled alloy was made at temperatures lower than 1058°C.

#### V.2.4 Effect of Annealing Time on the Annealed Texture

The effect of annealing time on texture was studied with two sheets with slightly different percent cold reduction (96% and 97% cold reduction) at two temperature levels, 1058°C and 1120°C. The annealing time used were 4 hrs, 6 hrs, 8 hrs and 16 hrs. For experimental diffi-

culties mentioned earlier, the longer annealings were performed in steps of 4 hr interrupted annealing. The intensity results are tabulated in Table XI. For the 96% cold reduction case 4 hr annealing at  $1058^{\circ}\text{C}$  appears to give the best result whereas at  $1120^{\circ}\text{C}$ , a 6 hr annealing was found to give the best result. Use of longer annealing time appears to increase the intensity at the pole location 1 for the 96% cold reduced material. Thus, use of shorter annealing time in the range of 4 to 6 hrs appears to produce a good result when the percent reduction in thickness is 96%. For the 97% cold reduced material, however, the results do not give any clear picture. For example, a 16 hrs annealing at  $1058^{\circ}\text{C}$  appears to produce the best result whereas at  $1120^{\circ}\text{C}$ , there is a considerable change in relative intensities (in more or less a random manner) at different pole locations and hence it is not easy to determine at which time the best texture was obtained. It is not clear why the pole intensities varied in random manner for different choice of annealing time. Since  $1120^{\circ}\text{C}$  was not considered as one of the favourable temperature for annealing, the present batch of Ni-Fe alloys, no further study was made to investigate the reason for this random variation in intensities.

### V.3 Identification of Other Process Variables

The above results indicate that for 48 permalloy used in this investigation 96% cold reduction followed by



texture. The texture produced, however, contained besides the desirable texture considerable amount of secondary textures which are undesirable from magnetic property point of view. Hence, possibility of other process variables were thought of. On chemical analysis of the first set of specimens, it was found that they contained very little of Mn (less than 0.1%) whereas about 0.5% Mn was put in. This trace amount of Mn was sufficient to make the material ductile enough for hot and cold rolling. Since addition of Mn to Ni-Fe alloy improves its ductility, it was thought probable that proper grain orientation could not be obtained because the material was not ductile enough due to lack of proper amount of Mn in the alloy. On this assumption it appears that a possible process variable is the Mn content of the alloy.

The copper type and brass type textures in fcc metals are not characteristics of particular elements or alloys. For example transition from copper type to brass type texture is possible even in pure Cu<sup>51</sup> through suitable choice of cold rolling temperature. For copper, rolling at liq. N<sub>2</sub> temperature produces Brass type texture whereas at room temperature complete copper type texture is produced. Similarly for stainless steel<sup>52</sup> it was found that a texture transition can be achieved by rolling at elevated temperature. The texture transition in metals and alloys has been qualitatively related to the stacking fault energy. Stacking fault energy depends on alloying element contents and fault frequency depends on temperature

of deformation. The change in stacking fault energy or stacking fault frequency when Fe is added to Ni is rather small. Moreover, in the present case Fe content is fixed. Effect of Mn additions on the stacking fault energy and stacking fault frequency is larger than that of Fe but in order to change these quantities considerably large amount of Mn, than is normally present in the permalloys, is needed. Thus, of the two variables Mn content and temperature of cold rolling, the more effective one for permalloy is expected to be the latter one. It should be noted here that none of the published literature indicate the necessity of warm rolling of permalloy to produce the desired texture.

#### V.4 Study of permalloys with new Process Variables

The next phase of work thus involved the study of the effect of Mn content and cold rolling temperature on the texture produced. For this study, the results obtained through the previous study (mentioned above) were utilized, namely that 96% cold reduction, 1058°C annealing for 4 hrs produced the best texture in 48 permalloy. For want of time this study was restricted to two levels of intended Mn contents, 0.5% Mn and 1.5% Mn, and three or four level of rolling temperatures varying between 100°C to 400°C. As mentioned earlier, the specimens had to be heated about 100°C above the desired cold rolling temperature and were rolled only when the temperature of the sheets reached the desired rolling temperature. The general effect of addition

of more Mn (on analysis the Mn was found to be 1.2%) was that during hot rolling, edge cracking was considerably reduced and the specimens appeared to be more ductile as they were more easy to cold roll.

#### V.4.1 Cold Rolled Texture

The cold rolled texture of 0.5% Mn at higher cold rolling temperature (200°C) showed (Fig. 39) no improvement over the room temperature one and at 400°C (Fig. 40) the cold rolled texture showed a tendency towards greater randomness. The cold rolled textures of 1.25% Mn alloys (Figs. 41 and 42), on the other hand, were found to show a sharp ear corresponding to the intensity distribution around pole C (Fig. 12) indicating that the developed copper type texture was sharper than the previous cases. The secondary texture represented by the poles D, E, F were not, however, eliminated.

#### V.4.2 Annealing Textures

The annealing texture data are shown as pole figures in Figs. 66 to 71 and the relative intensity data are shown in Table XII. The annealed texture of 0.5% Mn perm-alloy and for different cold rolling temperature showed no improvement of texture (see Table XII) indicating that an increase in cold rolling temperature alone (when Mn content was about the same) did not help in the improvement of texture. This result may be expected, since elevated temperature cold rolling did not produce appreciable change in texture compared to the room temperature cold rolling.

On annealing 48 permalloy with 1.35% Mn also did not show much change in texture when cold rolled at 150°C. However, when it was cold rolled at 250°C and annealed at 1058°C for 4 hrs, a favourable texture was produced (see table XII). In this case, the intensity of pole 6 as well as at pole 4, the two favourable textures, were quite high whereas the intensity of all other poles (1,2,3,5,7 and 8) were reasonably low. It is of interest to see that the high temperature (250°C) rolling of 1.25% Mn permalloy has been able to reduce the intensities at pole locations 1, 2, 3, 5 which was not possible through the change of any other process variables. The reproducibility of achieving this texture was checked by reannealing another specimen from the same stock. The two textures agreed quite well with each other.

From the results it appears that for achieving favourable texture in 48 permalloy, Mn content should be high and the rolling has to be performed at elevated temperature. Since only one higher level of Mn (1.2%) was tried, it is not possible to say from the present results what will be the optimum level of Mn in 48 permalloy because no magnetic loss experiment was performed with the present alloy. Similarly cold rolling at 250°C may not be the most appropriate rolling temperature to produce the best texture. More experimentation will be needed to find the appropriate Mn content and rolling temperature.

## V.5 Magnetic Study of 48 Permalloys

It has been stated earlier that magnetic measurements were done with a magnetometer because Epstein test frame required a large amount of material. Moreover, the test frame could not be calibrated within the limited time. The sample required for magnetic measurements with a magnetometer is a  $\frac{3}{16}$ " x  $\frac{1}{8}$ " piece of sheet. Since the required specimen size is rather small and it may have an imperfect cube texture, it is expected that the magnetic properties may vary for different specimens even when they are cut from the same annealed sheet. As no other alternate measuring facility was available, the magnetometer was utilised to have some first hand information regarding the change in magnetic property of permalloy sheets due to different mechanical and thermal treatments.

The magnetic test results (in terms of M vs H) are shown in Figs. 74 and 75. Fig. 74 shows the magnetic properties of sample 2 (94% C.R.) when treated differently - in the as cast state, cold rolled state, cold rolled and annealed (645°C and 1058°C) state. As is expected, the magnetic property (as indicated by the M vs. H curve) of the 1058°C annealed sheet is better than the other specimens. Two different samples from the same 1058°C annealed stock were tested and the results (Fig. 74) show that there is a considerable difference in the early part of the M vs H curve for the two samples. This observation supports our previous expectation that a small sample will not

represent the average magnetic property of an annealed sheet specimen.

Fig. 75 shows the  $M$  vs  $H$  curves of 48 permalloys with different percent reduction in thickness (90% to 98%) but with the same annealing time and temperature ( $1058^{\circ}\text{C}$  for 4 hrs). Here, sample 1 (90% C.R.) shows the best magnetic property whereas from the texture results sample 2(a) (96% C.R.) is expected to show the best result. In view of the observations made with samples cut from the same rolled and annealed sheet (Fig. 74), the difference in the  $M$  vs.  $H$  curves of all the specimens shown in Fig. 75 may be considered to be due to the small specimen size.

All the results presented here show that near saturation condition for the sample occur at a reasonably large field. This might possibly be due to the fact that several types of textures are present in the sheet specimens. Moreover, the alloys were not analysed for impurities, like  $\bar{C}$ . It is not known what effect is produced by the impurities on the magnetic properties.

Using the small specimens, an attempt was made to determine the residual magnetisation  $M_r$  and coercive force  $H_c$  for the specimen 2. Only the first quadrant part of the hysteresis loop was determined. The difference between the magnetisation and the demagnetisation curve was quite small. The typical  $M_r$  value was  $\sim 5$  emu/gm and  $H_c \sim 40\text{e}$ . The  $H_c$  values were obtained by extrapolation of the first quadrant demagnetisation curve into the <sup>second</sup> ~~first~~ quadrant (insert in Fig. 75). Since the magnetic field could not

be measured with accuracies better than  $\pm 1$  Oe and the characteristics of the magnet power supply (which was insensitive to the creation of low fields)  $H_c$  could not be determined with greater accuracy. No further magnetic measurement was possible because of the break down of the magnet and the magnetometer.



TABLE IX

Effect of Percent Reduction or Annealing Texture at a Fixed Temperature  
(1058°C) and time (4 hrs.)

Sample	Relative intensities of (111) reflection at different pole position								Fig. No.
	1	2	3	4	5	6	7	8	
1, 90 C.R.	20.2	22.0	28.3	28.5	15.2	58.3	9.8	9.2	43
1(a), 92 C.R.	46.5	21.9	30.6	69.5	17.7	127.2	6.4	6.03	44
2, 94 C.R.	62.2	22.2	31.2	78.7	15.5	162.9	10.5	13.2	48
2(a), 96 C.R.	50.5	31.0	34.6	85.1	20.2	212.7	6.3	6.8	50
3, 97 C.R.	61.1	26.1	51.2	70.4	30.2	190.9	8.3	7.5	58
3(a), 98 C.R.	52.1	31.5	32.6	88.7	45.3	135.5	8.4	8.9	59

TABLE X

Effect of Temperature on Annealing Texture of Cold Rolled Samples  
at Fixed Time (4 hrs.)

Sample	Relative intensities of (111) reflection at different pole location								Fig. No.
	1	2	3	4	5	6	7	8	
2, 94 , 900°C	20.1	18.5	22.6	21.0	16.0	30.1	7.1	6.3	-
2, 94 , 950°C	12.0	22.8	28.6	22.8	18.9	31.2	5.4	7.4	-
2, 94 , 1000°C	25.2	26.2	23.6	41.2	14.0	62.2	7.7	5.0	-
2, 94 , 1058°C	62.2	22.2	31.2	73.7	16.5	162.9	10.5	13.2	48
2, 94 , 1100°C	64.7	57.0	57.2	73.3	29.2	124.0	10.4	10.2	49
2a,96 , 1058°C	50.5	31.0	34.6	85.07	20.2	212.7	6.3	6.8	50
2a,96 , 1120°C	73.7	50.7	55.3	96.5	35.7	173.8	11.4	15.4	53

TABLE XI

Effect of Time of annealing on Texture Formation at Different

Temperature

Sample No.	Relative intensities of (111) reflection at different pole positions								Fig. No.
	1	2	3	4	5	6	7	8	
2(a), 1058°C, 4 hrs	50.5	31.0	34.6	85.07	20.2	212.7	6.3	6.8	50
2(a), 1058°C, 8 hrs	80.3	27.7	23.4	80.8	10.5	148.0	7.6	11.2	51
2(a), 1058°C, 16 hrs	96.6	42.7	33.1	73.4	26.0	210.6	9.4	13.0	52
2(a), 1120°C, 4 hrs	78.7	50.7	55.3	96.5	35.7	173.8	11.4	15.4	53
2(a), 1120°C, 6 hrs	75.0	32.7	26.3	113.1	24.2	181.7	9.2	11.5	54
2(a), 1120°C, 8 hrs	52.5	43.4	64.4	94.3	29.1	190.5	10.3	13.5	55
2(a), 1120°C, 10 hrs	92.4	40.5	48.9	123.1	31.4	220.6	10.2	11.5	56
3(a), 1058°C, 4 hrs	68.4	41.5	43.6	78.9	30.1	158.1	8.5	11.4	58
3a, 1058°C, 8 hrs	71.0	28.3	36.4	65.9	26.4	174.7	7.8	7.7	59
3a, 1058°C, 16 hrs	65.0	33.9	36.9	104.5	20.5	169.4	8.6	7.3	60

Table XI (Contd.)

Sample No.	Relative intensities of (111) reflection at different pole positions								Fig. No.
	1	2	3	4	5	6	7	8	
3(a), 1120°C, 4 hrs	52.1	31.5	32.6	88.7	45.3	135.5	8.4	8.9	61
3(a), 1120°C, 6 hrs	114.3	53.5	69.6	85.7	29.6	184.7	11.4	10.1	62
3(a), 1120°C, 8 hrs	34.6	23.5	29.4	101.9	15.0	164.1	8.1	10.7	63
3a, 1120°C, 10 hrs	74.1	44.3	29.1	82.6	35.2	156.0	10.7	14.2	64

TABLE XII

Effect of Cold Rolling Temperature and Mn Content For 96 Cold Rolled and Annealed (1058°C, 4 hrs) Samples.

Sample	Relative peak intensities of (111) reflection at the different pole positions								Fig. No.
	1	2	3	4	5	6	7	8	
6(b), 150°C(0.5 Mn)	54.8	18.3	22.3	69.5	21.8	97.3	8.0	4.2	-
4(b), 250°C(0.5 Mn)	22.0	11.4	11.5	22.2	3.5	72.2	3.8	5.7	66
6(b), 250°C(0.5 Mn)	48.4	25.9	24.1	72.0	22.8	145.0	8.8	7.9	71
4(c), 400°C(0.5 Mn)	14.5	13.0	30.2	19.2	9.4	64.2	6.3	6.7	67
5a, 150°C(1.25 Mn)	63.2	29.4	43.5	81.9	25.4	156.0	10.0	10.4	68
5b, 250°C(1.25 Mn)	19.4	15.6	20.1	63.8	13.6	119.7	4.6	3.3	69

## CHAPTER VI

## CONCLUSION

## CHAPTER VI

## CONCLUSION

From the present investigation on the development of cube texture<sup>of</sup> 48 permalloy, the following conclusions can be drawn:

- (1) Cold reduction without intermediate annealing does not produce prominent copper type texture. Prominent copper type texture alongwith some secondary texture is produced when cold reduction in thickness is 96 and above.
- (2) Prominent cube texture appears to be produced by annealing cold rolled material in a narrow temperature range around  $1058^{\circ}\text{C}$ . Higher annealing temperature appears to produce strong secondary textures.
- (3) Prominent cube texture could be produced by annealing cold rolled material at  $1058^{\circ}\text{C}$  for 4 hours. Longer annealing time invariably produced more pronounced secondary texture.
- (4) Elevated temperature cold rolling of permalloy followed by proper annealing appears to sharpen cube texture to some extent as the rolling temperature increases from  $100^{\circ}\text{C}$  to about  $200^{\circ}\text{C}$ . At still higher rolling temperatures the texture tends to become random.
- (5) Increase in Mn content, keeping all other process variables same, does not appear to improve the cold rolled as well as the annealed texture.



- (6) Increase in Mn content to about 1% and use of elevated temperature (about 250°C) for cold rolling appears to sharpen the cube texture in 48 permalloy.

## REFERENCES

## REFERENCES

- (1) P. Leech and C. Sykes, Phil. Mag. 1935, 27, 742-753.
- (2) R. Hultgreh, C.A. Zapffer, Trans. Am. Inst. Min. Met. Engers. 1935, 133, 58-68.
- (3) J. Pauleve, D. Dautreppe, J. Langier and L. Neel, 'Metaltic Solid Solution', New York, 1963, XLVIII (1-6).
- (4) J. Pauleve and D. Dautreppe, Compt. Reded 250, 1960, 3804.
- (5) L. Neel, J. Phys. Rad. 15, 1954, 225.
- (6) G.A. Kelsall, Physics, 5, 1934, 169.
- (7) R.M. Bozorrth, 'Ferromagnetism' Van No sland, New York, 1951, 154.
- (8) H. Hu and S.R. Goodman, Trans. AIME, 227, 1963, 627.
- (9) H.G. Muller, Z. Metall. 31, 1939, 322.
- (10) C.S. Barrett and T.B. Masalski 'Structure of Metals', McGraw Hill, 1966.
- (11) J.C. Benford. J. Appl. Phys. 4, 1963, 1307.
- (12) D.A. Collins and G.A. Aspden, J. Appl. Phys. 40, 1969, 1571.
- (13) S.L. Ames, J. Appl. Phys., 41, 1970, 1032.
- (14) M.J. Saviksi, J. Appl. Phys. 29, 1958, 353.
- (15) N. Anantharaman, J.A. Coles, R.M. Aspden - J. Appl. Phys. 38, 1967, 1170.
- (16) P.S. Cook and R.M. Richards, J. Inst. Metall, 1, 1940, 66.

- (17) P. Dahl and H. Powlek, Z. Metallkunde, 210, 1927, 684.
- (18) G. Wassermann and J. Grewen 'Tex Metallischer Werkstoffe' Springer-Verlag, Berlin, 1962, 705.
- (19) N.F. Littman, E.S. Harris, C.E. Ward, J. Appl. Phy. 33, 1962, 1229.
- (20) E. Alder and H. Pfeiffer, I.E.E.E. (Magnetics) 10, 1974, 172.
- (21) Colling and Aspden, J. Appl. Phys., 41, 1970, 1040.
- (22) M.J. Savitski, J. Appl. Phys. 29, 1958, 353.
- (23) S. Spachnen and M. Rostoker, Trans. AIME, 203, 1955, 921.
- (24) A.E. Berkwitz and E. Kneller 'Magnetism and Metallurgy' Vol. 2, Academic Press, New York, 1969, 734.
- (25) J.K. Kang, H. Scholofield and A.P. Markin, J. Appl. Phy. 38, 1967, 1178.
- (26) J.K. Kang and A.P. Martin, J. Appl. Phy. 38, 1967, 1179.
- (27) A.E. Berkwitz and E. Kneller 'Magnetism and Metallurgy' Vol.2, Academic Press New York, 1969, 739.
- (28) A.E. Berkwitz and E. Kneller 'ibid' 139.
- (29) A.E. Berkwitz and E. Kneller, 'ibid' 903.
- (30) A. Hnyes and R.S. Borns, Trans., ASM, 25, 1937, 129.
- (31) J.K. Wood, Trans. ASM, 39, 1947, 725.
- (32) A.E. Berkwitz and E. Kneller 'ibid' 702.
- (33) C.W. Rajhenau and J.H. Clusters, Philips, Res. Rep. 4 1949, 241.
- (34) D.J. Snee, J. Appl. Phy. 38, 1967, 1172.
- (35) W.D. Kehr, J. Appl. Phys. 41, 1970, 1857.
- (36) P.P. Coffi, Phy. Rev., 45, 1934, 742.

- (37) M. Stefan and Arto, Metals Science 11, 1977, 537.
- (38) G.A. Kelsall, Physics, 5, 1934, 169.
- (39) G.Y. Chin, Trans. IEEE, Magn., Mag-7, 1971, 102.
- (40) F. Pfeiffer, Z., Metall, 240, 1957, 996.
- (41) E.T. Ferguson, J. Appl. Phy. 29, 1957, 996.
- (42) English and G.Y. Chin, J. Appl. Phy. 38, 1967, 31183.
- (43) E.A. Nessibutt, R.D. Heidenrich and R.D. Borkank, J. Appl. Phy. (Supplenat).
- (44) A.A. Band, M.Tech. Thesis, I.I.T., Kanpur, 1972, 54.
- (45) P.V. Schigolev, Electrolytic and Chemical Polishing of Metals, Freund Publishing House, 1970, page - 176.
- (46) B.F. Decker, D. Harker and E.T. Asp., J. Appl. Phy. 19 1948, 388.
- (47) G.L. Kehl, 'The principles of Metallographic Laboratory Practice, McGraw Hill Book Company, Inc., New York, 1943, page-383.
- (48) W.D. Hannibal, Acta. Met. 3, 1959, 697.
- (49) Metals Hand Book, 1948, ASM, Cleveland, Ohio.
- (50) H. Hu and S.R. Goodman Trans. AIME 227, 1963, 627.
- (51) G. Sachs and J. Pretnak, Trans. AIME, 140, 1940, 359.
- (52) S.R. Goodman and H. Hu, TMS-AIME, 236, 1966, 710.

## APPENDIX

TABLE I PROGRAM FOR CALCULATION OF INTENSITY CORRECTION FACTOR FOR  
VARIOUS  $t$  AND  $\tau$  FOR DIFFERENT VALUES OF  $\tau$ .

```

$WATFOR      CEG230      PALLAB PALLAB PALLAB
C      W118      26THOCT., 788
$IBJOB
$IBFTC MAIN
C      DETERMINATION OF THE CORRECTION FACTOR USED FOR INTENSITY CORR
      DIMENSION ALPHA (100), B (100), C(100), D(100), GUT (100)
      DIMENSION X(100), Y(100), Z(100)
      PIM=3.14159/180.
      NTHETA=10
      NTHETA=5
      THETA=9.9
      THETA=10.3
      THETA=9.5
      THETA=9.
      DTHETA=0.1* PIM
      THETA=THETA*PIM
      DO 30 I THETA=1, NTHETA
      A=COS(THETA)
      DALPHA=5. * PIM

```



TABLE 1 CONTD.

```

11,
C1= +1.
LLL=10
ALP=0.
DO 5 L=1,LLL
ALP=ALP+DALPHA*C1
ALPHA(L)=ALP
B(L)=COS( THETA+ALPHA(L))
C(L)=COS(THETA-ALPHA(L))
IF(C(L).EQ.0.)GO TO 6
D(L)=B(L)/C(L)
GO TO 5
6 PRINT 11, L
5 CONTINUE
MMM=10
MMM=5
AMT=1.
AMT=2.
DAMT=0.1
DO 20 M=1,MMM
GUT(M)=AMT

```

TABLE 1 CONTD

```

E=GUT(M)/A
E1= GUT(M) * A
EE=EXP(-E1)
DO 10 N=1,LLL
  IF(B(N).EQ.O.) GO TO 7
  IF(C(N).EQ.O.) GO TO 8
  IF(B(N).EQ.C(N)) GO TO 9
  G=EXP(-GUT(M)/C(N))
  F=EXP(-GUT(M)/B(N))
  FACTN=E*EE*(1./D(N)-1.)/(G-F)
  FACTP=E*EE*(D(N)-1.)/(F-G)
  H=ALPHA(N)/PIM
  X(N)=H
  Y(N)=FACTP
  Z(N)=FACTN
  GO TO 10
7 PRINT 12, N
  GO TO 10
8 PRINT 13, N
  GO TO 10

```

```

9 PRINT 14, N,N
10 CONTINUE
  IF(M.EQ.(((M-1)/5)*5)) PRINT 4
  TH=THETA/PIM
  PRINT1,GUT(M),TH
  PRINT2
  PRINT3,(X(N),Y(N),Z(N),N=1,LLL
  AMT=AMT+DAMT
  GUT(M)=AMT
20 CONTINUE
  THETA=THETA+DTHETA
30 CONTINUE
  1  FORMAT(50x,4HMUT=F10.3,10x,6THETA=F10.3)
  2  FORMAT(1x,120(1H*),/,10x,2(5HALPHA,10x,9H(+)FACTOR,6X,9H(-)FACTOR,
    16X),/,1X,120(1H*))
  3  FORMAT(10X,90(1H*),/,7X,6E15.6
  4  FORMAT(1H1)
  11 FORMAT(1X,*C(*,1X,14,1X,*), IS ZERO HENCE SKIPPED*)
  12 FORMAT(1X,*B(*,1X,14,1X,*), IS ZERO HENCE SKIPPED*)

```

## TABLE 1 CONTD

13 FORMAT(IX,\*C(\*,IX,14,IX,\*) IS ZERO HENCE SKIPPED\*)

14 FORMAT(IX,\*B(\*,IX,14,IX,\*)EQUALS C)\*,X,14,IX,\*) HENCE SKIPPED\*)

STOP

END

\$ENTRY

Table 2: Intensity Correction factor for various  $\theta$  and  $\mu t$  values. $\theta = 9.0^\circ$ 

$\mu t \backslash \theta$	1.0	1.1	1.2	1.3	1.4	1.5	1.6	1.7
0	1.000	1.000	1.000	1.000	1.000	1.000	1.000	1.000
5.	1.039	1.042	1.045	1.048	1.051	1.054	1.057	1.060
10	1.054	1.059	1.063	1.067	1.072	1.076	1.080	1.085
15	1.071	1.078	1.084	1.091	1.098	1.104	1.111	1.118
20	1.090	1.100	1.110	1.120	1.131	1.141	1.152	1.162
25	1.113	1.128	1.143	1.158	1.174	1.189	1.205	1.221
30	1.142	1.163	1.185	1.208	1.230	1.250	1.277	1.301
35	1.180	1.211	1.242	1.275	1.308	1.341	1.376	1.411
40	1.234	1.278	1.323	1.369	1.417	1.466	1.517	1.570
45	1.313	1.375	1.440	1.507	1.578	1.651	1.728	1.807
50	1.434	1.525	1.621	1.722	1.829	1.942	2.062	2.188

Table 2 contd.

 $\theta = 9.0$ 

	1.8	1.9	2	2.1	2.2	2.3	2.4
0	1.000	1.000	1.000	1.000	1.000	1.000	1.000
5	1.065	1.066	1.069	1.073	1.076	1.079	1.082
10	1.089	1.094	1.098	1.103	1.107	1.112	1.116
15	1.125	1.132	1.139	1.146	1.153	1.160	1.167
20	1.173	1.184	1.195	1.206	1.216	1.227	1.239
25	1.237	1.254	1.270	1.287	1.304	1.321	1.338
30	1.325	1.350	1.375	1.400	1.426	1.452	1.479
35	1.447	1.484	1.522	1.561	1.600	1.641	1.622
40	1.624	1.680	1.737	1.797	1.852	1.921	1.986
45	1.891	1.977	2.068	2.162	2.260	2.362	2.468
50	2.321	2.462	2.610	2.767	2.932	3.106	3.289

Table 2 contd.

 $\theta = 9.1^\circ$ 

$\alpha$	1.0	1.1	1.2	1.3	1.4	1.5	1.6	1.7
0								
5	1.040	1.043	1.046	1.049	1.052	1.055	1.058	1.061
10	1.055	1.060	1.066	1.068	1.073	1.077	1.082	1.086
15	1.072	1.079	1.086	1.092	1.099	1.106	1.113	1.120
20	1.091	1.101	1.112	1.122	1.132	1.143	1.154	1.164
25	1.111	1.129	1.145	1.160	1.176	1.191	1.207	1.223
30	1.144	1.165	1.187	1.210	1.233	1.256	1.280	1.304
35	1.183	1.214	1.245	1.278	1.311	1.345	1.379	1.415
40	1.237	1.281	1.326	1.373	1.421	1.470	1.521	1.574
45	1.316	1.379	1.444	1.512	1.583	1.657	1.734	1.814
50	1.439	1.530	1.627	1.728	1.836	1.950	2.070	2.197

Table 2 contd.

	$\theta = 9.1$						
	1.8	1.9	2	2.1	2.2	2.3	2.4
0	1.000	1.000	1.000	1.000	1.000	1.000	1.000
5	1.065	1.068	1.071	1.074	1.077	1.080	1.083
10	1.091	1.095	1.100	1.104	1.109	1.113	1.118
15	1.127	1.134	1.141	1.148	1.155	1.162	1.170
20	1.175	1.186	1.197	1.207	1.219	1.230	1.241
25	1.240	1.256	1.273	1.290	1.307	1.324	1.345
30	1.328	1.353	1.378	1.403	1.429	1.456	1.483
35	1.451	1.488	1.526	1.565	1.605	1.645	1.687
40	1.629	1.685	1.743	1.803	1.864	1.927	1.993
45	1.898	1.985	2.075	2.170	2.268	2.371	2.477
50	2.331	2.473	2.622	2.779	2.945	3.120	3.305



Table 2 contd.

 $\theta = 9.2^\circ$ 

$\mu t$ - $\kappa$	1.0	1.1	1.2	1.3	1.4	1.5	1.6	1.7
5	1.041	1.044	1.047	1.050	1.053	1.056	1.059	1.063
10	1.056	1.061	1.067	1.070	1.074	1.079	1.083	1.088
15	1.073	1.080	1.087	1.094	1.100	1.107	1.114	1.121
20	1.093	1.103	1.103	1.124	1.134	1.145	1.155	1.166
25	1.116	1.131	1.147	1.162	1.178	1.194	1.209	1.226
30	1.146	1.168	1.168	1.212	1.235	1.259	1.282	1.306
35	1.185	1.216	1.248	1.280	1.314	1.348	1.383	1.418
40	1.240	1.284	1.284	1.376	1.425	1.474	1.526	1.579
45	1.320	1.383	1.448	1.517	1.588	1.662	1.740	1.820
50	1.444	1.536	1.536	1.735	1.843	1.958	2.079	2.207

Table 2 contd.

 $\theta = 9.2$ 

	1.8	1.9	2	2.1	2.2	2.3	2.4
0	1.000	1.000	1.000	1.000	1.000	1.000	1.000
5	1.066	1.069	1.072	1.075	1.079	1.082	1.085
10	1.092	1.097	1.101	1.106	1.111	1.115	1.120
15	1.128	1.136	1.143	1.150	1.157	1.164	1.171
20	1.177	1.188	1.199	1.210	1.221	1.232	1.244
25	1.242	1.259	1.276	1.292	1.310	1.327	1.345
30	1.331	1.356	1.381	1.407	1.433	1.460	1.487
35	1.455	1.492	1.530	1.569	1.609	1.650	1.692
40	1.634	1.690	1.749	1.809	1.870	1.934	2.000
45	1.904	1.992	2.033	2.178	2.277	2.380	2.488
50	2.341	2.484	2.634	2.792	2.959	3.135	3.320

Table 2 contd.

$\theta = 9.3^\circ$

$\frac{t}{\mu}$	1.0	1.1	1.2	1.3	1.4	1.5	1.6	1.7
5	1.041	1.045	1.048	1.051	1.054	1.057	1.031	1.064
10	1.057	1.062	1.066	1.071	1.075	1.080	1.084	1.089
15	1.074	1.081	1.088	1.095	1.102	1.109	1.116	1.123
20	1.094	1.105	1.115	1.125	1.136	1.146	1.157	1.168
25	1.118	1.133	1.148	1.164	1.180	1.196	1.212	1.228
30	1.148	1.170	1.192	1.215	1.238	1.261	1.285	1.30
35	1.188	1.219	1.251	1.283	1.317	1.351	1.386	1.422
40	1.243	1.287	1.333	1.380	1.429	1.479	1.530	1.584
45	1.324	1.387	1.453	1.522	1.593	1.668	1.746	1.827
50	1.449	1.541	1.639	1.742	1.851	1.966	2.088	2.216

Table 2 contd.

 $\theta = 9.3$ 

	1.8	1.9	2	2.1	2.2	2.3	2.4
0	1.000	1.000	1.000	1.000	1.000	1.000	1.000
5	1.068	1.072	1.073	1.077	1.080	1.083	1.087
10	1.095	1.100	1.103	1.108	1.112	1.117	1.122
15	1.132	1.139	1.145	1.152	1.159	1.166	1.174
20	1.181	1.192	1.201	1.212	1.223	1.235	1.246
25	1.247	1.264	1.278	1.295	1.313	1.330	1.348
30	1.337	1.362	1.385	1.410	1.437	1.464	1.491
35	1.463	1.500	1.535	1.574	1.614	1.655	1.697
40	1.644	1.701	1.754	1.814	1.877	1.941	2.007
45	1.919	2.000	2.091	2.137	2.286	2.390	2.498
50	2.362	2.506	2.646	2.805	2.972	3.144	3.336

Table 2 contd.

 $\theta = 9.4^\circ$ 

$\mu t$	1.0	1.1	1.2	1.3	1.4	1.5	1.6	1.7
$-\alpha$								
5	1.042	1.045	1.049	1.052	1.055	1.058	1.062	1.065
10	1.058	1.063	1.067	1.072	1.077	1.081	1.086	1.091
15	1.075	1.083	1.089	1.096	1.103	1.110	1.118	1.125
20	1.096	1.106	1.116	1.127	1.138	1.148	1.159	1.170
25	1.119	1.135	1.150	1.166	1.182	1.198	1.214	1.231
30	1.150	1.172	1.194	1.217	1.240	1.264	1.288	1.312
35	1.190	1.221	1.253	1.286	1.320	1.354	1.390	1.426
40	1.246	1.290	1.337	1.384	1.433	1.483	1.535	1.589
45	1.328	1.391	1.458	1.527	1.599	1.674	1.752	1.833
50	1.454	1.547	1.645	1.749	1.858	1.974	2.097	2.226

Table 2 contd.

 $\theta = 9.4$ 

	1.8	1.9	2.0	2.1	2.2	2.3	2.4
0	1.000	1.000	1.000	1.000	1.000	1.000	1.000
5	1.068	1.072	1.075	1.078	1.082	1.085	1.089
10	1.095	1.100	1.105	1.109	1.114	1.119	1.124
15	1.132	1.139	1.147	1.154	1.161	1.168	1.176
20	1.181	1.193	1.204	1.215	1.226	1.237	1.249
25	1.248	1.264	1.281	1.298	1.316	1.337	1.351
30	1.337	1.363	1.388	1.414	1.441	1.468	1.495
35	1.463	1.501	1.539	1.579	1.619	1.660	1.703
40	1.644	1.701	1.760	1.821	1.883	1.948	2.015
45	1.919	2.007	2.099	2.195	2.295	2.399	2.508
50	2.362	2.506	2.658	2.818	2.986	3.164	3.351

Table 2

Table 2 contd.

 $\theta = 9.5^\circ$ 

$\mu$	1.0	1.1	1.2	1.3	1.4	1.5	1.6	1.7
5	1.043	1.046	1.049	1.053	1.056	1.059	1.063	1.066
10	1.059	1.064	1.068	1.073	1.078	1.082	1.087	1.092
15	1.077	1.084	1.091	1.098	1.105	1.112	1.119	1.126
20	1.097	1.107	1.118	1.129	1.139	1.150	1.161	1.172
25	1.121	1.137	1.152	1.168	1.184	1.200	1.216	1.233
30	1.152	1.174	1.197	1.220	1.243	1.267	1.291	1.315
35	1.193	1.224	1.256	1.289	1.323	1.358	1.393	1.430
40	1.249	1.294	1.340	1.387	1.437	1.487	1.540	1.594
45	1.332	1.396	1.462	1.532	1.604	1.679	1.758	1.840
50	1.460	1.553	1.651	1.756	1.866	1.982	2.105	2.235

Table 2

Table 2 contd.

 $\theta = 9.5^\circ$ 

$\frac{-x}{\lambda t}$	1.0	1.1	1.2	1.3	1.4	1.5	1.6	1.7
5	1.043	1.046	1.049	1.053	1.056	1.059	1.063	1.066
10	1.059	1.064	1.068	1.073	1.078	1.082	1.087	1.092
15	1.077	1.084	1.091	1.098	1.105	1.112	1.119	1.126
20	1.097	1.107	1.118	1.129	1.139	1.150	1.161	1.172
25	1.121	1.137	1.152	1.168	1.184	1.200	1.216	1.233
30	1.152	1.174	1.197	1.220	1.243	1.267	1.291	1.315
35	1.193	1.224	1.256	1.289	1.323	1.358	1.393	1.430
40	1.249	1.294	1.340	1.387	1.437	1.487	1.540	1.594
45	1.332	1.396	1.462	1.532	1.604	1.679	1.758	1.840
50	1.460	1.553	1.651	1.756	1.866	1.982	2.105	2.235



Table 2 contd.

 $\theta = 9.5$ 

	1.8	1.9	2.0	2.1	2.2	2.3	2.4
0	1.000	1.000	1.000	1.000	1.000	1.000	1.000
5	1.070	1.073	1.076	1.080	1.083	1.087	1.090
10	1.097	1.101	1.107	1.111	1.116	1.121	1.126
15	1.134	1.141	1.149	1.156	1.163	1.171	1.178
20	1.183	1.194	1.206	1.217	1.229	1.240	1.252
25	1.250	1.267	1.284	1.302	1.319	1.336	1.355
30	1.341	1.366	1.391	1.418	1.445	1.471	1.499
35	1.467	1.505	1.543	1.583	1.624	1.665	1.708
40	1.649	1.707	1.766	1.827	1.890	1.954	2.021
45	1.926	2.015	2.108	2.204	2.304	2.409	2.518
50	2.372	2.517	2.670	2.831	3.000	3.17	3.367

Table 2 contd.

 $\theta = 9.6$ 

	1.8	1.9	2.0	2.1	2.2	2.3	2.4
0	1.000	1.000	1.000	1.000	1.000	1.000	1.000
5	1.071	1.074	1.078	1.081	1.085	1.088	1.092
10	1.098	1.103	1.108	1.113	1.118	1.123	1.128
15	1.135	1.143	1.150	1.158	1.165	1.178	1.180
20	1.185	1.197	1.208	1.219	1.231	1.243	1.254
25	1.252	1.270	1.287	1.304	1.322	1.340	1.358
30	1.343	1.369	1.395	1.421	1.448	1.476	1.503
35	1.471	1.509	1.548	1.588	1.629	1.671	1.713
40	1.654	1.712	1.772	1.833	1.896	1.961	2.029
45	1.933	2.022	2.116	2.213	2.314	2.419	2.529
50	2.383	2.529	2.682	2.844	3.014	3.194	3.384

Table 2 contd.

 $\theta = 9.6$ 

	1.0	1.1	1.2	1.3	1.4	1.5	1.6	1.7
0	1.000	1.000	1.000	1.000	1.000	1.000	1.000	1.000
5	1.044	1.047	1.050	1.054	1.058	1.061	1.064	1.067
10	1.060	1.065	1.069	1.074	1.079	1.084	1.089	1.093
15	1.078	1.085	1.092	1.099	1.106	1.114	1.121	1.128
20	1.098	1.109	1.129	1.130	1.141	1.152	1.163	1.174
25	1.123	1.138	1.154	1.170	1.186	1.202	1.219	1.235
30	1.154	1.176	1.196	1.222	1.245	1.269	1.294	1.318
35	1.195	1.227	1.259	1.292	1.327	1.361	1.397	1.433
40	1.252	1.297	1.343	1.391	1.441	1.492	1.545	1.598
45	1.336	1.400	1.467	1.537	1.609	1.685	1.764	1.847
50	1.465	1.559	1.560	1.763	1.874	1.991	2.115	2.245

Table 2 contd.

 $\theta = 9.7$ 

	1.0	1.1	1.2	1.3	1.4	1.5	1.6	1.7
0	1.000	1.000	1.000	1.000	1.000	1.000	1.000	1.000
5	1.044	1.048	1.051	1.055	1.058	1.062	1.065	1.069
10	1.061	1.066	1.071	1.075	1.080	1.085	1.090	1.095
15	1.079	1.086	1.093	1.101	1.108	1.115	1.123	1.130
20	1.100	1.110	1.121	1.132	1.144	1.154	1.165	1.176
25	1.125	1.140	1.156	1.172	1.188	1.205	1.221	1.238
30	1.156	1.117	1.201	1.224	1.248	1.272	1.297	1.321
35	1.197	1.229	1.262	1.296	1.330	1.365	1.401	1.437
40	1.255	1.300	1.347	1.395	1.446	1.496	1.549	1.603
45	1.340	1.404	1.472	1.542	1.615	1.691	1.771	1.854
50	1.470	1.565	1.664	1.770	1.881	1.999	2.124	2.255

Table 2 contd.

 $\theta = 9.7$ 

	1.8	1.9	2.0	2.1	2.2	2.3	2.4
0	1.000	1.000	1.000	1.000	1.000	1.000	1.000
5	1.073	1.076	1.079	1.083	1.086	1.090	1.094
10	1.100	1.105	1.110	1.115	1.120	1.125	1.130
15	1.137	1.145	1.152	1.160	1.168	1.175	1.183
20	1.188	1.199	1.210	1.222	1.234	1.245	1.257
25	1.255	1.272	1.289	1.307	1.325	1.343	1.361
30	1.347	1.372	1.399	1.425	1.452	1.480	1.507
35	1.475	1.513	1.552	1.593	1.634	1.676	1.719
40	1.660	1.718	1.778	1.839	1.903	1.968	2.036
45	1.940	2.230	2.124	2.221	2.323	2.429	2.539
50	2.394	2.540	2.694	2.857	2.029	3.20	3.400

Table 2 contd.

 $\theta = 9.8$ 

	1.0	1.1	1.2	1.3	1.4	1.5	1.6	1.7
0	1.000	1.000	1.000	1.000	1.000	1.000	1.000	1.000
5	1.045	1.052	1.053	1.056	1.059	1.063	1.067	1.070
10	1.062	1.067	1.072	1.077	1.081	1.087	1.091	1.096
15	1.080	1.087	1.095	1.102	1.109	1.117	1.124	1.132
20	1.101	1.112	1.123	1.134	1.145	1.156	1.167	1.118
25	1.126	1.143	1.158	1.174	1.119	1.207	1.224	1.241
30	1.158	1.181	1.204	1.227	1.251	1.275	1.299	1.324
35	1.200	1.232	1.265	1.299	1.333	1.368	1.404	1.441
40	1.258	1.301	1.351	1.399	1.449	1.501	1.554	1.609
45	1.344	1.409	1.476	1.547	1.620	1.697	1.777	1.861
50	1.476	1.571	1.671	1.777	1.889	2.008	2.133	1.265

Table 2 contd.

 $\theta = 9.8$ 

	1.8	1.9	2.0	2.1	2.2	2.3	2.4
0	1.000	1.000	1.000	1.000	1.000	1.000	1.000
5	1.074	1.077	1.081	1.084	1.088	1.092	1.099
10	1.101	1.106	1.111	1.117	1.122	1.127	1.132
15	<del>1.145</del>	1.147	1.154	1.162	1.170	1.178	1.185
20	1.190	1.202	1.213	1.225	1.237	1.248	1.260
25	1.258	1.275	1.292	1.310	1.328	1.346	1.364
30	1.350	1.376	1.402	<del>1.429</del>	1.456	1.484	1.512
35	1.479	1.517	1.557	1.597	1.639	1.681	1.724
40	1.665	1.723	1.783	1.846	1.909	1.975	2.044
45	1.948	2.038	2.132	2.230	2.323	2.439	2.555
50	2.405	2.552	2.707	2.871	3.043	3.225	3.417

Table 2 contd.

 $\phi = 9.9$ 

	1.8	1.9	2	2.1	2.2	2.3	2.4
0	1.00	1.00	1.00	1.00	1.00	1.00	1.00
5	1.075	1.079	1.082	1.086	1.090	1.093	1.096
10	1.103	1.108	1.113	1.118	1.123	1.129	1.134
15	1.141	1.149	1.156	1.164	1.172	1.180	1.188
20	1.192	1.203	1.215	1.227	1.239	1.251	1.263
25	1.260	1.278	1.295	1.313	1.331	1.349	1.367
30	1.353	1.379	1.406	1.433	1.460	1.488	1.515
35	1.483	1.522	1.561	1.602	1.644	1.686	1.727
40	1.670	1.729	1.789	1.852	1.916	1.983	2.049
45	1.955	2.046	2.141	2.239	2.342	2.449	2.556
50	2.416	2.564	2.720	2.884	3.058	3.241	3.424



Table 2 contd.

 $\theta = 10.00$ 

	1.8	1.9	2.0	2.1	2.2	2.3	2.4
0	1.000	1.000	1.000	1.000	1.000	1.000	1.000
5	1.076	1.080	1.084	1.087	1.091	1.095	1.099
10	1.105	1.110	1.115	1.120	1.125	1.131	1.136
15	1.143	1.151	1.158	1.166	1.174	1.182	1.190
20	1.191	1.206	1.218	1.230	1.242	1.254	1.266
25	1.263	1.280	1.298	1.316	1.334	1.353	1.371
30	1.356	1.383	1.409	1.436	1.464	1.492	1.520
35	1.487	1.526	1.566	1.607	1.649	1.691	1.735
40	1.676	1.735	1.796	1.858	1.923	1.990	2.058
45	1.963	2.054	2.149	2.248	2.352	2.459	2.571
50	2.427	2.576	2.733	2.896	3.073	3.256	3.451